SYNTHESIS, CHARACTERIZATION AND BIOLOGICAL APPLICATIONS OF POLYELECTROLYTE BRUSHES

A Dissertation

Presented to the Faculty of the Graduate School

of Cornell University

In Partial Fulfillment of the Requirements for the Degree of

Doctor of Philosophy

by

Rong Dong

August 2009

SYNTHESIS, CHARACTERIZATION AND BIOLOGICAL APPLICATIONS OF POLYELECTROLYTE BRUSHES

Rong Dong, Ph. D.

Cornell University 2009

Polyelectrolyte (PE) brushes refer to surface tethered polyelectrolyte chains with sufficiently high grafting density such that the polymer chains are forced to extend from the surfaces. Most physicochemical properties of PE brushes are stimuli-responsive and they are thus able to create "smart" surfaces for various applications. In addition, many biointerfaces inside biological systems possess "brush-like" structures and may also carry many ionizable groups. PE brushes can serve as realistic models to better understand the behaviors of those biological interfaces.

This dissertation describes the synthesis, characterization and applications for several types of PE brushes. Surface-initiated atom transfer radical polymerization in protic solvents was used to directly synthesize the PE brushes. A variety of characterization methods were used to understand the chemical structure and physical properties of the brushes. We were able to estimate the pKa of weak polyacid brushes and experimentally confirmed the variation of pKa inside the weak PE brushes. Poly(acrylic acid) (PAA) brushes were patterned on silica surfaces by a protocol modified from photolithography. The patterned PAA brushes were used to create arrays of biomolecules to study the signaling pathways of rat basophilic leukemia (RBL) mast cells. Cell adhesion on patterned PAA brush surfaces changed dramatically, depending on the size of the pattern, incubation temperature and thickness of the brushes. Positively charged poly((2-(methacryloyloxy)ethyl)

trimethylammonium chloride) (PMETA) brushes were shown to be promotive for neuron growth. Patterned PMETA brushes surrounded by a poly(ethylene glycol) monolayer guided neuron growth very well. Finally, several types of pH-responsive polymer brushes were used to tailor electrochemical properties of gold electrodes. Cyclic voltammetry of the modified electrodes showed that the redox process of charged electroactive compounds greatly depended on the nature of the brushes and pH of the medium. PE brushes could screen the electrodes against like-charged interferences and increase the selectivity of the electrodes in biosensing.

BIOGRAPHICAL SKETCH

Rong Dong was born in Hubei Province, China. She graduated from Peking University in July 2003 with a Bachelor's degree in Materials Chemistry. Since July 2004, she has pursued her Ph.D. in Chemistry at Cornell University under the supervision of Prof. Christopher K. Ober in the Department of Materials Science and Engineering.

Dedicated to my family

for their love, support and encouragement

ACKNOWLEDGMENTS

Throughout my Ph.D. study at Cornell, I have benefited from many people's generous help and intelligent advices. I would like to take this opportunity to express my deep gratitude to them.

I would start by thanking my advisor, Prof. Christopher K. Ober, for being always supportive and giving me the opportunity and freedom to work on the projects I am interested in. I am always deeply impressed by Chris's broad knowledge and in-depth understanding in both basic science and practical applications of materials science and engineering. His brilliant guidance has greatly benefited my graduate education and will continue to help me in the future. I also feel grateful for Chris's extraordinary patience, kind support and continuous encouragement and I greatly appreciate him as my advisor. I am very lucky to have an exceptional doctoral committee and wish to thank Prof. Barbara Baird and Prof. Manfred Lindau for their sparkling ideas and intelligent suggestions for my research projects. They have exposed the interesting biology research field to me. Without these professors' encouragement and guidance, this dissertation could never have reached the heights or explored the depths.

I am grateful to have the opportunity to work with several research groups and get help from many nice, intelligent people. Prof. Héctor Abruña has been very helpful by spending time to discuss electrochemistry with me. I have certainly learned a lot from him. I very much appreciate Dr. David A. Holowka's suggestions and discussions regarding mast cells. I also had a chance to work with Prof. Uli Wiesner's group and benefited a lot from his insightful suggestions. I would like to acknowledge Prof. Edward J. Kramer at UCSB for reading my manuscript and giving me invaluable feedbacks in spite of his busy schedule.

I especially want to thank my wonderful collaborators for their intelligent ideas and

persistent hard working. Special thanks go to Dr. Raymond Molloy, Ethan Chiang and Yi Liu. I could have never made the achievements without their contributions. I am also very thankful for my other collaborators: Dr. Andrew Burns, Dr. Khajak Berberian, Kassandra Kisler, Sunitha Ayers, Pangshun Zhu, and Alexis Torres. It was a great experience working with so many highly talented and motivated researchers at different disciplines.

The Ober group has always been the best source for help, support and friendship. In the beginning of my Ph.D. study, Dr. Ramakrishnan Ayothi, Dr. Yi Yi and Dr. Shinji Tanaka had helped me a lot by teaching me lab techniques and inspiring my research ideas. I can never say enough thanks for their generous help. I am also very thankful for Prof. Sitaraman Krishnan for his bright ideas and suggestions in several projects. I really appreciate that Dr. Wageesha Senaratne and Dr. Nelson Felix have taught me a lot in the area of their expertise. Mirjam Hemmelmann was very helpful and fun to work with during her visit at Cornell. I also want to thank Marvin Paik, Jing Sha and Priscilla Taylor for helping me characterizing some research samples. I am so grateful for the numerous help and kind support from all the other Ober group members and group alumni: Dr. Joan Bosworth, Dr. Anuja De Silva, Prof. Margarita Chatzichristidi, Dr. Shalin Jhaveri, Dr. Craig Weinman, Dr. Manabu Tanaka, Dr. Xavier Andre, Dr. Daewon Park, Dr. Da Yang, Dr. Fengxiang You, Dr. Qin Lin, Dr. Jin Kyun Lee, Eisuke Murotani, Dr. Woo Jin Bae, Dr. Harihara Subramanian, Dr. Young Jin Cho, Dr. Heloise Therien-Aubin, Abhinav Rastogi, Evan Schwartz, Drew Forman, Michelle Chavis, Zhaoli Zhou, Marie Krysak, Carol Newby, Christine Ouyang, Lin Chen, Liz Welch, and Reinhard Berger. I really appreciate that the Lindau group and the Baird group at Cornell have always been very friendly and helpful to me.

I gratefully acknowledge the funding support from the Cornell Nanobiotechnology center (NBTC), the Cornell Nanoscale Interdisciplinary Research Team and the

Cornell Center for Materials Research (CCMR) throughout my Ph.D. study. I would like to thank the technical support from the staff in NBTC, CCMR and the Cornell Nanofabrication Facility (CNF), especially Prof. Christopher Umbach for his help with AFM, Garry J. Bordonaro for his support in making photo-masks, and Carol Bayles for her advices with fluorescence microscopes.

I would like to take this opportunity to thank my family for their unconditional love and support. My parents have worked hard and sacrificed a lot to support me to pursue my dreams. Their hard working, honesty and positive attitudes toward life have always inspired me and helped me to look for my ways when I felt lost. I am lucky to have great parents-in-law who treated like their own daughter. Finally, I want to thank Mingwei Liu, my husband and my best friend, for spoiling me, sharing every moment of my life and cheering me up when I have difficulties during my Ph.D. study.

TABLE OF CONTENTS

Biographical Sketch	iii
Dedication	iv
Acknowledgements	v-vii
Table of Contents	viii
List of Schemes	ix
List of Figures	x-xii
List of Tables	xiii
Chapter 1: Recent Progress in Polyelectrolyte Brushes: Synthesis, Characterization and Applications	1-41
Chapter 2: Patterned Biofunctional Poly(acrylic acid) Brushes on Silicon Surfaces	42-79
Chapter 3: Dissociation Behavior of Weak Polyelectrolyte Brushes on a Planar Surface	80-100
Chapter 4: Investigating RBL Cell Behavior on Patterned Polymer Brush Surfaces	101-118
Chapter 5: Direct Synthesis of Quaternized Polymer Brushes and Their Applications for Guiding Neuronal Growth	119-138
Chapter 6: Tailoring electrode properties towards biosensor applications using pH-sensitive polymer brushes	139-155
Chapter 7: Conclusions	153-156

LIST OF SCHEMES

Scheme 2.1**:** Patterning of PEG and poly(acrylic acid) brushes on silicon surface 55

Scheme 2.2: Surface initiated polymerization of sodium acrylate using ATRP 55

Scheme 2.3: Protein immobilization on poly(acrylic acid) brush surface by EDC/NHS coupling 60

Scheme 2.4: Protein immobilization to PAA brushes through avidin-biotin interaction 62

Scheme 2.5: Immobilization of biotin using BSA as linkages 66

Scheme 4.1: Patterning of PAA brushes on a silicon surface 105

Scheme 4.2: Attaching DNP to PAA brushes using a PEG linker 106

Scheme 5.1: Generation of polymer brushes/PEG patterned surfaces based on photolithography 125

Scheme 5.2: Synthesis of cationic polymer brushes by SI-ATRP of META 128

LIST OF FIGURES

Figure 1.1: Swollen thickness of the PMETA brush as a function of NaCl concentration. 11

Figure 1.2: Schematic picture of the degree of dissociation within the weak PE brush. 12

Figure 1.3: A cartoon showing how dissociation behavior of weak polyacid brushes changes in solution at different pH. 15

Figure 1.4: Contact angle titration curves for poly(acrylic acid) brushes and poly(methacrylic acid) brushes on gold substrates. 17

Figure 1.5: Fluorescence image of BSA-FITC immobilized on PAA brush patterns in a background consisting of PEG monolayer. 23

Figure 2.1: C 1s XPS spectrum of poly(acrylic acid) (PAA) brush grown from a silicon surface. 57

Figure 2.2: Tapping-mode scanning probe microscopy height-images of unpatterned and patterned PAA brush grown on silicon substrates. 58

Figure 2.3: Fluorescence image of BSA-FITC immobilized on PAA brush patterns in a background consisting of PEG SAM. 59

Figure 2.4: Fluorescence microscopy image of avidin immobilized PEG/PAA patterned surface that was incubated with fluoresceinated biotin. 63

Figure 2.5: XPS survey scan and the high resolution C 1s spectrum of covalently immobilized avidin on PAA brush surface. 63

Figure 2.6: Fluorescence microscopy image of a streptavidin-immobilized BSA-PAA surface that was incubated with fluoresceinated biotin. 67

Figure 3.1: FTIR spectra of PAA brushes and PMAA brushes on gold surfaces treated with buffer solutions at different pH values. 87

Figure 3.2: FTIR titration curves for PAA brushes and PMAA brushes on gold substrates. 88

Figure 3.3: Contact angle titration curves measured using nonreactive spreading protocol for PAA brushes and PMAA brushes on gold substrates. 91

Figure 3.4: A cartoon showing how dissociation degree and swelling behavior of weak polyacid brushes change in solution at different pH. 94

Figure 3.5: The C 1s spectrum of PAA brushes at emission angle 0˚ with a four-peak fit. 96

Figure 3.6: Experimental dependence of charge fraction with emission angle and reconstructed depth profile of charge fraction within PAA brushes 97

Figure 4.1: Confocal fluorescence images of RBL cells incubated on patterned PAA brush (~ 30nm) surfaces at 37˚C for over twenty minutes. 109

Figure 4.2: Density of cell adhesion on pure silicon surface and patterned PAA brush surfaces with different pattern morphology. 110

Figure 4.3: Confocal fluorescence images of RBL cells incubated on patterned PAA brush (~ 30 nm) surface at room temperature and at 37˚C afterwards. 112

Figure 4.4: Confocal fluorescence images of RBL cells incubated on patterned PAA brush surfaces with different brush thicknesses. 113

Figure 4.5: Confocal fluorescence images of RBL cells incubated on patterned PAA-DNP brush (~ 8 nm) surface. 115

Figure 5.1: Thickness of PMETA brushes versus polymerization time in different solvents. 128

Figure 5.2: Grazing-angle reflectance FTIR spectra of PMETA brushes synthesized directly from META. 129

Figure 5.3: Confocal fluorescence image of rat hippocampal neurons cultured on PMETA brushes modified silicon substrates. 130

Figure 5.4: Optical image of a patterned PMETA brush/PEG surface. 132

Figure 5.5: Fluorescence and reflectance image of living hippocampal neurons using confocal microscopy. Cumulative histograms of neurite length 133

Figure 5.6: Reflectance (A) and Fluorescence (B) images of hippocampal neurons acquired by confocal microscopy. 134

Figure 6.1: Cyclic voltammograms of PDMAEMA brush modified gold electrodes for 1 mM $K_3Fe(CN)_6$ solution in 0.1 M MES buffer solution at different pH values. 146

Figure 6.2: FTIR spectra of PDMAEMA brushes on gold surfaces pretreated by solution used in the electrochemical experiments. 147

Figure 6.3: Cyclic voltammograms of PAA brush modified gold electrodes for 1 mM $K_3Fe(CN)_6$ solution in 0.1 M K_2SO_4 solution at different pH values. 148

Figure 6.4: Cyclic voltammograms of PAA brush modified gold electrode and bare gold electrode for 1 mM $K_3Fe(CN)_6$ solution in 0.1 M K_2SO_4 solution. 148

Figure 6.5: Cyclic voltammograms of PAA brush modified gold electrode, Nafion coated gold electrode and bare gold electrode for 1 mM ascorbic acid solution in 0.1 M K_2SO_4 solution at neutral pH. 150

Figure 6.6: Cyclic voltammograms of PAA brush modified gold electrode, poly(styrene sulfonate) brush modified gold electrode and bare gold electrode for 1 mM ascorbic acid solution in 0.1 M K_2SO_4 solution at neutral pH. 151

LIST OF TABLES

Table 2.1: Relative areas of the C 1s sub-peaks in the XPS spectrum of the avidin-tethered poly(acrylic acid) brush surface and number distribution of carbon atoms at the surface 65

Table 3.1: Area percentage of four peaks from the C 1s spectra of PAA brush at different emission angle 96

CHAPTER 1

RECENT PROGRESS IN POLYELECTROLYTE BRUSHES: SYNTHESIS, CHARACTERIZATION AND APPLICATIONS

Abstract

Polymer brushes have attracted tremendous interest in recent ten years, after the surface-initiated polymerization or so-called "grafting from" method was invented to synthesize polymer brushes. Polyelectrolye brushes (PE brushes) are of particular interest because of their unique properties and great potential for applications in the nanobiotechnology area. This review summarizes recent progress in synthesis, characterization and applications of PE brushes.

1.1. Introduction

PE brushes refer to surface tethered polyelectrolyte chains with sufficiently high grafting density such that the polymer chains are forced to extend from the surface. Unlike neutral polymer brushes, electrostatic interaction inside the PE brushes plays very important roles in regulating physicochemical properties of the brushes, which makes PE brushes extremely intriguing. Many theoretical studies have been done to understand the complicated behavior of polyelectrolyte brushes.[1] Furthermore, charge regulated properties are sensitive to external conditions, which makes PE brushes responsive to their environment and enables them to create "smart" surfaces. As a result, PE brushes possess great potential for applications in the nanobiotechnology area, including those ones already discussed for general polymer brushes.[2]

Surface-initiated atom transfer radical polymerization (SI-ATRP) in protic media enables direct synthesis of many types of PE brushes in an easy and controlled manner. Many recent studies began to explore applications of PE brushes in various fields.

Recent progress in the synthesis of PE brushes using SI-ATRP in protic media, physicochemical properties of PE brushes studied by both theoretical simulations and experimental characterization, and applications of PE brushes are discussed in detail this review.

1.2. Synthesis of PE brushes

Before the "grafting from" method was introduced by Rühe et al.,[3] PE brushes were formed mainly by adsorption of charged block copolymers, assembly of charged block copolymer at the air-water interface, or chemical attachment of charged polymers to solid surfaces (also referred to as "grafting to" method).[4] Due to steric hindrance, only brushes with very limited grafting density and thicknesses can be achieved using these methods. In addition, functional groups like carboxylic acid, may interfere with a surface reactive group, which makes the synthesis process very complicated. In the "grafting from" method, monomer molecules diffuse and attach to the growing chain end instead of bulky polymer chains, which greatly reduces steric hindrance. Because it is an *in situ* process, enthalpy released during the polymerization process also helps to overcome the energy cost caused by this steric effect. These factors in the "grafting from" method enable higher grafting density and larger thickness of polymer brushes. In addition, thickness and grafting density of the targeted brushes can be predesigned by choosing appropriate polymerization conditions and grafting density of the surface initiator. The invention of the "grafting from" method makes it possible to use existing knowledge of polymers to design and synthesize polymer brushes, which greatly aids progress in the field of polymer brushes.

In the first example of using surface-initiated polymerization to synthesize PE brushes, an azo initiator was used to initiate free radical polymerization of 4-vinylpyridine from the surface.[5] Permanent positive charge was introduced to the

brushes by quaternization. In terms of controlled radical polymerization, SI-ATRP is very popular due to the ease in preparing the ATRP surface initiator and the wide range of monomers that can be polymerized by ATRP. However, non-protic organic solvents used in traditional ATRP are not compatible with the hydrophilic monomers for PE brushes. As a result, PE brushes were usually derived from neutral polymer brushes by further reactions when synthesized by SI-ATRP.[6] Aqueous ATRP was first employed by Coca et al. to synthesis poly(2-hydroxylethyl acrylate),[7] following which Armes et al. reported the first ATRP of an acidic monomer in aqueous solution,[8] and demonstrated the possibility to synthesize polyacid directly using ATRP without the need of further reaction steps to introduce the ionizable groups. Shortly after this pioneering work, several other types of hydrophilic polymers were also successfully synthesized using ATRP in protic media.[9,10] Armes et al. used aqueous SI-ATRP to graft hydrophilic polymer brushes on silica nanoparticles.[11] The first example of direct synthesis of PE brushes using SI-ATRP was reported by Huck et al.[12] They synthesized triblock polymer brushes containing positively charged poly([2-(methacryloyloxy)ethyl] trimethylammonium chloride) (PMETA) brushes and negatively charged poly(sodium methacrylate) brushes using SI-ATRP in protic medium. Following this seminal work, SI-ATRP in protic media was widely used to synthesize other types of PE brushes.[13] The facile procedure and environmentally friendly solvents used in SI-ATRP in protic media make it an attractive method to synthesize polymer brushes. Some non-polar monomers, like methyl methacrylate, were also shown to be polymerized in a fast and controlled manner by using SI-ATRP in protic media.[14]

Matyjaszewski et al. discussed the synthesis of polymer brushes using SI-ATRP and side reactions involved in aqueous ATRP.[15] Many side reactions could occur when ATRP is conducted in protic solvents, such as disproportionation of the Cu^{I}

complex, reduction in the concentration of the Cu^{II} complexes via dissociation of the halide ligand, complexation of the dissociated complex with the solvent and the polar monomers, and disproportionation or hydrolysis of the initiator or dormant chain ends in protic solvents.

Because of these side reactions, ATRP in protic media is usually faster and less controllable than in non-polar organic solvents. Kinetics of ATRP in protic media is regulated by many factors, such as catalyst,[16] solvent,[17] monomer concentration,[18] and initiator.[19] For SI-ATRP, grafting density of initiator was shown to play an important role as well.[20] In the case of charged monomers, more factors could affect the growth kinetics of the brushes, such as pH value of the polymerization media.[8,21] These factors are discussed in more detail in the following text.

1.2.1. Catalyst. The kinetics of ATRP is closely related to the activity and concentration of the catalysts used in the polymerization process. By using cyclic voltammetry, [22] Coullerez et al. measured the redox potential of the CuBr with different complexing ligands in the aqueous media. They observed a good correlation between the redox potential and the apparent ATRP rate for polymerization of methoxy capped oligo(ethylene glycol) methacrylate in water. The general trend in the reducing properties in aqueous media of common ligands they studied is: Me_6-TREN < Bpy <HMTETA < PMDETA for bromo- and chlorocomplexes. However, Cu^I complexes in protic media also suffer from disproportionation. The Cu^I complexes of PMDETA and Me_6-TREN are not suitable for aqueous ATRP due to very fast disproportionation. As a result, bpy and HMTETA are better candidates as ligands for ATRP in protic media. Kim et al.[17(d)] studied the effect of Cu^I complex concentration on the kinetics of SI-ATRP of methyl acrylate (MA). They showed that the brush thickness resulting from a 4h SI-ATRP reached a maximum at a catalyst concentration

of 100 μM. At smaller concentrations the polymerization was too slow, and larger concentrations the polymerization was fast but terminated too soon.

Tsarevsky et al.[15(b)] discussed in detail the mechanism for deactivation of catalysts in protic solvents and possible methods to reduce the deactivation. According to them, heterolytic dissociation of the Cu^{II}-Br bonds in aqueous media[23] and the subsequent coordination of monomer or solvent to the catalyst are the main reasons for poorer control of aqueous ATRP. One way to improve the control over ATRP in protic media is to choose catalysts containing halide ligands that are less prone to heterolytic dissociation (higher K_x). Heterolytic dissociation of Cu^{II} complexes can be greatly affected by ligands and solvents. Ligands that form more stable complexes with catalyst than solvents or monomers do result in higher K_x. Decreasing the solvent polarity or adding halide salts can also shift the heterolytic dissociation toward the effective status of the Cu^{II} complexes, which will be discussed in detail in the next section. Another way to improve the control over ATRP in protic media is to increase the initial concentration of Cu^{II} complex,[16,17(c)] to ensure the presence of sufficient concentration of deactivator even after its dissociation in protic solvents. Tsarevsky et al. [17(c)] reported that addition of Cu^{II} complex into the polymerization medium reduced polymerization rate and also decreased polydispersities of the polymer product. In terms of polymer brushes, Cheng et al.[16] showed that the $[Cu^{I}]/[Cu^{II}]$ ratio greatly affected kinetics and conformation of PE brushes synthesized by SI-ATRP in protic media. Using QCM measurements, they observed *in situ* polymer brush growth with different $[Cu^{I}]/[Cu^{II}]$ ratios. Their results clearly showed that polymer brush growth rate was much slower when the ratio was small. By measuring the swelling ratios of the brushes grown at different $[Cu^{I}]/[Cu^{II}]$ ratios, they suggested that brushes grown at higher $[Cu^{I}]/[Cu^{II}]$ ratios possessed smaller grafting density and thus had larger swelling ratios when placed in good solvents.

In protic solvents, many side reactions took place to the catalysts used in ATRP and deactivated them, which has huge effects on the kinetics of PE brush growth. Close attention should be paid to the catalyst composition, especially concentration of the Cu^{II} deactivator, when PE brushes are synthesized by SI-ATRP in protic media.

1.2.2. Solvent. Because deactivation of the catalysts plays the key role in determining the kinetics of ATRP in protic solvents and the deactivation is tightly related to the solvent properties,[15(b)] the kinetics of ATRP in protic solvents is greatly affected by the properties of solvents used in the reaction, such as polarity,[17(a),17(c)] additional salt[17(b),17(c)] and pH values[8,21] etc. Li et al. [17(a)] explored the effect of different solvents during the synthesis of PMETA using ATRP. They have shown that adding methanol or 2-propanol to water solvent reduced the polymerization rate and resulted in narrower molecular weight distribution. Tsarevsky et al. [17(c)] also showed that a lower percentage of water in the solvent resulted in slower but more controllable polymerization. However, using methanol as a cosolvent caused transesterification of the monomer with methanol and generated significant amount of methyl methacrylate in the polymer product. Since a secondary alcohol was much less prone to transesterification, this problem was eliminated by using 2-propanol/water mixture as solvent.

ATRP catalysts were partially deactivated by dissociation and complexation during polymerization in protic solvent. Tsarevsky et al. [17(c)] proposed the idea of adding halide salts into the polymerization solution to suppress the deactivation of catalysts. Sankhe et al.[17(b)] also showed that addition of alkali halide salt, such as sodium chloride, enabled steady and continued growth of PE brushes with improved degree of control. For acid monomers, the pH of the polymerization medium determines how the monomer molecules interact with the catalyst complexes.[8] Armes et al.[8] reported that bipyridine ligands became protonated and no longer solubilized the $Cu^{I}Br$ catalyst

such that the acid monomers failed to polymerize at pH values lower than 6. But when the pH value of the polymerization media is too high, reduced propagation rates due to electrostatic repulsion between the monomer and the growing chains, complexation between monomer and the catalyst, and possible chemical bond cleavage caused by the hydrolysis of esters, work against brush growth. As a result, the optimum pH value for ATRP of sodium methacrylate lies between 8 and 9. Tugulu et al.[21(a)] explored the effect of pH, ionic strength and temperature on SI-ATRP of sodium methacrylate in detail. They showed that SI-ATRP of sodium methacrylate worked best at pH ~9 and ionic strength did not show a significant effect on the polymerization kinetics. As discussed in this section, solvent properties play very important roles in direct synthesis of PE brushes using SI-ATRP in protic media. Choosing the right solvent composition sometimes can be the vital part for SI-ATRP of certain types of monomers in protic solvents.

1.2.3. Monomer Concentration. It is well known that polymerization kinetics is tightly related to monomers. In addition to the chemical nature of the monomer and interaction between the monomer and the substrates, monomer concentration was also shown to have a huge impact on brush growth when polymer brushes were synthesized using aqueous SI-ATRP.[18] Grafting density and brush thickness were shown to increase with monomer concentration, especially in the low monomer concentration region. Kizhakkedathu et al.[18(a)] discussed the factors that caused the effect of monomer concentration in detail. They suggested that one reason could be the insufficient diffusion rate of monomer molecules to the initiation surface relative to the initiation rate at low monomer concentration. Such effect is enhanced even more in protic solvents, because of all the side reactions between the growing chain ends and the protic solvents. Basically, monomer molecules are competing with the solvents for the growing chain ends. Higher monomer concentration works in favor for

propagation of polymer brush chains. For PE brushes, electrostatic repulsion between charged monomers and growing chains is another factor that contributes to the effect of monomer concentration. When poly(acrylic acid) brushes were synthesized by direct polymerization of sodium acrylate using aqueous SI-ATRP as described before,[24] we observed a huge decrease in the brush thickness when the monomer concentration was reduced from 32 wt% to 24 wt%.[25] Because many SI-ATRP reactions in protic solvents are very fast, it is not always easy to control the brush thickness by controlling the polymerization time. One can take advantage of the effect of monomer concentration on brush growth to control the brush thickness to some extent.

1.2.4. Initiator. It is well known that initiator is a very important component for ATRP.[26] Zeng et al.[19] compared ATRP of 2-(dimethylamino)ethyl methacrylate in aqueous media using different initiators. They showed that molecular weight distribution of the synthesized polymer very much depended on the initiator, even though all initiators showed good solubility in the polymerization media. In terms of polymer brush synthesis, brush growth and brush conformation could be affected by more factors, such as the chain length,[27] grafting density[20] and wettability of the surface tethered initiator.

Jones et al.[20(a)] studied SI-ATRP of methyl methacrylate and glycidyl methacrylate on gold surfaces covered with self-assembled monolayers (SAMs) containing different percentages of initiator. They observed an almost linear relationship between initiator density and the growth rate of the polymer brush without a clear maximum initiator density. They speculated that the large "cutoff" initiator density was most likely due to consistent poor initiator efficiency at all initiator densities. However, Bao et al.[20(b)] reacted a preformed SAM with different percentages of compounds that can initiate ATRP to control the initiator density on gold surfaces. They showed that the initiator

efficiency increased a great deal when the initiator coverage dropped to 10% or lower because of reduced bimolecular termination. They attributed the difference between their results and the results of Johns et al. to the different initiator distribution within the mixed SAMs. Liu et al.[20(c)] also observed an increase of the initiator efficiency with decreasing initiator density. By controlling the density of the surface initiator, thickness and grafting density of polymer brushes could be tuned.

Although it has not yet been investigated, wettability of surface tethered initiator could also affect polymer brush growth, especially for hydrophilic monomers. Surfaces covered with ATRP initiators tend to be hydrophobic because of their hydrophobic head groups and hydrophobic hydrocarbon chains. Hydrophilic monomers do not wet these hydrophobic surfaces well, which leads to a difficult initiation step for SI-ATRP. Slight modification of the surface initiators with hydrophilic groups might make a big difference on SI-ATRP of hydrophilic monomers.

1.3. Characterization of PE Brushes

Physicochemical properties of PE brushes respond to their surrounding environment because of the ionizable functional groups carried on the brushes, which makes it both interesting yet complicated to understand the properties of PE brushes. In recent years, much effort in characterizing PE brushes has been made to better understand the physicochemical properties of PE brushes. Several reviews do an excellent job in summarizing the general synthesis and properties of PE brushes.[28] In the following text, we will summarize the recent progress in characterizing the properties of PE brushes that are closely related to their ionization, including swelling, dissociation behavior, surface energy and permeability of the brushes.

1.3.1. Swelling. PE brushes are usually very hydrophilic and tend to swell when placed in humid air or an aqueous solution.[28(a)] In most cases, electrostatic interactions

between the charged groups inside the PE brushes dominate the driving force for the swelling. As a result, the swelling behavior of PE brushes greatly depends on factors that can adjust the electrostatic interactions, such as pH and ionic strength of the solution, nature of the ionizable groups, grafting density of the brushes, etc. Good understanding of the swelling behavior of PE brushes is very important for their application. Many theoretical simulations[29] and characterization techniques that can measure thickness, such as dynamic light scattering (DLS),[30] atomic force microscopy (AFM),[31] ellipsometry,[32] and neutron reflectometry[33] have been used to study the swelling behavior of PE brushes.

For both neutral and charged brushes, swelling ratio decreases with increasing grafting density.[34] For PE brushes, swelling behavior for strong PE brushes and weak PE brushes are different, mainly because that the degree of dissociation is almost fixed in strong PE brushes, but not in weak PE brushes. Swelling behavior of strong PE brushes is not sensitive to pH given a constant electrolyte concentration of the medium.[30(b)] The relation between the swelling ratio of the strong PE brushes and the salt concentration of the medium changes with the salt concentration. Several research groups used different experimental methods to characterize swelling behavior of strong PE brushes.[31(e),32(c),33(a)] They all showed that the swelling ratio of strong PE brushes was constant when the salt concentrations were low, which was defined as the osmotic brush region. When the salt concentration in the medium was increased to a value comparable to the salt concentration within the brushes, the brushes entered a so-called salted brush region. In this region, the swelling ratio of strong PE brushes decreased with increasing salt concentration, as shown in Figure 1.1.

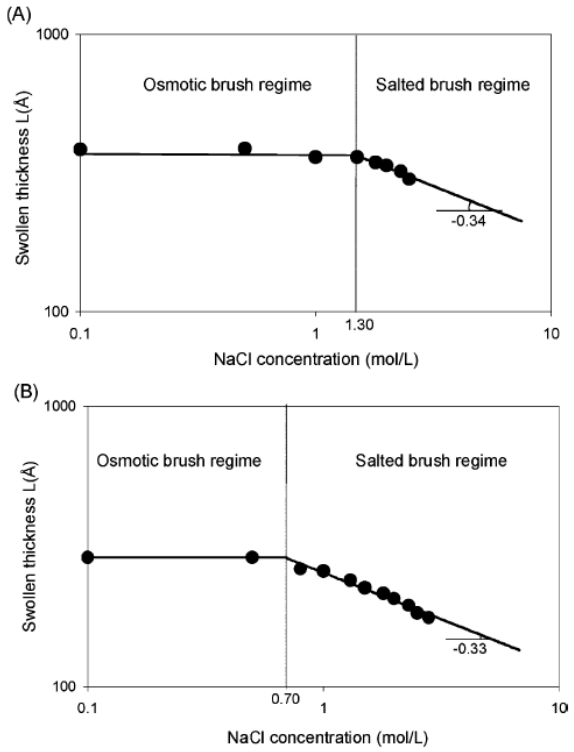

Figure 1.1: Swollen thickness of the PMETA brush as a function of NaCl concentration. The data are shown for brushes with grafting densities of $\sigma = 0.230$ (A) and 0.123 nm^{-2} (B). The crossover NaCl concentrations between the osmotic and salted-brush regimes are 1.30 and 0.70 mol/L for $\sigma = 0.230$ and 0.123 nm^{-2}, respectively. (Reprinted from Ref. 33(a) with permission from the American Chemical Society)

Swelling behavior of the weak PE brushes depends on both pH value and ionic strength of the medium.[30(a)] The effect of pH over the swelling behavior of weak PE brushes is very straightforward.[32(b),33(a)] When the changes in pH cause higher degree of dissociation in the brushes, the brushes swell more because of the increased electrostatic repulsion between the chains. Information about the collective

dissociation behavior of the weak PE brushes could be extracted by plotting the swelling ratios versus the pH values of the medium.

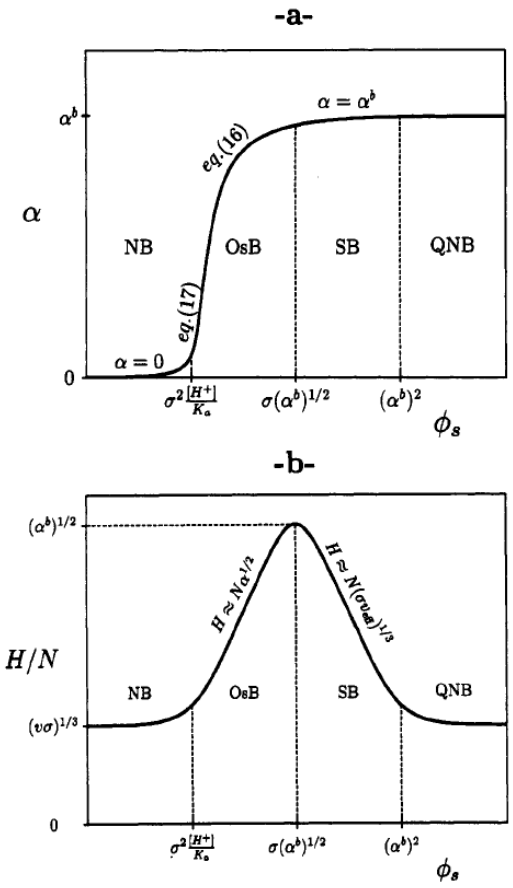

Figure 1.2: Schematic picture of the degree of dissociation within the weak PE brush (a) and the thickness of weak PE brush (b) as a function of the salt concentration**.** (Reprinted from Ref. 29(h) with permission from the American Chemical Society)

However, the swelling behavior of weak PE brushes depends on the ionic strength of the medium in a more complex manner, because the degree of dissociation of weak PE brushes increases with the ionic strength of the medium, as shown in Figure 1.2a. As a result, the thickness of the weak PE brushes increases with the salt concentration instead of remaining constant in the osmotic brush region. When the salt concentration is large enough to screen the electrostatic interactions within the weak PE brushes, the

brushes enter the salted brush region and the brush thickness decreases with the salt concentration, as shown in Figure 1.2b. Such swelling behavior of the weak PE brushes was confirmed by the experimental data from several groups. [30(b),32(b),32(e)]

1.3.2. Dissociation Behavior. In strong PE brushes, the ionizable groups are permanently charged over a large pH range, which is very straightforward and will not be discussed in detail. However, the dissociation behavior of weak PE brushes strongly depends on pH of the medium, as discussed in section 3.1. Because of the high segment density within polymer brushes, ionizable groups are much more difficult to dissociate in the brush environment than in the free polymer chains.[35] Polymer chains carrying charges must extend from the surface because of the electrostatic repulsion forces, which results in a large entropy loss of the system. To gain greater entropy and also to reduce the energy cost caused by the repulsion, it is favorable for many acid groups within the brushes to remain uncharged to minimize the energy of the whole system. The pKa values of weak PE brushes strongly depend on the grafting density and thickness of the brushes as well as the ionic strength of the medium.[35,36]

Direct titration of weak PE brushes is not as straightforward as in solution. However, many physicochemical properties of weak PE brushes, such as swelling, [32(b),33(a)] absorbance of infrared light,[37, 40(a)] surface zeta potential,[38] electrostatic force,[39] surface energy,[37,40] and permeability[41] etc. are tightly correlated with the pH of their environment. By plotting parameters of those physicochemical properties versus pH of the medium, one should be able to extract information about dissociation behavior of the brushes. In these properties, zeta potential could directly quantify the amount of charge on the surface. However, it was mostly used in colloidal systems. For planar surfaces, zeta potential was derived from streaming current data.[38(c)] Fourier transform

infrared spectroscopy (FTIR) is another technique that could quantify the degree of dissociation of PE brushes carrying certain types of functional groups, such as carboxylic acid and phosphate, which absorb IR differently depending on their charge status.[37,40(a)] Other physical properties can not be used to quantify the amount of charges or degree of dissociation of PE brushes, but titration curves based on those properties could still provide rich information about the dissociation behavior of PE brushes.

It must be noted that some of those properties such as electrostatic forces and surface energy, are only sensitive to the uppermost layer of the brush while the others represent the collective behavior of the whole brush layer. Theoretical simulations[29(h),35] and experimental results all showed that the pKa value of ionizable groups within weak PE brushes was a function of their distance from the substrate surface. The ionizable groups buried deeper inside the brushes are more difficult to dissociate than those closer to the brush periphery and have larger pKa. Because pKa of the weak PE brushes is not uniform within the brushes, it might be very helpful to differentiate the two types of physicochemical properties during data analysis to understand the weak PE brush system more accurately. A simple cartoon is shown in Figure 1.3 to illustrate how dissociation behavior of weak polyacid brushes changes with the pH of the medium.[41]

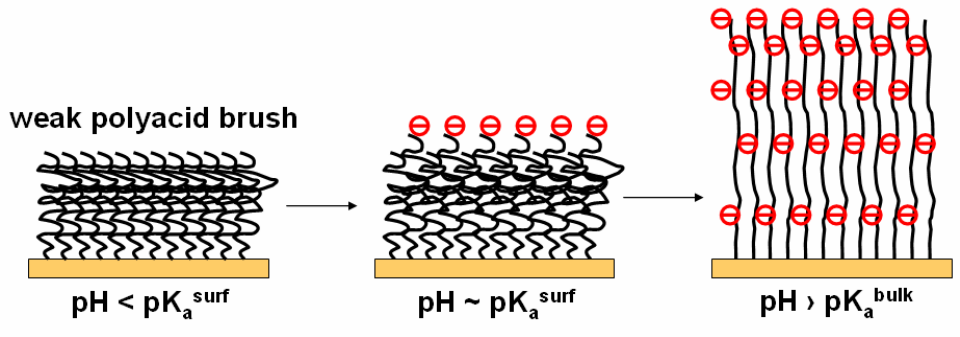

Figure 1.3: A cartoon (not to scale) showing how dissociation behavior of weak polyacid brushes changes in solution at different pH values. (Reprinted from Ref. 37 with permission from the American Chemical Society)

When the pH of the medium is very low, the weak PE brushes are all protonated and the brushes are collapsed. When the pH of the medium reaches the pKa of the top layer of the brushes, the top layer of the brushes dissociate and the brushes become hydrophilic. Upon further increase of the pH, a larger fraction of the brushes becomes charged and the brushes swell because of the electrostatic interaction. Such dissociation behavior of the weak PE brushes is very unique and might be very useful to understand the properties of charged "brush like" structures within biological systems.

1.3.3. Surface Energy. Surface energy is a very important parameter of the surfaces used in many industrial fields, such as packaging, painting for marine anti-fouling and anti-fog, and water proof materials, etc. A good understanding of surface energy of PE brushes is critical for their application. The surface energy of substrates covered with ionizable groups has been shown to depend on the degree of dissociation of the ionizable groups.[42] Ionic strength and pH of the medium could change the degree of ionization of weak PE brushes as discussed in the previous two sections. Thus they

could change the surface energy of weak PE brushes.[37,40] The most common method to characterize surface energy is contact angle measurements. Several research groups have used contact angle measurements to study the wettability of PE brushes.

Luzinova et al.[43] reviewed studies on adaptive and environmentally sensitive polymer surfaces, including the responsive wetting behavior of polymer films and PE mixed brushes. Houbenov et al.[40(c)] and Ionov et al.[40(b)] measured advancing water contact angle of surfaces modified by several types of PE brushes treated at different pH values. They showed that the wetting behavior of surfaces covered with poly(acrylic acid) brushes, poly(2-vinylpyridine) brushes and a mixture of the two brushes were all responsive to pH. Ionov et al.[44] applied the responsive wetting behavior of poly(2-vinylpyridine) brushes in a switchable channel and a pH sensor. Zhou et al.[40(a)] showed that the wettability of surfaces modified with poly[2-(methacryloyloxy)ethyl]phosphate brushes could be reversibly switched between three different states by adjusting pH values of the medium. Dong et al.[37] used contact angle measurements based on a nonreactive spreading protocol[42(b)] to study the dissociation behavior of weak polyacid brushes and achieved nice titration curves with smooth transition between plateau regions at low and high pH, as shown in Figure 1.4. When pH of the medium increased, more acid groups dissociated and the water contact angle dropped, indicating an increase of the surface energy of the brushes.

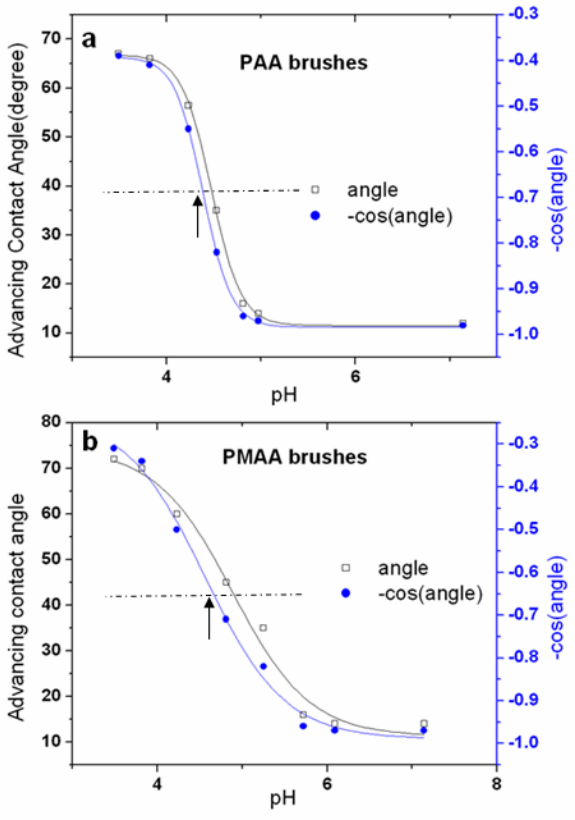

Figure 1.4: Contact angle titration curves for poly(acrylic acid) brushes (graph a) and poly(methacrylic acid) brushes (graph b) on gold substrates. The black rectangles correspond to the contact angle (θ) data points and the blue filled circles correspond to -cos(θ) data points. (Reprinted from Ref. 37 with permission from the American Chemical Society)

Surface energy of PE brushes was also shown to depend on the nature of the counterions.[31(b),45] Azzaroni et al. [31(b),45(a)] showed that counterions, such as ClO_4^- and SCN^-, induced "hydrophobic collapse" of PMETA brushes and turned the brushes into hydrophobic materials. But some types of couterions, like PO_4^{3-} and SO_4^{2-}, made PMETA brushes more hydrophilic.[45(d)] The hydrophobic character of the counterions follows the trend: ClO_4^- > SCN^-> I^->Br^->Cl^-> PO_4^{3-}. Cheng et al.[46] showed that large

thickness can also induce a hydrophobic change to poly[2-(methacryloyloxy)ethyl] dimethyl(3-sulfopropyl)ammonium hydroxide brushes. They showed that the brushes changed from hydrophilic to hydrophobic when the brush thickness increased above a certain value, which depended on the grafting density and conformation of the brushes. They suggested that the unique wetting behavior of zwitterionic polymer brushes was due to interchain association when the segment density within the zwitterionic polymer brushes was sufficiently high.

As a summary for this section, surface energy of PE brushes can be tuned by many parameters, such as pH and ionic strength of the medium, the nature of the counterions, and thickness of the brushes. Since surface energy is a very important property that regulates the interactions between the surfaces and their environment, it is very important to understand and control the wettability of the PE brushes for different application purposes.

1.3.4. Permeability. Permeability of PE brushes or PE brush modified membranes is very important for their use in the areas of chromatography, water purification, biosensing and the like. Because the permeability of PE brushes is related to their swelling, charge and wettability properties, it is responsive to the pH and ionic strength of the medium. Ito et al.[47] have grafted various types of signal-responsive polymers on surfaces of porous polymer membrane or glass substrates. They measured the rate of water permeation through these modified membranes at different conditions and found that the permeation rate decreased with increasing brush thickness. A "polymer brush membrane" model was proposed to explain this phenomenon. When the brushes change from collapsed state to swollen state upon stimuli, the size of the pores between the brushes becomes smaller, leading to a reduced permeation rate. This is in contrast of the "hydrogel membrane" model, where microchannels inside the membrane opened up for permeation upon swelling.

In these two models, the authors only considered the effect of the free volume of the brushes on the permeation rate. Electrostatic interaction between polymer brushes and the solute was not counted. However, the electrostatic interaction is a critical factor in determining the permeability of the PE brushes in many circumstances. Zhou et al.[41(b)] have used electropolymerization to modify gold electrode surfaces with stimuli-responsive polymer brushes. They used cyclic voltammetry and electrochemical impedance spectroscopy to study the redox process of charged $Fe(CN)_6^{3-/4-}$ on modified electrodes under different conditions. Their results showed that the impedance of the electrodes modified with neutral brushes was smaller when the brushes were expanded, meaning that the permeation of ions was larger when the brushes were in the swollen state, which is similar as the "hydrogel model" in Figure 1.5. However, when poly(acrylic acid) brushes were used to modify electrode surfaces, the permeation of negatively charged $Fe(CN)_6^{3-/4-}$ ions was hindered when the brushes were expanded at pH higher than 7. In this case, the electrostatic repulsion between the negatively charged brushes and negatively charged ions was the major factor that caused the reduced permeability. Motornov et al.[41(d)] measured the electrochemical impedance of poly(2-vinylpyridine) brush- or poly(dimethylsiloxane)/poly(2-vinylpyridine) mixed brush-modified electrodes in solution containing $Fe(CN)_6^{3-/4-}$ ions at different pH values. They achieved nice titration curves on both modified brush surfaces by plotting the impedance of the modified electrodes versus pH of the solution. However, the mixed brush modified electrode surface showed broader impedance variation upon pH change. Zhou et al.[41(a)] studied the redox process of $Fe(CN)_6^{3-/4-}$ on PMETA brush modified electrode surfaces. They observed that the effect of the salt concentration on the impedance of the brush modified electrodes strongly depended on the nature of the negatively charged counterions. Collapse of the brushes induced by hydrophilic ions did not have large effect on the impedance of the

brush modified electrodes. However, collapse induced by hydrophobic ions caused large increase in the impedance of the modified electrodes. In this case, wettability of the brushes played important roles in the permeability of the brushes.

Reznik et al.[48] used fluorescence correlation spectroscopy to probe the diffusive transport of fluorescent rhodamine-6G cations within poly(styrene sulfonate) brushes. This technique is very useful in studying local charge transport properties within PE brushes. Yameen et al. [49 (a)] modified macroporous silicon membranes with poly(sulfopropyl methacrylate) brushes and explored their application as proton conducting membranes. Nagase et al.[49(b)] modified silica beads with poly(*N*-isopropylacrylamide-*co*-2-(dimethylamino)ethylmethacrylate) brushes and they showed that biomolecules with different structures could be separated by using the modified silica beads as the stationary phases in chromatography. PE brushes could dramatically change the permselectivity of membranes and selectivity of electrodes, which could be very useful in the field of water purification, chromatography and biosensing.

1.4. Applications of PE Brushes

PE brushes have many interesting properties that are responsive to their environment, as discussed before. As a result, they have great potential for applications in many research and industrial fields, such as protein immobilization, biointerface, lubrication, chromatography, nanoparticle immobilization, biosensors, painting, and water purification. In the following text, we will review recent progress in some of these applications.

1.4.1. Protein Immobilization. Protein immobilization is a critical step in the field of biosensors, protein purification and protein condensation. Proteins can be immobilized onto PE brushes in three ways, physical uptake, specific binding and covalent

conjugation. Polymer brush modified membranes, surfaces and colloidal particles are very good substrates for protein immobilization, because of their better stability in solutions than polymer films and larger protein loading capacity than SAMs.

PE brushes can take up proteins directly through physical adsorption. Saito et al.[50] investigated protein adsorption on porous hollow-fiber membranes grafted with polymer chains containing ionizable groups. Ballauff et al.[51] explored the details of the adsorption of bovine serum albumin (BSA) and other proteins onto colloidal particles covered with PE brushes. They found that the protein adsorption very much depended on ionic strength but not as much on the pH value of the medium. Ballauff et al.,[51] Czeslik et al.,[52] and de Vos et al.[53] all found that proteins could bind to poly(acrylic acid) (PAA) brushes regardless of the sign of the net charge of the proteins. They suggested that the "counterion evaporation" was the driving force for proteins to adsorb to like-charged PE brushes. Upon adsorption, the positive charge patches on the protein surfaces became multivalent counterions of the PE brushes, causing the release of the counterions and entropy gain of the system, which conquered the repulsive electrostatic interaction and the steric hindrance between the proteins and the brushes. By taking up the proteins at low ionic strength and releasing the proteins at high ionic strength, proteins could be recycled for multiple usages. By investigating the secondary structures of the proteins using FTIR, Ballauff et al.[51(b)] and Czeslik et al.[52(d)] showed that the secondary structures of the released proteins were almost fully preserved. They also showed that enzymes embedded inside the PE brushes kept almost their full activity.[51(e)] Poly(2-(dimethylamino)ethyl methacrylate) (PDMAEMA) brushes were also used to uptake proteins.[54] Savina et al.[54(a)] showed that the conformation of the brush chains affected the adsorption of proteins in a large extent. Kusumo et al.[54(b)] did not observe uptake of positively charged lysozyme by PDMAEMA brushes, which is different from what other groups have observed for

PAA brushes. They suggested that this difference might due to the small size and conformational stability of lysozyme molecules which restricted them from interacting with PDMAEMA brushes. The physical uptake method is simple and reversible upon changing ionic strength, which is very useful for recovery of the proteins and brush modified substrates. However, the reversibility also makes the protein immobilization unstable in many conditions.

PE brushes with functional groups, such as nitrilotriacetate (NTA) complexes, can also be used to immobilize proteins containing histidine tags through specific binding. Bruening et al.[55] have modified porous alumina membrane with polymer brushes containing NTA-Cu^{2+} complexes and used these modified membranes to bind proteins via coordination of Cu^{2+} to histidine residues. They showed that the efficiency of protein elution with ethylenediaminetetraacetic acid solutions was essentially 100%. Cullen et al.[56] also used polymer brushes containing NTA-Cu^{2+} complexes to immobilize ribonuclease A. They showed that the binding capacity through metal-ion complexes was almost twice as much as by covalent immobilization. However, the relative activity of the immobilized protein for covalent immobilization was greater than that of metal-ion complexation. This immobilization method through specific binding could provide higher capacity of protein loading than the other two methods. However, the enzyme activity may be disrupted if the histidine units lie in the active site.

Proteins contain many functional groups that could form covalent bonds with appropriate substrates. PE brushes with functional groups, such as carboxylic acid and amine groups, can be used to immobilize protein through covalent conjugation. Cullen et al.[56] and Dong et al.[13(c)] have attached proteins to PAA brushes by forming amide bonds between proteins and the brushes. Covalent conjugation method provides stable

protein immobilization, which is very useful for applications that require long-term stability, such as *in vivo* biosensors.

Because of the good stability of polymer brushes in various chemical environments, polymer brushes could be lithographically patterned and used to create protein arrays.[13(c)] In Figure 1.5, fluorescently labeled BSA was covalently attached to patterned PAA brushes with polyethylene glycol (PEG) monolayer in between. Arrays of proteins or other types of biomolecules can also be achieved using this procedure. These arrays of biomolecules can be used for biosensing, tissue engineering, and cell-based assays to study fundamental cell behavior.

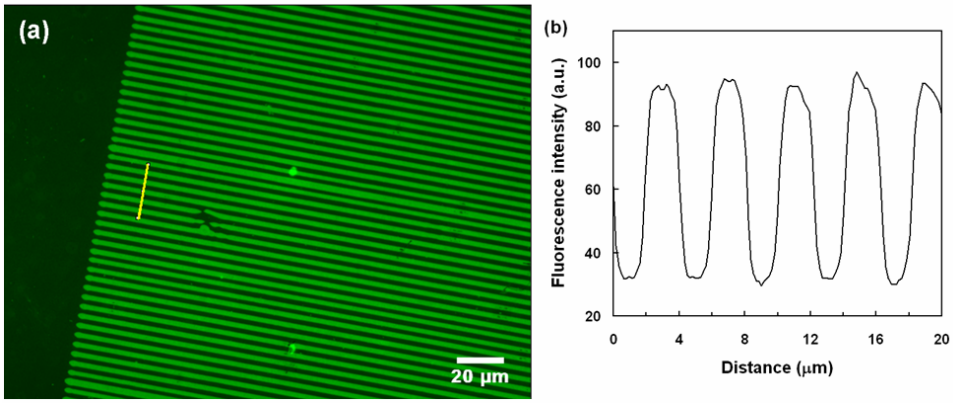

Figure 1.5. (a) Fluorescence image of BSA-FITC immobilized on 2 μm wide PAA brush patterns in a background consisting of PEG monolayer. The darker regions are the PEG covered substrate where there was no covalent binding or nonspecific adsorption of BSA-FITC. (b) Intensity profile along a line section shown in (a). (Adapted from Ref. 13(c) with permission from the American Chemical Society)

1.4.2. Biointerface. The ability to design and control the properties of a biointerface is very important in the fields of biomedical devices, bioimplants, biosensing, tissue engineering and the like. SAMs and polymer brushes provide powerful tools to tailor

surface properties. Senaratne et al.[2] discussed the potential applications of SAMs and polymer brushes in the field of biotechnology in detail. Different applications require different properties for the biointerface, such as antibacterial, anti-biofoulding or biocompatible activities.

Antibacterial activity is highly desirable for biomedical materials, especially implanted materials. Infection from bacteria could be a serious problem for bioimplantation. Positively charged poly(quaternary ammonium) compounds have been widely recognized as good antibacterial materials.[57] When covalently attached to surfaces as polymer brushes, quaternary polymers provide much more robust surface modification and retained good antibacterial activity.[58] The bacterial killing efficiency was shown to increase with the concentration of the quaternary groups on the surfaces[58(a)] and the thickness of brushes[58(d)] as well. Lee et al.[58(b)] showed that the quaternary brush modified glasses could recover most of their antimicrobial activity by washing the surfaces with detergent solution after usage. They also used AFM to investigate the morphology change during the bacteria killing process and they suggested that the quaternary ammonium brushes caused cell death by disrupting the cell membranes and allowing release of the intracellular contents. By comparing the antibacterial activity of quaternary brushes containing alkyl chains with different lengths, Roy et al.[58(e)] showed that brushes with shorter alkyl chains (C_8) had better antibacterial activity than longer chains (C_{12} and C_{16}). It was also suggested that negatively charged PE brushes loaded with silver counterions might potentially work well as antibacterial surfaces.[59]

Anti-biofouling activity is another property that is very useful for surface painting materials. While antibacterial materials kill bacteria that already attach to the surfaces, anti-biofouling materials prevent the settlement of bacteria or other types of cells and work against the formation of biofilms. Compounds containing PEG segments are the

most widely used materials for anti-biofouling purposes.[60] Zwitterionic polymers, such as poly(2-methacryloyloxyethyl phosphorylcholine) (PMPC), were shown to resist adsorption of proteins and cells as well.[61] Ishihara et al.[61(a)] suggested that the anti-biofouling property of PMPC was mainly because phospholipids in plasma were adsorbed immediately on the surface of PMPC and formed a stable adsorbed layer with a biomembrane-like structure, which interacted minimally with proteins and cells. When synthesized on silicon surfaces as polymer brushes using SI-ATRP, PMPC brushes were shown to be resistant to adsorption of proteins and cells.[62] Jiang et al. synthesize a series of zwitterionic brushes and investigated their anti-biofouling properties at different conditions.[63] They compared the protein resistance property of several anti-fouling polymer brushes and found that the brushes containing carboxybetaine methacrylate (CBA) side groups possessed the largest protein resistance activity.[63(c)] They found that protein adsorption on the polymer brushes containing CB groups depended on the spacer between the positively and negatively charged atoms.[64(d)] The protein adsorption increased at smaller salt concentrations and lower pH values, which was more evident for the brushes with a longer spacer group.

Many positively charged polymers were used to coat surfaces for neuron culture studies.[64] Positively charged polymer brush modified surfaces could potentially work well as neuron culture substrates as well.[65] Antibacterial quaternary polymer brush modified surfaces were shown to work well as substrates for rat hippocampal neurons and the patterned brushes could guide neurons to grow well.[66] Because of the robustness of polymer brushes in a chemical environment, multiple components can be introduced to the patterned polymer brush surfaces and complex devices could be built up to study novel neuron behaviors. As a summary, PE brushes provide powerful tools to tailor surface properties towards different biomedical applications and open new avenues for novel studies.

1.4.3. Lubrication. Articular joints in the human body are known to exhibit very low friction and wear. The cartilage coating these joints has polymeric molecules protruding from them, such as hyaluronan and lubricin, which are charged polymers.[67] Raviv et al. showed that polyelectrolytes coated to surfaces rubbing across an aqueous medium resulted in superior lubrication and they suggested that chemically bound polyelectrolyte brushes may serve as realistic models for biolubrication.[68] They attributed the superior lubrication to the resistance to the mutual interpenetration between the PE brush layers arising from steric effects and counterion osmotic pressures, as well as the fluidity of the hydration layers surrounding the PE brushes. Kobayashi[69] synthesized dense PMPC brushes on silicon surfaces and characterized the frictional properties of PMPC brushes by sliding a glass ball probe on the brush modified surfaces in air and various solvents. They observed an extremely low friction coefficient both in humid air and in aqueous medium. Ohsedo et al.[70] grafted poly(sodium 4-styrenesulfonate) brushes with different thicknesses onto hydrogels and measured the sliding friction between the modified hydrogel and a glass substrate in water media. They found that the presence of polymer brush could dramatically reduce the friction especially when the polymer brushes were short. However, the friction properties of weak poly(acrylic acid) brushes were shown to be similar to neutral polymer brushes.[71]

The superior lubrication properties of strong PE brushes or zwitterionic brushes can be extremely useful in the field of artificial implants as biolubrication interfaces. PMPC brushes were used in the polymeric surfaces for artificial implanting and greatly reduced the friction and amount of wear in the implanted artificial joints.[72] These lubrication properties of PE brushes can also be very useful in industry and other fields to reduce mechanic wear in machines and increase energy efficiency.

1.4.4. Metal Nanoparticle Immobilization. Nanoparticles potentially have unique properties due to the quantum confinement effects and their large surface area relative to their volume.[73] Metal nanoparticles can be very useful in the field of optoelectronics, sensors, catalysis, and medicine. To prevent aggregation of nanoparticles during their synthesis, a polyelectrolyte matrix was used as carrier systems to synthesize metal nanoparticles before.[74] PE brushes were also used to immobilize opposite-charged metal complexes. By reducing the metal ions attached inside the PE brushes, metal nanoparticles could be easily prepared.[75] Because of the robustness and versatility of polymer brushes, the nanoparticles can be synthesized on colloidal particle surfaces or patterned brush surfaces and might provide more opportunities for application of nanoparticles.

Yu et al.[76] have synthesized platinum nanoparticles inside cationic polymer brushes on spherical particle surfaces and they compared the activity of the platinum nanoparticles synthesized inside the brushes and microgels as catalysts for chemical reactions. They showed that the activity of platinum nanoparticles was much higher when they were synthesized inside the brushes.[76(b)] Li et al.[77] synthesized palladium nanoparticles inside water-dispersible polymer brush-grafted polymeric particles and used them to catalyze the hydrogenation of styrene in an aqueous/organic biphasic system. Azzaroni et al.[78] attached metal ions, which worked as catalyst for metallization, to patterned quaternary PE brushes and used these patterned surfaces to guide metallization and formed patterned metal thin films. The rate of metallization and thickness of the metal film could be controlled by controlling the amount of the adsorbed catalysts.

Metal or semiconductor nanoparticles immobilized in responsive polymer brushes were used to sense the chemical environment of the medium.[79] The swelling and collapse of responsive polymer brushes caused a change of distance between the

immobilized nanoparticles and surfaces, which altered the surface plasma resonance spectra or fluorescence intensity. By detecting these signals, information about pH or polarity of the solvents could be extracted.

1.4.5. Sensors. SAMs and thin polymer films have been widely used in the field of sensors for a long time.[80] As discussed before, polymer brush contains higher density of functional groups than SAMs and can be used to immobilize multiple layers of proteins. Compared to physically cast thin polymer films, covalently tethered polymer brushes provide a much more stable surface modification both chemically and mechanically. Polymer brushes combined the good features of SAMs and thin polymer films. In addition, PE brushes are responsive to the environment and they can tailor the surface properties in a variety of ways. As a result, PE brushes could potentially play very important roles in the area of sensors.

In the previous section, several examples of applications of PE brushes in the area of sensors were mentioned.[79] Kurosawa et al.[81] synthesized PAA brushes on quartz crystal microbalance surfaces and used them for immunosensors. They showed that the response was 10 times larger by using polymer brushes to immobilize the antibody than by using the traditional method based on SAMs. As mentioned before, patterned positively charged polymer brushes were used to guide neuron growth.[66] By integrating these patterned brushes and micro-scale biosensors on the same device, one could study some novel cellular behaviors *in vivo* and *in situ*.

Charged SAMs and polymer films were widely used to change the selectivity of electrodes in electrochemical sensors.[82] PE brushes were shown to change the permeability of charged electroactive compounds dramatically,[41] which can also be very useful in tailoring the selectivity of biosensors. Because of their high stability under various conditions, PE brush modified biosensors could have a longer lifetime than polymer film coated biosensors. In addition, we have found that PAA brushes

could screen negatively charged interferences better than Nafion™ thin films,[83] which makes PE brushes even more attractive for applications in the area of sensors.

1.5. Conclusions.

PE brushes attracted a great deal of attention in recent years, both theoretically and experimentally. PE brushes have many interesting physicochemical properties that are responsive to their environment, which lead to many useful applications in various areas. This review summarized recent progress in synthesis, characterization and applications of PE brushes. SI-ATRP in protic solvents is an easy and straightforward method to synthesize many types of PE brushes directly in a controllable fashion. Because of the side reactions of ATRP in protic solvents, the polymerization kinetics is affected by many factors, including catalyst, solvent, monomer concentration, and initiator. How these factors affect the growth of PE brushes was discussed. The applications of PE brushes are closely related to their physicochemical properties, such as swelling behavior, dissociation degree, surface energy and permeability. Various characterization methods used to study these properties of PE brushes were discussed. Finally, the recent literature on applications of PE brushes in a variety of research fields was summarized. We believe that PE brushes provide very powerful and interesting tools to tailor surface properties. They will have great potential for applications in the field of protein immobilization, biointerface studies, lubrication, chromatography, nanoparticle immobilization, biosensors, coatings, and water purification.

Acknowledgements

The authors wish to thank Prof. Barbara Baird, Prof. Manfred Lindau, and Prof. Hector Abruña for their contributions to our understanding of the topics covered in

this review. Authors also acknowledge the support of NSF-funded Cornell Nanobiotechnology Center (NBTC) and Cornell Nanoscale Interdisciplinary Research Team (NIRT).

REFERENCES

[1] (a) Pincus, P. *Macromolecules* **1991,** 24, 2912; Ross, R. S.; Pincus, P. *Macromolecules* **1992,** 25, 2177. (b) Israëls, R; Leermakers, F. A. M.; Fleer, G. J.; Zhulina, E. B. *Macromolecules* **1994**, 27, 3249. (c) Zhulina, E. B.; Birshtein, T. M.; Borisov, O. V. *Macromolecules* **1995**, 28, 1491.

[2] Senaratne, W.; Luisa Andruzzi, L.; Ober, C. K. *Biomacromolecules* **2005,** 6, 2427-2448.

[3] Prucker, O.; Rühe, J. *Macromolecules* **1998,** 31, 592.

[4] (a) Halperin, A.; Tirrell, M.; Lodge, T. P. *Adv. Polym. Sci.* **1992,** 100, 31. (b) Mir, Y.; Auroy, P.; Auvray, L. *Phys. Rev. Lett.* **1995,** 75, 2863. (c) Tran, Y.; Auroy, P.; Lee, L. T.; Stamm, M. *Phys. Rev. E.* **1999,** 60, 6984. (d) Dubreuil, F.; Guenouna, P. *Eur. Phys. J. E* **2001, 5**, 59-64.

[5] Biesalski, M.; Rühe, J. *Macromolecules* **1999,** 32, 2309-2316.

[6] (a) Matyjaszewski, K.; Miller, P. J.; Shukla, N.; Immaraporn, B.; Gelman, A.; Luokala, B. B.; Siclovan, T. M.; Kickelbick, G.; Vallant, T.; Hoffmann, H.; Pakula, T. *Macromolecules* **1999,** 32, 8716-8724. (b) Treat, N. D.; Ayres, N.; Boyes, S. G.; Brittain, W. J. *Macromolecules* **2006,** *39,* 26-29. (c) Tran, Y.; Auroy, P. *J. Am. Chem. Soc.* **2001,** 123, 3644-3654.

[7] Coca, S.; Jasieczek, C. B.; Beers, K. L.; Matyjaszewski, K. *J. Polym. Sci. Part A: Polym. Chem.* **1998,** 36, 1417-1424.

[8] Ashford, E. J.; Naldi, V.; O'Dell, R.; Billingham, N. C.; Armes, S. P. *Chem. Commun.* **1999,** 14, 1285-1286.

[9] Wang, X.-S.; Lascelles, S. F.; Jackson, R. A.; Armes, S. P. *Chem. Commun.* **1999,** 1817–1818.

[10] Wang, X.-S.; Jackson, R. A.; Armes, S. P. *Macromolecules* **2000,** 33, 255-257.

[11] Perruchot, C.; Khan, M. A.; Kamitsi, A.; Armes, S. P. *Langmuir* **2001,** 17, 4479.

[12] Osborne, V. L.; Jones, D. M.; Huck, W. T. S. *Chem. Commun.* **2002,** 17, 1838-1839.

[13] (a) Chen, X. Y.; Randall, D. P.; Perruchot, C.; Watts, J. F.; Patten, T. E.; von Werne, T.; Armes, S. P. *J. Colloid Interface Sci.*, **2003,** 257, 56–64. (b) Chen, M.; Briscoe, W. H.; Armes, S. P.; Cohen, H.; Klein, J.; *ChemPhysChem* **2007,** 8, 1303 – 1306. (c) Dong, R; Krishnan, S.; Baird, B. A.; Lindau, M.; Ober, C. K. *Biomacromolecules* **2007,** 8, 3082-3092. (d) Ramstedt, M.; Cheng, N.; Azzaroni, O.; Mossialos, D.; Mathieu, H. J.; Huck, W. T. S. *Langmuir* **2007,** 23, 3314-3321. (e) Azzaroni, O.; Brown, A. A.; Huck, W. T. S. *Angew. Chem. Int. Ed.* **2006,** 45, 1770.

[14] Jones, D. M.; Huck, W. T. S. *Adv. Mater.* **2001,** 13, 1256-1259.

[15] (a) Pyun, J.; Kowalewski, T.; Matyjaszewski, K. *Macromol. Rapid Commun.* **2003,** 24, 1043-1059. (b) Tsarevsky, N. V.; Matyjaszewski, K. *Chem. Rev.* **2007,** 107, 2270.

[16] Cheng, N.; Azzaroni, O.; Moya, S.; Huck, W. T. S. *Macromol. Rapid Commun.* **2006,** 27, 1632–1636.

[17] (a) Li, Y.; Armes, S. P.; Jin, X.; Zhu, S. *Macromolecules* **2003,** 36, 8268-8275. (b) Sankhe, A. Y.; Husson, S. M.; Kilbey II, S. M. *J. Polym. Sci. Part A: Polym. Chem.* **2007,** 45, 566–575. (c) Tsarevsky, N. V.; Pintauer, T.; Matyjaszewski, K. *Macromolecules* **2004,** 37, 9768-9778. (d) Kim, J.; Huang, W.; Miller, M. D.; Baker, G. L.; Bruening, M. L. *J. Polym. Sci. Part A: Polym. Chem.* **2003,** 41, 386–394.

[18] (a) Kizhakkedathu, J. N.; Takacs-Cox, A.; Brooks, D. E. *Macromolecules* **2002,** 35, 4247. (b) Kizhakkedathu, J. N.; Brooks, D. E. *Macromolecules* **2003,** 36, 591-598. (c) Kizhakkedathu, J. N.; Norris-Jones, R.; Brooks, D. E. *Macromolecules*, **2004**, 37, 734.

[19] Zeng, F.; Shen, Y.; Zhu, S.; Pelton, R. *J. Polym. Sci. Part A: Polym. Chem.* **2000,** 38, 3821.

[20] (a) Jones, D. M.; Brown, A. A.; Huck, W. T. S. *Langmuir* **2002,** 18, 1265-1269. (b) Bao, Z.; Bruening, M. L.; Baker, G. L. *Macromolecules*, **2006**, 39, 5251-5258. (c) Liu, Y.; Klep, V.; Zdyrko, B.; Luzinov, I. *Langmuir* **2004,** 20, 6710-6718.

[21] (a) Tugulu, S.; Barbey, R.; Harms, M.; Fricke, M.; Volkmer, D.; Rossi, A.; Klok, H.- A. *Macromolecules* **2007,** 40, 168-177. (b) Jain, P.; Dai, J.; Baker, G. L.; Bruening, M. L. *Macromolecules*, **2008**, 41, 8413-8417.

[22] Coullerez, G.; Carlmark, A.; Malmstro1m, E.; Jonsson, M. *J. Phys. Chem. A,* **2004,** 108, 7129.

[23] Pintauer, T.; Reinohl, U.; Feth, M.; Bertagnolli, H.; Matyjaszewski, K. *Eur. J. Inorg. Chem.* **2003**, 2082.

[24] Dong, R; Krishnan, S.; Baird, B. A.; Lindau, M.; Ober, C. K. *Biomacromolecules* **2007,** 8, 3082-3092.

[25] Dong, R; Chiang, E.; Holowka, D.; Baird, B. A.; Ober, C. K. *Investigating RBL Cell Behavior on Patterned Polymer Brush Surfaces, in preparation.*

[26] Matyjaszewski, K.; Xia, J. *Chem. Rev.* **2001,** 101, 2921-2990.

[27] Akgun, B.; Boyes, S.G.; Granville, A.M.; Brittain, W.J. *Am. Chem. Soc., Div. Polym. Chem.* **2003**, 44(1), 514-515.

[28] (a) Rühe, J; Matthias Ballauff, M.; Markus Biesalski, M.; Peter Dziezok, P.; Gröhn, F.; Johannsmann, D.; Houbenov, N.; Hugenberg, N.; Konradi, R.; Minko, S.; Motornov, M.; Netz, R. R.; Schmidt. M.; Seidel, C.; Stamm, M.; Stephan, T.; Usov, D.; Zhang, H. *Adv. Polym. Sci.* **2004,** 165, 79–150. (b) Ballauff, M. *Prog. Polym. Sci.* **2007,** 32, 1135–1151. (c) Naji, A.; Seidel, C.; Netz, R. R. *Adv. Polym. Sci.* **2006,** 198, 149–183. (d) Minko, S. *J. Macromolecular Sci., Part C: Polym. Rev.* **2006,** 46, 397.

[29] (a) Seidel, C. *Macromolecules*, **2003**, 36, 2536-2543. (b) Romet-Lemonne, G.; Daillant, J.; Guenoun, P.; Yang, J.; Mays, J.W. *Phys. Rev. Lett.* **2004,** 93, 148301. (c)

Biesheuvel, P. M. *J. Colloid Interface Sci.* **2004,** 275, 97–106. (d) Hehmeyer, O. J.; Arya, G.; Panagiotopoulos, A. Z.; Szleifer, I. *J. Chem. Phys.* **2007,** 126, 244902. (e) Sandberg, D. J.; Carrillo, J. Y.; Dobrynin, A. V. *Langmuir* **2007,** 23, 12716-12728. (f) Jiang, T.; Wu, J. *J. Chem. Phys.* **2008,** 129, 084903. (g) Jiang, T.; Wu, J. *J. Phys. Chem. B*, **2008**, 112, 7713-7720. (h) Israëls, R; Leermakers, F. A. M.; Fleer, G. J. *Macromolecules* **1994**, 27, 3087-3093. (i) Kumar, N. A.; Seidel, C. *Macromolecules* **2005,** 38, 9341-9350.

[30] (a) Guo, X.; Ballauff, M. *Langmuir* **2000**, *16*, 8719. (b) Guo, X.; Ballauff, M. *Phys. Rev. E*, **2001,** 64, 051406. (c) Mei, Y.; Lauterbach, K.; Hoffmann, M.; Borisov, O. V.; Ballauff, M.; Arben Jusufi, A. *Phys. Rev. Lett.* **2006,** 97, 158301. (d) Xu, Y.; Bolisetty, S.; Drechsler, M.; Fang, B.; Yuan, J.; Ballauff , M.; Müller, A. H. E. *Polymer* **2008,** 49, 3957–3964.

[31] (a) Farhan, T.; Azzaroni, O.; Huck, W. T. S. *Soft Matter* **2005,** 1, 66–68. (b) Azzaroni, O.; Moya, S.; Farhan, T.; Brown, A. A.; Huck, W. T. S. *Macromolecules* **2005,** 38, 10192-10199. (c) Moya, S. E.; Azzaroni, O.; Kelby, T.; Donath, E.; Huck, W. T. S. *J. Phys. Chem. B*, **2007**, 111, 7034-7040. (d) Kaholek, M.; Lee, W.; Feng, J.; LaMattina, B.; Dyer, D. J.; Zauscher, S. *Chem. Mater.* **2006,** 18, 3660-3664. (e) Ye, M.; Zhang, D.; Han, L.; Tejada, J.; Ortiz, C. *Soft Matter,* **2006,** 2, 243–256. (e) Balastre, M.; Li, F.; Schorr, P.; Yang, J.; Mays, J. W.; Tirrell, M. V. *Macromolecules* **2002,** 35, 9480-9486.

[32] (a) Biesalski, M.; Rühe, J. *Macromolecules* **2002,** 35, 499. (b) Biesalski, M.;Johannsmann, D.; Rühe, J. *J. Chem. Phys.* **2002,** 117, 4988. (c) Biesalski, M.; Johannsmann, D.; Rühe, J. *J. Chem. Phys.* **2004,** 120, 8807. (d) Rupert Konradi, R.; Rühe, J. *Macromolecules* **2005,** 38, 4345-4354. (e) Zhang, H.; Rühe, J. *Macromolecules* **2005,** 38, 4855-4860. (f) Ayres, N.; Boyes, S. G.; Brittain, W. J.

Langmuir **2007,** 23, 182-189. (g) Ayres, N.; Cyrus, C. D.; Brittain, W. J. *Langmuir* **2007,** 23, 3744-3749.

[33] (a) Sanjuan, S.; Perrin, P.; Pantoustier, N.; Tran, Y. *Langmuir* **2007,** 23, 5769-5778. (b) Geoghegan, M.; Ruiz-Pérez, L.; Dang, C. C.; Parnell, A. J.; Martin, S. J.; Howse, J. R.; Jones, R. A. L.; Golestanian, R.; Topham, P. D.; Crook, C. J.; Ryan, A. J.; Sivia, D. S.; Websterc, J. R. P.; Menelled, A. *Soft Matter* **2006,** 2, 1076–1080.

[34] Tran, Y.; Auroy, P.; Lee, L-T. *Macromolecules*, **1999**, 32, 8952-8964.

[35] (a) Nap, R.; Gong, P.; Szleifer, I. *J. Polym. Sci., Part B: Polym. Physics.* **2006**, 44, 2638. (b) Gong, P.; Genzer, J.; Szleifer, I. *Phys. Rev. Lett.* **2007,** 98, 018302. (c) Gong, P.; Wu, T.; Genzer, J.; Szleifer, I. *Macromolecules* **2007,** *40,* 8765-8773.

[36] Smalley, J. F.; Chalfant, K.; Feldberg, S.W.; Nahir, T.M.; Bowden, E.F. *J. Phys. Chem. B* **1999,** *103,* 1676-1685.

[37] Dong, R.; Lindau, M.; Ober, C. K. *Langmuir* **2009,** 25, 4774-4779.

[38] (a) Chen, X.; Randall, D. P.; Perruchot, C.; Watts, J. F.; Patten, T. E.; von Werne, T.; Armes, S. P. *J. Colloid Interface Sci.* **2003,** 257, 56–64. (b) Houbenov, N.; Sergiy Minko, S.; Stamm, M. *Macromolecules* **2003,** 36, 5897-5901. (c) Zimmermann, R.; Norde, W.; Stuart, M. A. C.; Werner, C. *Langmuir* **2005,** 21, 5108-5114. (d) Zhang, J.; Chen, K.; Zhao, H. *J. Polym. Sci., Part A: Polym. Chem.* **2008,** 46, 2632–2639.

[39](a) Hayashi, S.; Takashi Abe, T.; Nobuyuki Higashi, N.; Masazo Niwa, M.; Kurihara, K. *Langmuir* **2002,** 18, 3932-3944. (b) Dominguez-Espinosa, G.; Synytska, A.; Drechsler, A.; Gutsche, C.; Kegler, K.; Uhlmann, P.; Stamm, M.; Kremer, F. *Polymer* **2008,** 49, 4802–4807.

[40] (a) Zhou, F.; Huck, W. T. S. *Chem. Commun.* **2005,** 5999–6001. (b) Ionov, L.; Houbenov, N.; Sidorenko, A.; Stamm, M.; Luzinov, I.; Minko, S. *Langmuir*, **2004**, 20, 9916. (c) Houbenov,N.; Minko,S.; Stamm**,** M. *Macromolecules* **2003,** 36, 5897-5901.

(d) Motornov, M.; Minko, S.; Eichhorn, K.; Nitschke M.; Simon, F.; Stamm, M. *Langmuir* **2003,** 19, 8077-8085. (e) Zhou, F.; Huck, W. T. S. *Phys. Chem. Chem. Phys.* **2006,** 8, 3815–3823.

[41] (a) Zhou, F.; Hu, H.; Yu, B.; Osborne, V. L.; Huck, W. T. S.; Liu, W. *Anal. Chem.* **2007,** 79, 176. (b) Zhou, J.; Wang, G.; Hu, J.; Lu, X.; Li, J. *Chem. Commun.* **2006,** 4820–4822. (c) Zhou, J.; Lu, X.; Hu, J.; Li, J. *Chem. Eur. J.* **2007,** 13, 2847–2853. (d) Motornov, M.; Sheparovych, R.; Katz, E.; Minko, S. *ACS Nano*, **2008**, 2, 41-52. (e) Schepelina, O.; Zharov, I. *Langmuir* **2008,** 24, 14188-14194. (f)

[42] (a) Holmes-Farley, S.R.; Reamey, R.H.; McCarthy, T.J.; Deutch, J.; Whitesides, G.M. *Langmuir* **1985**, 1, 725-740. (b) Creager, S.E.; Clarke, J. *Langmuir* **1994**, 10, 3675-3683. (c) Liu, Y.; Navasero, N.M.; Yu, H. *Langmuir* **2004**, 20, 4039-4050. (d) Badre, C.; Mayaffre, A.; Letellier, P.; Turmine, M. *Langmuir* **2006**, 22, 8424-8430.

[43] Luzinova, I.; Minko, S.; Tsukruk, V. V. *Prog. Polym. Sci.* **2004,** 29, 635–698.

[44] Ionov, L.; Minko, S.; Stamm, M.; Gohy, J.; Jérôme, R.; Scholl, A. *J Am Chem Soc* **2003,** 125, 8302.

[45] (a) Azzaroni, O.; Brown, A. A.; Huck, W. T. S. *Adv. Mater.* **2007**, 19, 151–154. (b) Döbbelin, M.; Arias, G.; Loinaz, I.; Llarena, I.; Mecerreyes, D.; Moya, S. *Macromol. Rapid Commun.* **2008,** 29, 871–875. (c) Spruijt, E.; Choi, E.; Huck, W. T. S. *Langmuir* **2008,** 24, 11253-11260. (d) Moya, S.; Azzaroni, O.; Farhan, T.; Osborne, V. L.; Huck, W. T. S. *Angew. Chem. Int. Ed.* **2005,** 44, 4578 –4581.

[46] Cheng, N.; Brown, A. A.; Azzaroni, O.; Huck, W. T. S. *Macromolecules* **2008,** 41, 6317-6321.

[47] (a) Park, Y. S.; Ito, Y.; Imanishi, Y. *Chem. Mater.* **1997,** 9, 2755-2758. (b) Ito, Y.; Ochiai, Y.; Park, Y. S.; Imanishi, Y. *J. Am. Chem. Soc.* **1997**, 119, 1619. (c) Ito, Y.;

Nishi, S.; Park, Y. S.; Imanishi, Y. *Macromolecules* **1997**, 30, 5856. (d) Ito, Y.; Park, Y. S.; *Polym. Adv. Technol.* **2000,** 11, 136-144.

[48] Reznik, C.; Darugar, Q.; Wheat, A.; Fulghum, T.; Advincula, R. C.; Landes, C. F. *J. Phys. Chem. B*, **2008**, 112, 10890-10897.

[49] (a) Yameen, B.; Kaltbeitzel, A.; Langner, A.; Duran, H.; Müller, F.; Gösele, U.; Azzaroni, O.; Knoll, W. *J. Am. Chem. Soc.* **2008**, 130, 13140–13144. (b) Nagase, K.; Kobayashi, J.; Kikuchi, A.; Akiyama, Y.; Kanazawa, H.; Okano, T. *Biomacromolecules* **2008,** 9, 1340–1347.

[50] (a) Kawai, T.; Sugita, K.; Saito, K.; Sugo, T. *Macromolecules* **2000,** 33, 1306-1309. (b) Koguma, I.; Sugita, K.; Saito, K.; Sugo, T. *Biotechnol. Prog.* **2000,** 16, 456-461. (c) Kawai, T.; Nakamura, M.; Sugita, K.; Saito, K.; Sugo, T. *Biotechnol. Prog.* **2001,** 17, 872-875. (d) Okamura, D.; Saito, K.; Sugita, K.; Tamada, M.; Takanobu Sugo, *J. Chromatogr*. *A* **2002,** 953, 101–109. (e) Iwanade, A.; Umeno, D.; Saito, K.; Sugo, T. *Biotechnol. Prog.* **2007,** 23, 1425-1430.

[51] (a) Wittemann, A.; Haupt, B.; Ballauff, M. *Phys. Chem. Chem. Phys.* **2003,** 5, 1671–1677. (b) Wittemann, A.; Ballauff, M. *Anal. Chem.*, **2004**, 76, 2813-2819. (c) Czeslik, C.; Jansen, R.; Ballauff, M.; Wittemann, A.; Royer, C. A.; Gratton, E.; Hazlett, T. *Phys. Rev. E* **2004,** 69, 021401. (d) Rosenfeldt, S.; Wittemann, A.; Ballauff, M.; Breininger, E.; Bolze, J.; Dingenouts, N. *Phys. Rev. E* **2004,** 69, 061403. (e) Haupt, B.; Neumann, T.; Wittemann, A.; Ballauff, M. *Biomacromolecules* **2005,** 6, 948-955. (f) Henzler, K.; Haupt, B.; Ballauff, M. *Anal. Biochem.* **2008,** 378, 184–189.

[52] (a) Czeslik, C.; Jackler, G.; Steitz, R.; von Grnberg, H. *J. Phys. Chem. B*, **2004**, 108, 13395-13402. (b) Hollmann, O.; Gutberlet, T.; Czeslik, C. *Langmuir*, **2007**, 23, 1347-1353. (c) Hollmann, O.; Steitzb, R.; Czeslik, C. *Phys. Chem. Chem. Phys.* **2008,** 10, 1448–1456. (d) Reichhart, C.; Czeslik, C. *Langmuir* **2009,** *25,* 1047-1053.

[53] de Vos, W. M.; Biesheuvel, P. M.; de Keizer, A.; Kleijn, J. M.; Stuart, M. A. C. *Langmuir* **2008,** 24, 6575-6584.

[54] (a) Savina, I. N.; Galaev, I. Y.; Mattiasson, B. *J. Chromatogr. A* **2005,** 1092, 199–205. (b) Kusumo, A.; Bombalski, L.; Lin, Q.; Matyjaszewski, K.; Schneider, J. W.; Tilton, R. D. *Langmuir* **2007,** 23, 4448-4454.

[55] (a) Sun, L.; Dai, J.; Baker, G. L.; Bruening, M. L. *Chem. Mater.* **2006,** 18, 4033-4039. (b) Jain, P.; Dai, J.; Baker, G. L.; Bruening, M. L. *Macromolecules* **2008,** 41, 8413-8417. (c) Bruening, M. L.; Dotzauer, D. M.; Jain, P.; Ouyang, L.; Baker, G. L. *Langmuir* **2008,** 24, 7663-7673.

[56] Cullen, S. P.; Liu, X.; Mandel, I. C.; Himpsel, F. J.; Gopalan, P. *Langmuir* **2008,** 24, 913-920.

[57] (a) Ikeda, T.; Hirayama, H.; Yamaguchi, H.; Tazuke, S.; Watanabe, M. *Antimicrob. Agents Chemother.* **1986**, *30*, 132-136. (b) Tiller, J. C.; Liao, C.; Lewis, K.; Klibanov, A. M. *PNAS* **2001**, 98, 5981. (c) Krishnan, S.; Ward, R. J.; Hexemer, A.; Sohn, K. E.; Lee, K. L.; Angert, E. R.; Fischer, D. A.; Kramer, E. J.; Ober, C. K. *Langmuir* **2006,** 22, 11255-11266.

[58] (a) Cen, L.; Neoh, K. G.; Kang, E. T. *Langmuir* **2003**, 19, 10295. (b) Lee, S. B.; Koepsel, R. R.; Morley, S. W.; Matyjaszewski, K.; Sun, Y.; Russell, A. J. *Biomacromolecules* **2004**, 5, 877. (c) Cheng, Z.; Zhu, X.; Shi, Z. L.; Neoh, K. G.; Kang, E. T. *Ind. Eng. Chem. Res.* **2005,** 44, 7098-7104. (d) Huang, J.; Murata, H.; Koepsel, R. R.; Russell, A. J.; Matyjaszewski, K. *Biomacromolecules* **2007,** 8, 1396-1399. (e) Roy, D.; Knapp, J. S.; Guthrie, J. T.; Perrier, S. *Biomacromolecules* **2008,** 9, 91–99.

[59] Ramstedt, M.; Cheng, N.; Azzaroni, O.; Mossialos, D.; Mathieu, H. J.; Huck, W. T. S. *Langmuir* **2007,** 23, 3314-3321.

[60] Andruzzi, L.; Senaratne, W.; Hexemer, A.; Sheets, E. D.; Ilic, B.; Kramer, E. J.; Baird, B.; Ober, C. K. *Langmuir*, **2005**, 21, 2495-2504.

[61] (a) Ishihara, K.; Oshida, H.; Endo, Y.; Ueda, T.; Watanabe, A.; Nakabayashi, N. *J. Biomed. Mater. Res.* **1992**, 26, 1543-1552. (b) Ishihara, K.; Nomura, H.; Mihara, T.; Kurita, K.; Iwasaki, Y.; Nakabayashi, N. *J. Biomed. Mater. Res.* **1998**, 39, 323-330. (c) Kitano, H.; Kawasaki, A.; Kawasaki, H.; Morokoshi, S. *J. Colloid Interface Sci.* **2005,** 282, 340–348. (d) Chapman, R. G.; Ostuni, E.; Takayama, S.; Holmlin, R. E.; Yan, L.; Whitesides, G. M. *J. Am. Chem. Soc.* **2000**, 122, 8303–8304.

[62] (a) Iwata, R.; Suk-In, P.; Hoven, V. P.; Takahara, A.; Akiyoshi, K.; Iwasaki, Y. *Biomacromolecules* **2004,** 5, 2308-2314. (b) Feng, W.; Brash, J.; Zhu, S. *J. Polym. Sci., Part A: Polym. Chem.* **2004**, 42, 2931–42.

[63] (a) Zhang, Z.; Chao, T.; Chen, S.; Jiang, S. *Langmuir*, **2006**, 22, 10072-10077. (b) Zhang, Z.; Chen, S.; Chang, Y.; Jiang, S. *J. Phys. Chem. B* **2006**, 110, 10799–10804. (c) Ladd, J.; Zhang, Z.; Chen, S.; Hower, J. C.; Jiang, S. *Biomacromolecules*, **2008**, 9, 1357-1361. (d) Zhang, Z.; Vaisocherová, H.; Cheng, G.; Yang, W.; Xue, H.; Jiang, S. *Biomacromolecules* **2008,** 9, 2686–2692. (e) Li, G.; Xue, H.; Cheng, G.; Chen, S.; Zhang, F.; Jiang, S. *J. Phys. Chem. B* **2008,** 112, 15269–15274.

[64] (a) Soekarno, A.; Lom, B.; Hockberger, P. E. *Neuroimage* **1993,** 1, 129-144. (b) Bledi, Y.; Domb, A. J.; Linial, M. *Brain Research Protocols* **2000**, 5, 282-289. (c) Wang, J-H.; Hung, C-H.; Young, T-H. *Biomaterials* **2006,** 27, 3441-3450.

[65] Ruhe, J.; Yano, R.; Lee, J.-S.; Koberle, P.; Knoll, W.; Offenhausser, A. *J. Biomater. Sci. Polym. Ed.* **1999**, 10, 859-874.

[66] Dong, R.; Molloy, R. P.; Linda, M.; Ober, C. K. *Direct synthesis of quaternized polymer brushes and their application for guiding neuronal growth, in preparation.*

[67] (a) Jin, M. S.; Grodzinsky, A. J. *Macromolecules* **2001**, 34, 8330–8339. (b) Zappone, B.; Ruths, M.; Greene, G. W.; Jay, G. D.; Israelachvili, J. N. *Biophys. J.* **2007,** 92, 1693.

[68] (a) Raviv, U.; Klein, J. *Science* **2002**, 297, 1540–1543. (b) Raviv, U.; Giasson, S.; Kampf, N.; Gohy, J. F.; Jérôme, R.; Klein, J. *Nature* **2003,** 425, 163-165. (c) Kampf, N.; Raviv, U.; Klein, J. *Macromolecules* **2004,** 37, 1134-1142. (d) Raviv, U.; Giasson, S.; Kampf, N.; Gohy, J. F.; Jérôme, R.; Klein, J. *Langmuir,* **2008**, 24, 8678-8687.

[69] Kobayashi, M.; Terayama, Y.; Hosaka, N.; Kaido, M.; Suzuki, A.;Yamada, N.; Torikai, N.; Ishiharae, K.; Takahara, A. *Soft Matter,* **2007,** 3, 740–746.

[70] Ohsedo, Y.; Takashina, R.; Gong, J. P.; Osada, Y. *Langmuir* **2004,** 20, 6549-6555.

[71] Liberelle, B.; Giasson, S. *Langmuir* **2008,** 24, 1550-1559.

[72] (a) Moro, T.; Takatori, Y.; Ishihara, K.; Konno, T.; Takigawa, Y.; Matsushita, T.; Chung, U.; Nakamura, K.; Kawaguchi, H. *Nat. Matter* **2004**, 3, 829–836. (b) Kyomoto, M.; Moro, T.; Miyaji, F.; Hashimoto, M.; Kawaguchi, H.; Takatori, Y.; Nakamura, K.; Ishihara, K. *J. Biomed. Mater. Res. Part A,* **2007,** 86A, 2, 439-447.

[73] Wang, T. C.; Rubner, M. F.; Cohen, R. E. *Langmuir* **2002**, 18, 3370.

[74] (a) Clay, R. T.; Cohen, R. E. *Supramol. Sci.* **1995**, 2, 183. (b) Joly, S.; Kane, R.; Radzilowski, L.; Wang, T.; Wu, A.; Cohen, R. E.; Thomas, E. L.; Rubner, M. F. *Langmuir* **2000**, 16, 1354.

[75] (a) Boyes, S. G.; Akgun, B.; Brittain, W. J.; Foster, M. D. *Macromolecules* **2003,** 36, 9539-9548. (b) Azzaroni, O.; Brown, A. A.; Cheng, N.; Wei, A.; Jonasc, A. M.; Huck, W. T. S. *J. Mater. Chem.* **2007,** 17, 3433–3439.

[76] (a) Mei, Y.; Sharma, G.; Lu, Y.; Ballauff, M.; Drechsler, M.; Irrgang, T.; Kempe, R. *Langmuir* **2005,** 21, 12229-12234. (b) Mei, Y.; Lu, Y.; Polzer, F.; Ballauff, M. *Chem. Mater.* **2007,** 19, 1062-1069.

[77] Li, D.; Dunlap, J. R.; Zhao, B. *Langmuir* **2008,** 24, 5911-5918.

[78] Azzaroni, O.; Zheng, Z.; Yang, Z.; Huck, W. T. S. *Langmuir* **2006,** 22, 6730-6733.

[79] (a) Tokareva, I.; Minko, S.;. Fendler, J. H.; Hutter, E. *J. Am. Chem. Soc.* **2004**, 126, 15950-15951. (b) Ionov, L.; Sapra, S.; Synytska, A.; Rogach, A. L.; Stamm, M.; Diez, S. *Adv. Mater.* **2006**, 18, 1453–1457. (c) Gupta, S.; Uhlmann, P.; Agrawal, M.; Chapuis, S.; Oertel, U.; Stamm, M. *Macromolecules* **2008,** 41, 2874-2879.

[80] (a) Willner, I.; Katz, E. *Angew. Chem., Int. Ed.,* **2000,** 39, 1180-1218. (b) Emr, S. A.; Yucynych, A. M. *Electroanalysis* **2005,** 7, 913-923.

[81] Kurosawa, S.; Aizawa, H.; Talib, Z. A.; Atthoff, B.; Hilborne, J. *Biosens. Bioelectron.* **2004,** 20, 1165–1176.

[82] (a) Dalmia, A.; Liu, C.C.; Savinell. R. F. *J. Electroanal. Chem.* **1997,** 430, 205-214. (b) Rice, M.E.; Oke, A.F.; Bradberry, C.W.; Adams, R.N. *Brain Res.* **1985,** 340, 151. (c) Wightman, R.M.; May, L.J.; Michael, A.C. *Anal. Chem.* **1988,** 60, 769A.

[83] Dong, R.; Liu, Y.; Abruña, H. D.; Lindau, M.; Ober, C. K. *Tailoring electrode properties towards biosensor applications using pH-sensitive polymer brushes, in preparation.*

CHAPTER 2

PATTERNED BIOFUNCTIONAL POLY(ACRYLIC ACID) BRUSHES ON SILICON SURFACES

Abstract

Protein patterning was carried out using a simple procedure based on photolithography wherein the protein was not subjected to UV irradiation and high temperatures or contacted with denaturing solvents, strongly acidic or basic solutions. Self-assembled monolayers of poly(ethylene glycol) (PEG) on silicon surfaces were exposed to oxygen plasma through a patterned photoresist. The etched regions were back-filled with an initiator for surface-initiated atom transfer radical polymerization (ATRP). ATRP of sodium acrylate was readily achieved at room temperature in an aqueous medium. Protonation of the polymer resulted in patterned poly(acrylic acid) (PAA) brushes. A variety of biomolecules containing amino groups could be covalently tethered to the dense carboxyl groups of the brush, under relatively mild conditions. The PEG regions surrounding the PAA brush greatly reduced nonspecific adsorption. Avidin was covalently attached to PAA brushes and biotin tagged proteins could be immobilized through avidin-biotin interaction. Such an immobilization method based on specific interactions is expected to better retain protein functionality than direct covalent binding. Using biotin-tagged bovine serum albumin (BSA) as a model, a simple strategy was developed for immobilization of small biological

molecules using BSA as linkages, while BSA can simultaneously block nonspecific interactions.

Key words. Protein patterning, aqueous ATRP, poly (acrylic acid) brushes, XPS, avidin, bovine serum albumin, streptavidin, biotin

2.1. Introduction

The ability to pattern biomolecules, especially proteins, onto a substrate is very important for a variety of biological studies and applications including biosensors, studies of cell-surface interactions, cell patterning and the like.[1, 2] Though concentrated efforts have been made on protein patterning, many methods are based on nonspecific physical adsorption on hydrophobic surfaces, wherein the proteins tend to unfold and partially denature[3] upon adsorption. The complexity of creating patterned substrates that combine self-assembled monolayers (SAM) bearing functional groups to immobilize proteins with SAMs that are resistant to nonspecific protein adsorption leads to difficulties in effective surface construction. Veiseh et al. have created patterned surfaces containing both carboxylic acid groups and PEG and used the surface for cell patterning studies.[4,5] In their work, it was necessary to use a gold-patterned silicon substrate and a combination of thiol-gold and silane chemistry to create the chemically patterned substrates. While the formation of self-assembled monolayers of ω-mercapto carboxylic acids on gold covered substrates is widely reported,[6,7,8,9] reports on direct functionalization of a silicon surface with carboxyl-terminated alkylchlorosilanes (or alkoxysilanes) are relatively rare. Some of the advantages of silicon surfaces are that they are inexpensive, molecularly flat, form thermally stable siloxy linkages with organosilanes and are compatible with the well-established microfabrication techniques of the electronic industry. However, the fact

that carboxyl-terminated alkylsilanes (which are required to form SAMs on silicon surfaces) are difficult to synthesize, may have limited their use.[10] Moreover, strong interactions between the carboxyl head group of the silane and the silanol groups on the surface may complicate the process of SAM formation. To avoid this complication, vinyl-, carboalkoxy- or bromo-terminated alkylsilanes have been converted to carboxylic acid after self-assembly and reaction with the surface silanol groups.[11,12,13]

Here we report the synthesis of PAA brushes by the atom transfer radical polymerization (ATRP) of sodium acrylate in aqueous media to generate carboxylic acid groups on a silicon surface. Besides providing a high surface density of –COOH groups for protein immobilization, the PAA brushes are expected to impart biocompatibility, [14] and are more robust and self-healing towards defects than carboxyl-terminated SAMs. Our synthetic methods enable the direct and efficient formation of PAA brushes in contrast to prior studies[15] that involved hydrolysis of poly(*tert*-butyl acrylate) brushes by means of complex synthetic procedures and the use of potentially undesirable organic solvents.

We also describe the patterning of these PAA brushes using optical lithography as an effective alternative to microcontact printing. The creation of a patterned surface using multicomponent, microcontact printing (μCP) has become a widely used method. Usually, one compound is printed onto a substrate and the patterned substrate is back-filled with another compound. The substrate used in μCP is often gold and not silicon, probably because the technique is more suited for thiol chemistry than the moisture sensitive silane chemistry. In addition, depending on the nature and roughness of the stamp and substrate, defects of the monolayer are difficult to avoid in a large patterned area.

Conventional photolithography has also been used previously to pattern multicomponent silanes on silicon surfaces. To carry out surface modification, we

have patterned photoresists on silicon surfaces followed by reaction of the exposed area with a silane initiator. A silicon surface may be first coated with PEG monolayer prior to patterning a photoresist. After the photoresist is patterned, oxygen plasma cleaning may be used to etch the exposed PEG and also regenerate silanol groups on the etched surface to attach surface initiator. Thus, Wang et al. have used photolithography to pattern PEG on a silicon surface and removed the exposed PEG via wet etching,[16] and Senaratne et al. used electron beam lithography to pattern PEG monolayer on silicon surface and back-filled the etched regions with organosilane molecules containing terminal dinitrophenyl groups.[17] While effective, electron beam lithography is expensive and time consuming, and not suitable for patterning large areas.

In this work, after a patterned PEGylated silicon surface was created using optical lithography, it was back-filled with a surface initiator for ATRP. PAA brushes were grown in the regions with tethered initiator molecules, by aqueous ATRP of sodium acrylate and subsequent formation of acid by rinsing with deionized water. As proof of concept we demonstrate covalent immobilization of fluorescently labeled bovine serum albumin (BSA) onto PAA brushes yielding well defined BSA patterns. We also demonstrate immobilization of biotin-tagged proteins through avidin-biotin interaction by showing that fluoresceinated biotin can be immobilized onto PAA brush region after avidin was attached to the brush. We also look into the immobilization of small biological molecules onto PAA brushes using BSA as linkages. After immobilizing biotinylated BSA onto PAA brush, the substrates were incubated with streptavidin and fluoresceinated biotin sequentially. Because BSA is a protein blocking agent, nonspecific adsorption of streptavidin onto the surface is further reduced. The binding of streptavidin is only due to the specific streptavidin-biotin interaction. This method can be extended to BSA tagged with other ligands, such as dinitrophenyl groups, to

engineer spatially confined stimuli for the study of immunoglobulin receptor signaling. The avidin or streptavidin patterned surfaces may also be combined with ink-jet printing or nano-array techniques for multiple protein patterning. The following section reviews prior methods of fabrication of carboxylate functionalized surfaces.

Carboxylate Functionalized Surfaces. The spontaneous reaction of amine containing biomolecules with activated carboxylic acids makes silicon surfaces functionalized with carboxyl groups a versatile platform for microarray technology. A variety of biological molecules can be covalently immobilized on such substrates under mild conditions of pH and temperature. The use of silicon as substrate allows the state-of-the-art approaches to the microfabrication of computer chips to be transferred to 'biochip' production.[18, 19] As noted above, reports of direct functionalization of silicon oxide surfaces with carboxylic acid groups remains relatively rare and patterned carboxyl functionalized surfaces are rarer still.

In an alternative approach to prepare carboxyl functionalized silicon surfaces, Boukherroub et al. have used thermal hydrosilylation of ω-alkenyl carboxylic acid with hydrogen-terminated silicon surface.[20] The same reaction was found to occur at room temperature when irradiated with 300 nm UV light.[21] Voicu et al. prepared DNA microarrays using photopatterning of undecylenic acid on a hydrogen-terminated silicon surface.[18] Irradiation of an air exposed Si-H surface through a patterned mask lead to the formation of oxide squares in the exposed regions. In a complex series of steps, the unexposed surface, consisting of Si-H groups, was reacted with ω-alkenyl carboxylic acid in the presence of UV light. The –COOH groups were then reacted an amine terminated PEG and the PEGylated surface was immersed in aqueous hydrofluoric acid solution to restore Si–H groups in the oxide squares. These new silane groups were reacted with ω-alkenyl carboxylic acid under UV irradiation and finally the –COOH groups in this region were activated with *N*-hydroxylsuccinimide

(NHS) to bind DNA. Although an elegant method, a simpler procedure for micropatterning a silicon surface with –COOH and PEG groups would be desirable. More recently, Asanuma et al. have noted that the carboxyl groups could themselves react with hydrogen terminated silicon, instead of the terminal $–CH=CH_2$ group, [22,23] necessitating the use of an ester-terminated alkene followed by deprotection of the carboxyl group after SAM formation. Alternative methods to prepare silicon surfaces that are densely functionalized with carboxyl groups will be quite useful.

Protein Patterning. The spatially defined presentation of a protein or biochemical ligand of interest against a protein-resistant background is of importance in several areas of biotechnology and biomedical research,[24] for example, in the design of supports for immobilizing antigens or antibodies in enzyme-linked immunosorbent assays (ELISA). Patterned arrays of carboxylated and PEGylated regions are useful for this purpose. The –COOH groups can be readily activated by forming acyl chlorides and nitrophenyl or succinimide esters, which undergo spontaneous reaction with the amine groups in a protein (N-terminal or ε-amino groups of lysine).[5,21] PEG is used to prevent nonspecific protein adsorption.[25,26,27] Potential advantages of dense microarrays in the field of genomics and proteomics have been discussed by Bhatnagar et al.[28] These include reduction in the volumes of analyte and reagents, and higher signal-to-noise ratios. The basic criterion in the design of a protein microarray is that the protein must retain its native conformation (and hence its biological activity) after immobilization. Thus, the use of harsh solvents, strongly acidic or basic buffers, and exposure to UV and high temperatures are all undesirable.[29] Several methods have been used to micropattern proteins on surfaces, as discussed in the reviews by Blawas and Reichert and Kane et al.

López et al. have patterned a gold surface with methyl-terminated and PEGylated SAMs and have used physical adsorption of proteins on the hydrophobic methyl-

terminated regions.[30] Physisorption of a protein on a surface is predominantly driven by hydrophobic interactions, especially in aqueous solutions of high ionic strength. In the absence of competing proteins the adsorption is essentially irreversible. However, many proteins lose their native solution conformation, and hence activity, upon immobilization on a hydrophobic surface.[31] Physical adsorption on untreated glass has been used to pattern albumin[32] but in high ionic strength buffers where electrostatic interactions are weak, desorption of the protein from the hydrophilic glass substrate is very likely. Covalent immobilization on hydrophilic substrates, as discussed by Lahiri et al.,[8,33] is more desirable.[15,34]

Photochemical techniques involving aryl azide chemistry, nitrobenzyl caging chemistry and diazirine chemistry have also been used, but these methods involve potentially denaturing UV irradiation of the protein. Padeste et al. have used a UV lithography process, wherein a protein immobilized surface is first covered by a protective sucrose layer, cured in an oven, spin-coated with a photoresist, irradiated with UV using a lithographic mask, developed to remove exposed photoresist, and treated with oxygen plasma to remove the protein from the exposed region.[35] The sucrose layer is believed to protect the protein from organic solvents and alkaline solutions used in the process, which would otherwise denature the protein. Similarly, Lee et al. have used agarose as a protective layer in photolithographic patterning of proteins.[36] In addition, they have discussed the problems associated with microcontact printing, PDMS-based microfluidic systems, and parylene-based peel-off process for direct patterning of proteins.

Jun et al. have formed patterns of HO– and CH_3O– terminated PEG regions on chlorine-terminated silicon surfaces using the soft lithographic techniques of microcontact printing and micromolding in capillaries (MIMIC).[37] The HO–terminated PEG regions were activated by either oxidation to aldehyde or using *N*,*N*′-

disuccinimidyl carbonate, followed by covalent immobilization of protein molecules. The MIMIC technique has also found application in the work of Delamarche et al.[38] and Patel et al.[39]

Protein patterning on a sub-micron length scale has been achieved using electron beam lithography of organosilane self-assembled monolayers[25, 40] and surfaces of block copolymers as templates.[41] Zhang et al. created patterns of biotin in a hydrophobic perfluoroalkyl background, but could avoid nonspecific adsorption by incubating the patterned surface with streptavidin for only a short time.

In this paper we describe immobilization of proteins on patterned hydrophilic PAA brushes through covalent binding and avidin-biotin interaction. UV lithography was used to pattern a silicon surface covered with PEGylated SAM. An initiator for ATRP was then attached to regions not covered by PEG. ATRP of sodium acrylate in water at or near room temperature, using the surface-tethered initiator, resulted in facile formation of patterned polymer brushes that were used to selectively immobilize fluorescently labeled proteins. The patterned proteins showed a sharp contrast against a protein resistant PEG background when observed under a fluorescence microscope.

2.2. Experimental section

2.2.1. Materials. Allyl 2-bromo-2-methylpropionate (CAS no. 40630-82-8, 98 %), chlorodimethylhydrosilane (CAS no. 1066-35-9, 98 %), Pt on activated carbon (10 wt %), triethylamine (CAS no. 121-44-8, 99.5 %), sodium acrylate (CAS no. 7446-81-3, 97 %), CuBr (CAS no. 7787-70-4, 99.999 %), $CuBr_2$ (CAS no. 7789-45-9, 99.999 %), 2,2′-bipyridine (CAS no. 366-18-7, ≥ 99 %), *N*-hydroxylsuccinimide (NHS, CAS no. 6066-82-6, 98 %), *N*-(3-dimethylaminopropyl)-*N*′-ethylcarbodiimide hydrochloride (EDC, CAS no. 25952-53-8, ≥ 98%), egg white avidin, bovine serum albumin labeled with fluorescein isothiocyanate (BSA-FITC), biotin-tagged bovine serum albumin

(BSA-biotin, 8-16 mol biotin per mol albumin), streptavidin (from streptomyces), 5(6)-(biotinamidohexanoylamido)pentylthioureidylfluorescein (fluorescein-tagged biotin, CAS no. 134759-22-1, ≥ 90 %), phosphate buffered saline (PBS) tablets and 4-morpholineethanesulfonic acid (MES, CAS no. 4432-31-9, ≥ 99%), were purchased from Sigma-Aldrich and used without out further purification. 2-[Methoxy(polyethylenoxy)propyl]trichlorosilane (PEGylated silane, $CH_3O(CH_2CH_2O)_{6-9}(CH_2)_3SiCl_3$, 90 %) was purchased from Gelest. Anhydrous toluene (99.8 %) was purchased from Acros. All the other solvents for rinsing and cleaning were obtained from Fisher. The PBS buffer solution was prepared by dissolving the PBS tablet in water to yield 0.01 M phosphate buffer, 0.0027 M potassium chloride, 0.137 M sodium chloride, and a pH of 7.4 at 25 °C. A 3.8 pH MES solution was prepared by dissolving 50 mM MES in water. The pH of this solution was 3.8.[42] The MES buffer solution was prepared by dissolving MES (50 mM) and NaOH (3 mM) in water to obtain a pH of about 5. Distilled deionized water and ultra-pure nitrogen (99.99 %, Airgas) were used throughout.

2.2.2. Patterning of PEG on Silicon Wafer. Silicon wafers, rinsed with acetone and blown dry under nitrogen gas, were cleaned with oxygen plasma cleaner (Harrick Scientific) for 5 min. Self-assembled monolayers of PEG were prepared by either vapor deposition or solution deposition technique. The silicon wafers were immersed in a 1 % (v/v) solution of the PEGylated silane in anhydrous toluene containing catalytic amounts of triethylamine for about 12 h at room temperature, followed by rinsing with anhydrous ethanol and drying with nitrogen. After deposition, the substrates were baked at 115 °C for 10 min. S1813 positive tone photoresist (Shipley) was spin-coated onto the PEG functionalized silicon wafers at 4000 rpm for 30 s and soft-baked at 115 °C for 1 min, resulting in a film about 1 μm thick. The wafer was then exposed to UV light (λ = 405 nm, 17 mW/cm^2) passed through patterns of lines

with widths of 2 or 5 μm, for 2 s using HTG System III-HR Contact Aligner. After development in a tetra-methyl ammonium hydroxide solution (AZ 300 MIF), the exposed PEG regions were etched using oxygen plasma. The remaining photoresist was stripped off using acetone, resulting in PEG stripes on a silicon surface. The PEG patterned surfaces were used immediately in the next step of attaching the ATRP initiator.

2.2.3. Synthesis of Surface Initiator and Immobilization of Initiator. Hydrosilylation of allyl 2-bromo-2-methylpropionate was carried out using a literature procedure to obtain the ATRP initiator, 3-(chlorodimethylsilyl)propyl 2-bromo-2-methylpropionate (CAS no. 370870-81-8, cf. **2** in Scheme 2.2).[43] The PEG patterned silicon substrates were immersed in toluene solution of the initiator (5 mM) and triethylamine (0.05 mM) for 18 hours. The wafers were then removed from the solution and washed with ethanol, water, and acetone sequentially. They were blown dry under nitrogen gas and used for surface-initiated polymerization. Plain silicon substrates without patterned PEG were similarly modified with the ATRP initiator.

2.2.4. Surface Initiated Polymerization of Sodium Acrylate. The substrates (1 cm × 1 cm) were placed in a dry Schlenk flask. The flask was evacuated and back-filled with nitrogen three times. Sodium acrylate (1.88 g, 20 mmol), CuBr (57.4 mg, 0.4 mmol), $CuBr_2$ (9.0 mg, 0.04 mmol), and 2,2′-bipyridine (137.4 mg, 0.88 mmol) were added to another 25 mL Schlenk flask equipped with a magnetic stir bar. Air in this flask was evacuated and replaced with nitrogen thrice. Four milliliters of water, which was purged with nitrogen for at least 30 min, was transferred to the Schlenk flask containing the monomer using a cannula. The mixture was stirred at room temperature under nitrogen for about 10 min until a brown solution was obtained. The solution was then transferred into the Schlenk flask containing the patterned substrates using a cannula. Polymerization was carried out at 30 °C for 2 hours, after which the

substrates were taken out of the solution and gently sonicated in water–ethanol mixture for 5 min. They were then rinsed with water and ethanol, blown dry under nitrogen gas, and characterized by AFM. Un-patterned polymer brushes on silicon were characterized by ellipsometry, and X-ray photoelectron spectroscopy (XPS).

2.2.5. Immobilization of BSA-FITC. The wafers (1 cm × 1 cm) with patterned PEG and PAA brushes were equilibrated in PBS buffer solution (pH ~ 7.4) for 30 min. They were then immersed in 5 mL of MES solution (50 mM, pH ~ 3.8) containing EDC (40 mg) and NHS (24 mg). After 10 min, the substrates were taken out of the solution, rinsed with MES buffer, and covered with a 100 μg/mL solution of BSA-FITC in MES buffer solution (pH ~ 5.0). After 1 h of incubation in darkness, the substrates were thoroughly rinsed and left in PBS buffer solution (pH ~ 7.4) overnight to deactivate unreacted NHS ester.

2.2.6. Immobilization of Avidin and Incubation with Fluoresceinated Biotin. Avidin was immobilized on PEG-PAA patterned silicon surfaces as described in section 2.5, but 100 μg/mL solution of avidin in MES buffer solution (pH ~ 5.0) was used instead of BSA-FITC. The protein-immobilized surface was incubated in a solution of 100 μg/mL fluoresceinated biotin in a PBS buffer solution, in the dark for 1 h. Finally, the substrates were washed with PBS buffer solution (pH ~ 7.4) and observed under a fluorescence microscope. A PEG-PAA patterned substrate without avidin was incubated with fluoresceinated biotin in PBS buffer solution for an hour and used as a control. Avidin was also immobilized onto non-patterned PAA brush surfaces. These surfaces were then characterized by X-ray photoelectron spectroscopy.

2.2.7. Immobilization of BSA-biotin and making biotin-streptavidin-biotin sandwich. Biotinylated BSA was immobilized onto PAA brushes of the PEG-PAA patterned substrates using EDC/NHS mediated coupling, as described in section 2.5. A 100 μg/ mL solution of the protein in MES buffer solution (pH ~ 5.0) was used. The

BSA-biotin functionalized substrates were incubated with 100 μg/mL of streptavidin in a PBS buffer solution (pH ~ 7.4) for 1 h. After rinsing several times to remove free streptavidin, the substrates were incubated with a 100 μg/mL solution of fluoresceinated biotin (in PBS buffer solution) in the dark for 1 h. The substrates were finally rinsed with PBS buffer solution and imaged under a fluorescence microscope. The control surfaces were prepared in an identical manner, except that BSA was used instead of biotinylated BSA.

2.2.8. X-ray Photoelectron Spectroscopy. X-ray photoelectron spectroscopy (XPS) measurements were performed using a Kratos Axis Ultra Spectrometer (Kratos Analytical, Manchester, UK) with a monochromatic Al Kα X-ray source (1486.6 eV) operating at 280 W (14 kV, 20 mA). Charge neutralization was carried out by injection of low energy electrons and the C–C 1s peak was corrected to a binding energy of 285 eV. The pass energy of the analyzer was set at 20 eV for high resolution spectra and 80 eV for survey scans, and data were acquired at energy steps of 0.5 eV and 0.1 eV, respectively. The high resolution spectra were fitted using a Tougaard background and Gaussian-Lorentzian (sum) line shapes for sub-peaks.

2.2.9. Fluorescence Microscopy. Fluorescence microscopy was performed using an Olympus BX51 upright microscope with a 40x UPlan Fluorite 40x dry objective (N.A. 0.75). Images were acquired using a Roper CoolSnap HQ CCD camera and Image Pro image acquisition and processing software. Fluorescein and FITC were observed with a 450 nm excitation and 550 nm emission filter sets. False color fluorescence images reported here were processed using the ImageJ 1.36b software. All sets of control and test images were processed in an identical manner. Moreover, representative line sections of as obtained and unprocessed images are also shown, in order to compare fluorescence intensity from different parts of the patterned surfaces.

2.2.10. Contact Angles, Surface Topography and Film Thickness. Contact angles were measured using a NRL contact angle goniometer (Ramé-Hart Model 100-00) at room temperature. Dynamic water contact angle measurements were performed by addition and retraction of a drop of water on the surface. Surface topography and roughness were determined using Veeco Dimension 3100 Scanning Probe Microscope in the tapping mode. Thicknesses of the PEG layer and the PAA brush were measured by Woollam variable angle spectroscopic ellipsometer at a 70° angle of incidence. A Cauchy model (Cauchy layer/silicon substrate) was used to fit the data, in which Cauchy layer was representative of the PEG layer or the PAA brush.

2.3. Results and Discussion

2.3.1. PEG-PAA Patterned Surfaces. The overall procedure for forming PEG-PAA patterns on a silicon substrate is shown in Scheme 2.1. Ellipsometry showed that the thickness of the PEG layer was about 2.2 nm. Photolithography was used in this study to create patterns of PEG SAM on silicon; however, the patterned PEG surface can also be prepared by other techniques such as microcontact printing or electron beam lithography. The siloxane bonds at the SAM-silicon interface are relatively stable and withstand the high temperatures (~ 115 °C) involved in the patterning process. The regions not covered by the PEG were back-filled with the ATRP initiator. PAA brushes were grown by ATRP at room temperature.

Scheme 2.1. Patterning of PEG and poly(acrylic acid) brushes on silicon surface

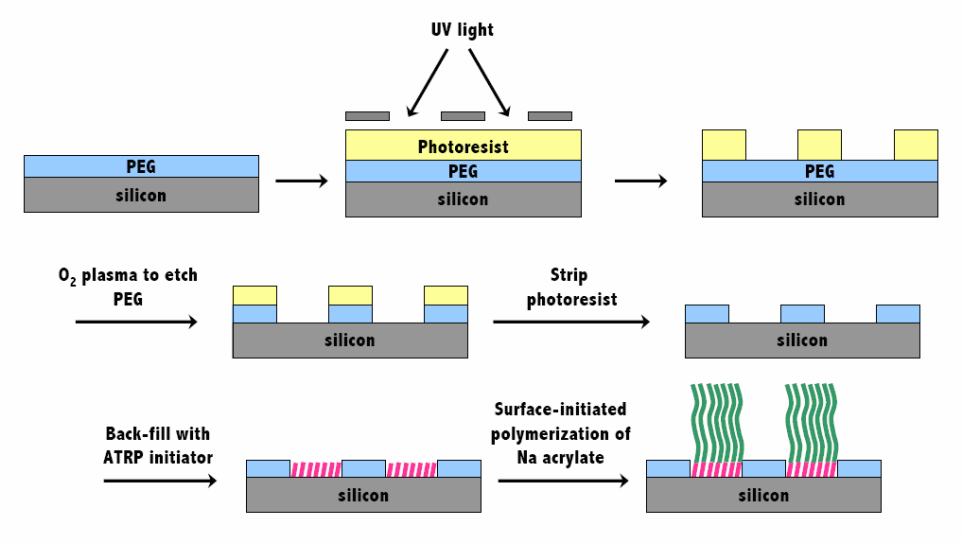

Scheme 2.2. Surface initiated polymerization of sodium acrylate using ATRP

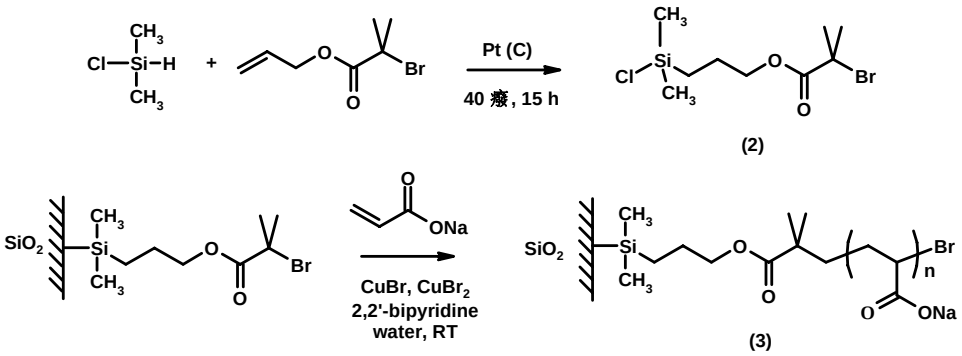

2.3.2. PAA Brushes. Due to the possibility of interaction of the carboxylic acid groups with the ATRP catalyst,[44] poly(acrylic acid) is usually prepared by hydrolysis of poly(*tert*-butyl acrylate).[45] Matyjaszewski et al. have reported an ATRP synthesis of polystyrene-*block*-poly(*tert*-butyl acrylate) brushes on silicon surfaces which were converted to polystyrene-*block*-poly(acrylic acid) by refluxing the surfaces in aqueous hydrochloric acid solution.[46] Similarly, Kurosawa et al. have prepared poly(acrylic acid) brushes by plasma polymerization of allyl alcohol on a quartz surface, reaction

of the surface –OH groups with 2-bromo-2-methylpropionyl bromide, growth of *tert*-butyl acrylate brushes by ATRP, and conversion of the *t*BA groups to acrylic acid by refluxing with trifluoroacetic acid in dichloromethane.[47] However, this method is problematic if the surface bound initiator also contains an ester group, which can also undergo hydrolysis resulting in removal of polymer chains from the surface. Treat and co-workers have recently reported the formation of poly(acrylic acid) brushes by high temperature deprotection of poly(*tert*-butyl acrylate).[48] Pyrolysis of the *tert*-butyl ester at 200 °C for 30 min produced carboxylic acid with isobutylene as side product. However, this procedure may not be compatible with our strategy shown in Scheme 2.1. The pyrolysis may have undesirable effects on the PEG SAMs.

Ashford et al. observed that aqueous ATRP of sodium methacrylate resulted in controlled molecular weights and narrow molecular weight distributions.[49,50] Osborne and co-workers have also prepared triblock copolymer brushes containing a poly(methacrylic acid) block by aqueous ATRP of sodium methacrylate. Grazing incidence FT-IR spectra showed that rinsing the brush surface with water protonated the anion and removed the Na^+ ions from the brush.[51]

We have found that ATRP growth of sodium acrylate brushes may be successfully performed in water at room temperature using the CuBr/2,2′-bipyridine catalyst system. Reactions for the synthesis of surface-initiated ATRP initiator, 3-(chlorodimethylsilyl)propyl 2-bromo-2-methylpropionate, and the poly(sodium acrylate) brushes are shown in Scheme 2.2. About 10 % of $CuBr_2$ (relative to CuBr) was used to moderate the polymerization rate. X-ray photoelectron spectra revealed the absence of Na^+,[52] suggesting that the carboxylate anions were fully protonated. XPS studies also indicated the absence of CuBr or $CuBr_2$ at the brush surface.[53] XPS of PAA brushes on silicon surfaces were shown in Figure 2.1.

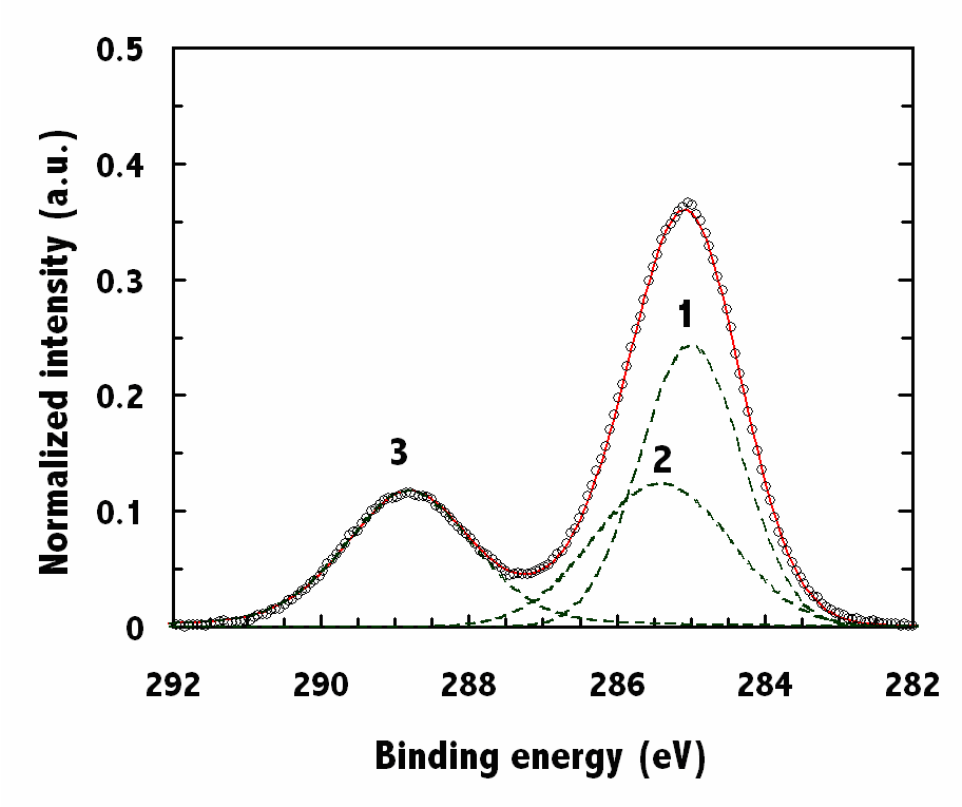

Figure 2.1. C 1s XPS spectrum of poly(acrylic acid) (PAA) brush grown from a silicon surface. Sub-peaks 1 and 2 arise from alkyl carbon atoms along the PAA backbone, while peak 3 is due to –C(=O)-OH.

The advancing and receding water contact angles of the PAA brush surface were $\theta_{AW} = 45°$ and $\theta_{RW} = 9°$, respectively. Treat et al. have reported $\theta_{AW} = 48°$ and $\theta_{RW} = 34°$,[45] while Husemann et al. observed an advancing water contact angle of 15°.[54] If the brush thicknesses are comparable, the reason for the differences in contact angles must lie in the thermal and solvent treatments of the brushes before contact angle measurements. The brush surface was rinsed with water and ethanol and dried it at room temperature in a vacuum oven before measuring the contact angles. Both ellipsometry and AFM (Figure 2.2) showed that the dry thickness of PAA brushes was about 30 nm.

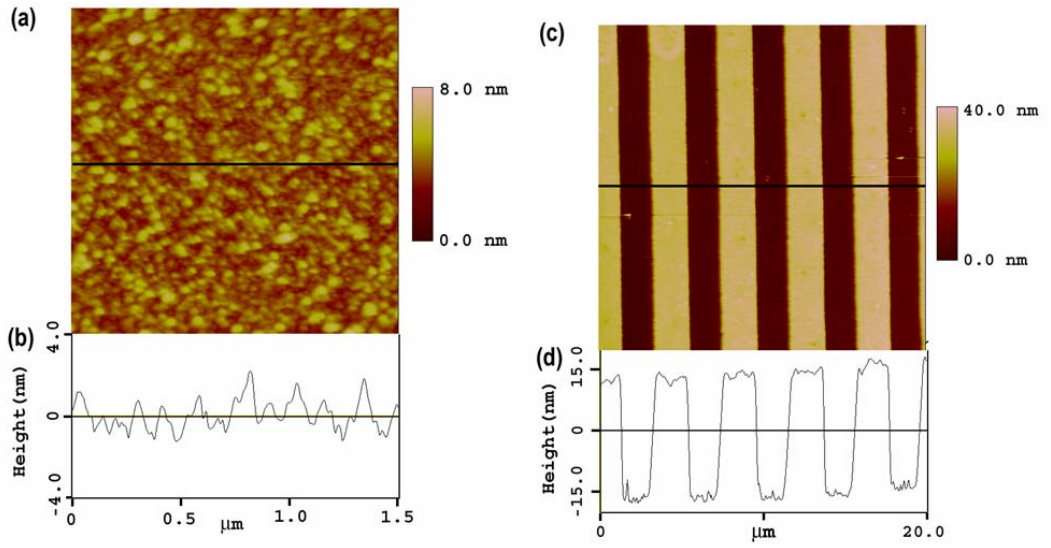

Figure 2.2. Tapping-mode scanning probe microscopy height-images of (a) PAA brush grown by surface initiated polymerization, and (c) 2 µm wide alternating stripes of PEG SAM and PAA brush on silicon substrates. The height profiles of transverse sections near the centers of the scan regions are shown in (b) and (d), respectively.

Figure 2.2a shows a height image of a PAA brush surface obtained by scanning probe microscopy. The surface was rinsed with ethanol after polymerization and dried under a stream of nitrogen at room temperature. The rms roughness was 0.7 nm. The height image of a patterned silicon surface with 2 µm wide PAA stripes juxtaposed to PEG-covered stripes is shown in Figure 2.2b. The ATRP initiator selectively attached to regions not covered by PEG and could successfully initiate polymerization of the sodium acrylate monomer. The surface composition of PAA brush was characterized using X-ray photoelectron spectroscopy. The C 1s peak could be deconvoluted into three sub-peaks positioned at binding energy values of 285 eV, 285.4 eV and 288.8 eV, and with relative areas of 42 %, 29 %, and 29 %, respectively. The curve-fitting results are in accord with previously reported XPS characterization of poly(acrylic acid)

surfaces.[55] The PEG self-assembled monolayer showed two peaks, at 286.5 eV and 285 eV, respectively. The former peak, with a relative area of 87 %, corresponds to the ether carbon atoms of the PEG group. The hydrocarbon peak arises from the propyl carbon atoms in the PEGylated molecules used for preparing the SAM.

2.3.3. Protein patterning through covalent immobilization. The patterned PAA brushes were further characterized using the binding of fluorescently labeled BSA. Figure 2.3 is a fluorescence image of a pattern with 2 μm wide stripes of PAA in a PEGylated background. BSA-FITC was selectively immobilized on the PAA regions resulting in fluorescence, while the PEG regions were dark. The fluorescence intensity did not change significantly even after washing with 0.5 M sodium chloride solution in water, indicating that protein immobilization on the PAA brush was very stable.[56]

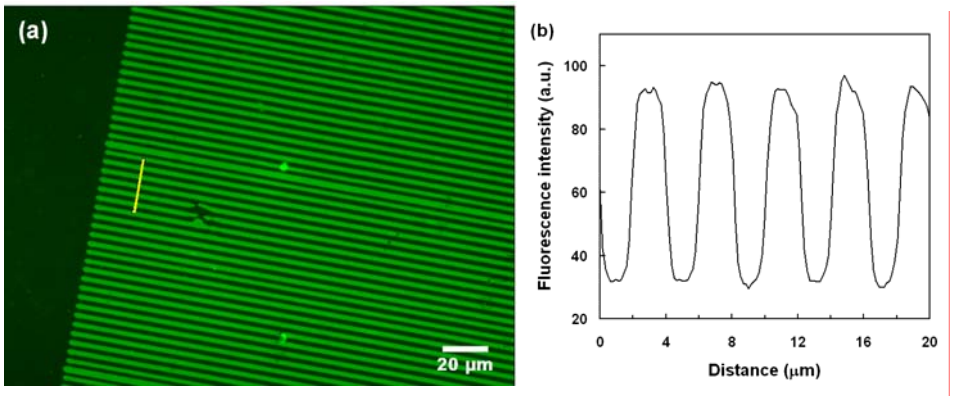

Figure 2.3. (a) Fluorescence image of BSA-FITC immobilized on 2 μm wide PAA brush patterns in a background consisting of PEG SAM. The darker regions are the PEG covered substrate where there was no covalent binding or nonspecific adsorption of BSA-FITC. (b) Intensity profile along a line section shown in (a).

Covalent immobilization of proteins on the PAA brush was carried out as shown in Scheme 2.3 using a published procedure.[8,57] Activated *N*-hydroxysuccinimidyl esters of the polymer carboxylic acids were first generated by a reaction mediated by the water-soluble carbodiimide, EDC. The reaction was performed in 50 mM MES solution (pH ~ 3.8). The NHS esters were then reacted with ε-amino groups of lysine residues in a MES buffer solution (pH ~5.0). After immobilization, the surfaces were washed and incubated with a PBS buffer solution (pH ~ 7.4) to hydrolyze residual NHS esters.

Scheme 2.3. Protein immobilization on poly(acrylic acid) brush surface by EDC/NHS coupling

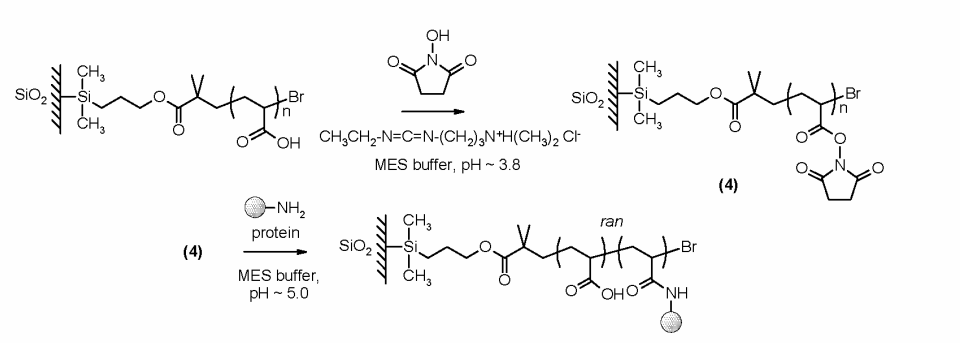

Lahiri et al. have found that the highest levels of protein immobilization were obtained when the pH of the coupling buffer was one unit below the pI of the protein, that is, when the protein was positively charged.[8] A favorable electrostatic interaction between the positively charged protein and the negatively charged $–COO^-$ group was hypothesized to be responsible for this effect. However, they have also noted certain ambiguities in this hypothesis. Because the carboxylic acid groups were quantitatively converted to NHS esters before protein coupling, the surface is expected to be largely neutral in the ester form. But it is likely that the hydrolysis of the NHS ester is fast

relatively to the coupling of the protein, in which case the surface would be negatively charged. Moreover, protonation of the ε-amino groups of lysine residues is of concern at lower values of pH. The reduced nucleophilicity due to protonation is unfavorable for the coupling reaction. Nevertheless, Lahiri et al. have achieved immobilization of a variety of proteins in solutions with pH values of 7 or lower. The ε-amino groups of the lysine has a pK_a of 10.4.[58] Therefore, almost all of the $-NH_2$ groups are expected to be protonated at these pH values. Yet, significant amounts of proteins attached to the carboxylated surfaces. We used a MES buffer solution of pH ~ 5.0 for immobilizing both BSA (pI = 4.9) and avidin (pI = 10.8). Initial experiments using fluorescence microscopy showed that acidic media resulted in higher amounts of BSA immobilization (data not shown). We also used XPS to characterize the BSA immobilization onto un-patterned PAA brushes on silicon surface, which is shown in the supporting information.

2.3.4. Protein patterning using avidin-biotin affinity. In section 2.3.3, we discussed covalent immobilization of BSA on PAA brushes. Although the covalent binding method is simple and provides stable immobilization, it usually involves a multi-point attachment of proteins to surfaces, resulting in a random orientation of the immobilized protein, and a loss of activity associated with structural deformation.[59] Single-point attachment of proteins is expected to result in a more controlled and oriented immobilization. The avidin-biotin interaction is widely used for controlled immobilization of proteins. Because each avidin molecule has four biotin-binding sites, avidin-biotin complex formation has also been used for multi-layer immobilization of proteins and enzymes.[60] Here, we created patterned arrays of avidin, on a PEGylated background, for further functionalization with biotinylated molecules. Avidin was covalently attached to PAA brushes through EDC/NHS coupling. Biotin-tagged proteins may then be immobilized onto the surface through avidin-biotin interaction,

which was demonstrated by attachment of fluoresceinated biotin to avidin modified regions, as shown in Scheme 2.4.

Scheme 2.4. Protein immobilization to PAA brushes through avidin-biotin interaction

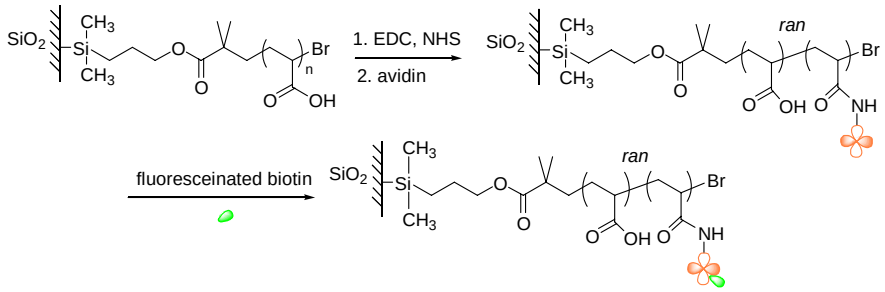

The attachment of avidin to the PAA brush was confirmed by fluorescence microscopy. The binding of fluorescein-tagged biotin to avidin[61] resulted in the image shown in Figure 2.4. The control surface, where the PEG/PAA patterned surfaces were incubated with fluorescein-labeled biotin showed negligible binding of biotin (data not shown). X-ray photoelectron spectroscopy was used to characterize the binding of avidin to un-patterned PAA brushes. Figure 2.5a shows the XPS survey scan of a PAA brush surface with immobilized avidin, which is qualitatively similar to the XPS spectrum of avidin reported by Nehilla et al.[62] We carried out a detailed analysis of the high resolution C 1s spectrum, to determine the extent of attachment of avidin to PAA brush. Avidin is a well-characterized glycoprotein, and is amenable to such an analysis. It consists of four identical polypeptide chains, each containing about 128 amino acid residues.[63] Each subunit has a carbohydrate moiety attached at the asparaginyl residue 17 (Asn_{17}). The oligosaccharides attached to the four subunits can be compositionally different, but contain, on an average, 5 mannose and 3 *N*-acetylglucosamine moieties per subunit.[64]

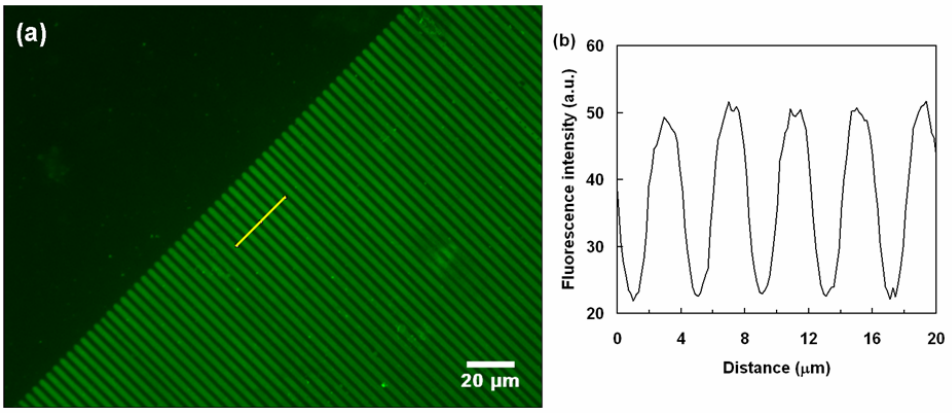

Figure 2.4. (a) Fluorescence microscopy image of avidin immobilized PEG/PAA patterned surface that was incubated with fluoresceinated biotin; and (b) intensity profile along a line section shown in (a).

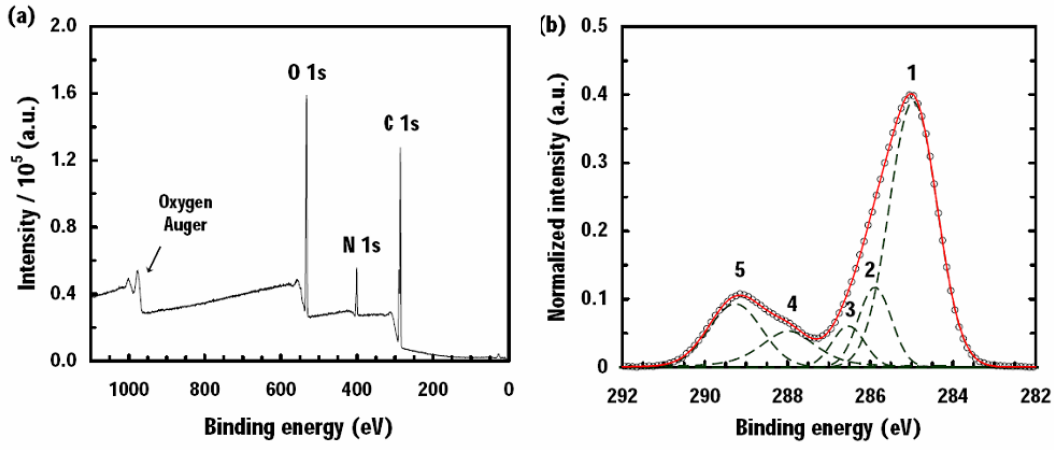

Figure 2.5. (a) XPS survey scan of covalently immobilized avidin on PAA brush surface, and (b) the high resolution C 1s spectrum, resolved into component peaks. The peak assignments are: (1) C–C, C–H (2) C–N (3) C–OH, C–O–C, (4) C=O (amide), and (5) C=O (carboxylic acid). The circles represent the experimental data points. The continuous line is the best-fit curve. The dashed curves are fitted sub-peaks.

Figure 2.5b shows a high resolution C 1s XPS spectrum of an avidin-PAA surface. Deconvolution of the C 1s peak into sub-peaks was performed on the basis of high resolution C 1s XPS spectra of model poly(amino acid) surfaces reported by Bomben and Dev.[65] Using a series of homopolymeric amino acids, Bomben and Dev found that deconvolution of the C 1s peak into only three sub-peaks, corresponding to the C–H or C–C hydrocarbon peak at 285.0 eV, the amide C=O peak at 287.8 eV, and the amine C–N peak at 286.3 eV, resulted in good agreements between the experimental ratios of peak areas with the theoretical ratios. The theoretical areas of peaks were calculated from the known poly(amino acid) structure. The use of more than 3 peaks was not found to be necessary. However, the hydroxylated amino acids, threonine (Thr) and serine (Ser), were not studied by Bomben and Dev. Avidin has a high content of these amino acids (20 residues of Thr and 9 residues of Ser per subunit). In fact, the fraction of Thr residues in avidin (~ 0.16) is higher than that of any other amino acid residue. Moreover, the oligosaccharides attached to Asn_{17} contain mannose and *N*-aceylglucosamine moieties, which are also highly hydroxylated. These oligosaccharides constitute about 10 % of the total mass of the glycoprotein. Hence, in addition to the three characteristic poly(amino acid) peaks used by Bomben and Dev,[62] a C–O (alcohol or ether) peak is also expected near 286.5 eV in the XPS spectrum. In addition, a carboxylic acid C=O peak due to the PAA brush will be observed near 289 eV. As can be seen from Figure 2.5b, the experimental spectrum could be fitted very well (correlation coefficient, r = 0.999) using these five sub-peaks.[66] Gauss-Lorenztian sums were used as the line shapes for curve fitting. Table 2.1 shows the peak positions and relative areas of the fitted sub-peaks. Using the experimentally known ratios of C–C and C=O peak areas for poly(acrylic acid) the individual contributions of avidin and poly(acrylic acid) to the peak areas were also calculated as given in Table 2.1.

Table 2.1. Relative areas of the C 1s sub-peaks in the XPS spectrum of the avidin-tethered poly(acrylic acid) brush surface and number distribution of carbon atoms at the surface

Peak	Position (eV)	Carbon atom	Percentage of C 1s peak area		
			Total	Avidin	Poly(acrylic acid)
1	285.0	C–C (or C–H)	56.3	23.9	32.4
2	285.9	C–N	11.8	11.8	–
3	286.5	C–O	6.0	6.0	–
4	288.0	C=O (amide)	11.0	11.0	–
5	289.3	C=O (acid)	14.9	1.0	13.9

The relative areas of sub-peaks shown in Table 2.1 are in good agreement with the known composition of avidin: C–C 44.48 %, C–N 21.94 %, C–O 10.90 %, C=O (amide) 20.91 %, and C=O (acid) 1.77 %. The expected distribution of carbon atoms in avidin was calculated from its amino acid and oligosaccharide compositions as reported by DeLange and Huang.[63, 67] These values are also in accord with the relatives areas of C 1s sub-peaks in the XPS spectrum of pure avidin (data not shown).

It is evident from the values reported in Table 2.1 that about 54 % of the C 1s peak area is from avidin. The avidin molecules can be localized on the silicon surface in two distinctly different ways. First, they can form a monolayer on top of the PAA brush, without diffusing into the brush. Second, they can penetrate the brush layer. For a monolayer of avidin with a thickness, d, of ~ 4.8 nm[68] and an electron escape depth, λ, of ~ 3.3 nm,[69] the expected contribution of avidin to the C 1s peak area is about 76.6 %,[70] which is higher than the experimentally determined value of 54 %. Thus, we either have less than a complete coverage of avidin at the PAA surface, or a situation

where the protein molecules penetrate the PAA brush. Prior studies[71,72] have shown that protein molecules do not just bind to the surfaces of PAA brushes, but can also penetrate and interact with the brush interior.

2.3.5. Patterning small biological molecules using BSA as linkages. In sections 2.3.4 and 2.3.5, we discussed two methods to pattern proteins that have several functional groups available for modification with other biomolecules and ligands. A single molecule of BSA has 60 lysine residues, and hence 60 amino groups that can react with carboxylic acids. Thus, BSA can function as a multi-site linkage between biofunctional ligands, such as biotin or 2,4-dinitrophenyl (DNP) moieties, and patterned PAA brushes. Moreover, BSA is commonly used to "block" nonspecific adsorption of biomolecules on surfaces.[73] Here, we used biotinylated BSA to pattern biotin molecules on silicon surfaces. The PAA regions were selectively functionalized with biotinylated BSA by covalent coupling. The surfaces were then incubated with a PBS buffer solution of streptavidin (pI ~ 5.3). Biotin-streptavidin complex formation (affinity constant ~ 10^{15} M^{-1}) resulted in an almost irreversible immobilization of streptavidin on the PAA regions. The streptavidin binding was characterized by complexation of fluoresceinated biotin with streptavidin. The series of reactions are represented in Scheme 2.5.

Scheme 2.5. Immobilization of biotin using BSA as linkages

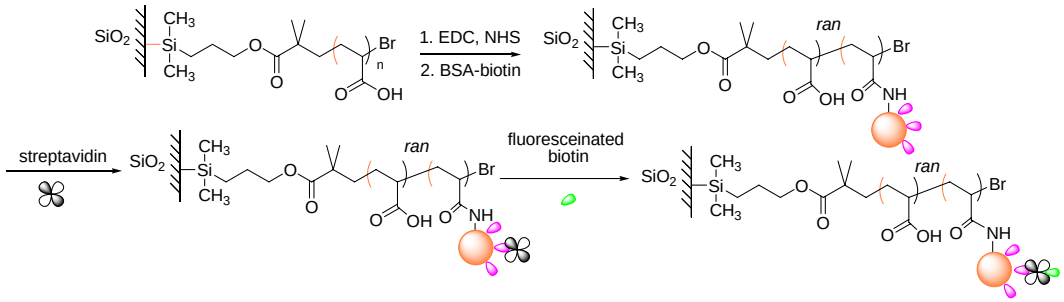

Figure 2.6a shows a fluorescence microscopy image of streptavidin immobilized on 5 μm wide PAA brushes. The control experiment was carried out by covalently immobilizing BSA onto PEG/PAA patterned surfaces, incubating the BSA functionalized patterned surface with streptavidin, and finally incubating with biotin-fluorescein. It is evident from Figure 2.6b that there was no streptavidin attachment in the absence of biotin, which confirmed the specificity of streptavidin attachment onto the biotinylated patterns and showed that both BSA and PEG prevented the nonspecific adsorption of streptavidin. Such surfaces can minimize nonspecific interactions between biological molecules inside the patterned regions and the regions surrounding the patterns as well.

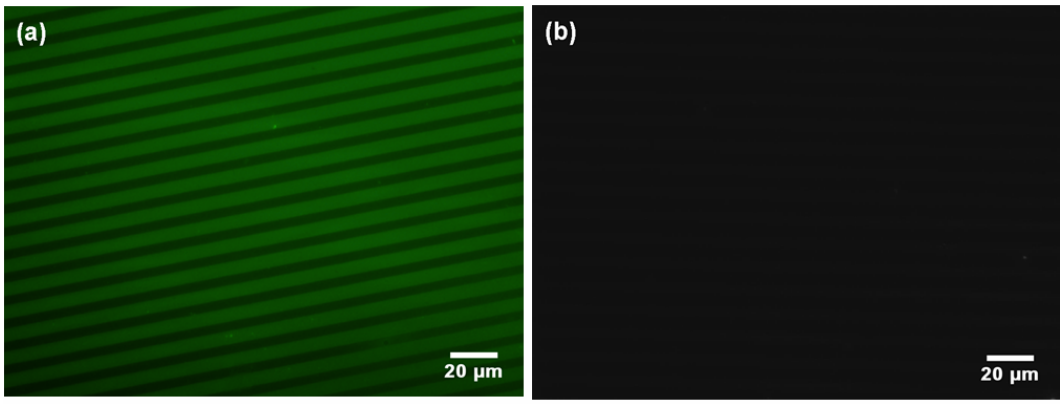

Figure 2.6. (a) Fluorescence microscopy image of a streptavidin-immobilized BSA-PAA surface that was incubated with fluoresceinated biotin. Immobilization of streptavidin was achieved through biotinylated BSA, which was covalently tethered to the PAA stripes. The darker regions correspond to PEG. (b) A control patterned surface where the BSA was not tagged with biotin. No streptavidin, and hence, fluoresceinated biotin attached to the surface.

4. Conclusions

A versatile procedure was developed to pattern biological molecules with low-level nonspecific adsorptions. PEG monolayer was patterned based on photolithography. Surface-initiated atom transfer radical polymerization of sodium acrylate was successfully carried out in water at room temperature on patterned surfaces where PEG was etched. Poly(acrylic acid) brushes acted as robust templates for protein immobilization by providing a high density of –COOH groups on the surface, while PEG surrounding the brushes restricted proteins into the brush region further.

Two different strategies for protein immobilization were discussed. First, protein (BSA) molecules were directly immobilized on PAA brushes through covalent linkages. Second, a protein such as avidin was attached, which could then be used to bind different biotinylated molecules through the almost irreversible avidin-biotin interaction. We also used a simple strategy to immobilize small biological molecules like biotin using BSA as linkages. We have utilized the effectiveness of BSA in blocking nonspecific interactions by immobilizing biotin-tagged BSA to the patterned brushes. We found that the attachment of streptavidin was only through specific recognition of biotin. Streptavidin did not bind in the absence of the latter. Moreover, by itself being a polypeptide, BSA offers a non-denaturing environment for immobilizing other proteins. Thus, this method can be expanded to immobilize a range of antigens, or ligands for biosensing applications, and to study cell-surface interactions. The problem of nonspecific binding can be greatly reduced by this approach.

Acknowledgements

This research was supported by the NSF-funded NIRT program (ECS-0103297-NIRT), the Cornell Nanobiotechnology Center (NBTC) and the Office of Naval Research (N00014-02-1-0170). It made use of the facilities at NBTC, Cornell NanoScale Science and Technology Facility (CNF), and Cornell Center for Materials Research (CCMR), all of which are supported by NSF. The NIRT and NBTC support for RD and the ONR support for SK are gratefully acknowledged. XPS spectra of the avidin immobilized PAA surfaces were acquired by Robert W. Hengstebeck at the Materials Characterization Laboratory of the Pennsylvania State Univeristy.

REFERENCES

[1] Blawas, A. S.; Reichert, W. M. Protein patterning. *Biomaterials* **1998,** *19,* 595-609.

[2] Kane, R. S.; Takayama, S.; Ostuni, E.; Ingber, D. E.; Whitesides, G. M. Patterning proteins and cells using soft lithography. *Biomaterials* **1999,** *20,* 2363-2376.

[3] Seigel, R. R.; Harder, P.; Dahint, R.; Grunze, M.; Josse, F.; Mrksich, M.; Whitesides, G. M. On-line detection of nonspecific protein adsorption at artificial surfaces. *Anal. Chem.***1997**, *69*,3321-3328.

[4] Veiseh, M.; Zhang, Y.; Hinkley, K.; Zhang, M. Q. Two-dimensional protein micropatterning for sensor applications through chemical selectivity technique *Biomedical Microdevices* **2001**, *3*, 45-51.

[5] Veiseh, M.; Zhang, M. Effect of silicon oxidation on long-term cell selectivity of cell-patterned Au/SiO_2 platforms. *J. Am. Chem. Soc.* **2006**, *128*, 1197-1203.

[6] Nuzzo, R. G.; Dubois, L. H.; Allara, D. L. Fundamental studies of microscopic wetting on organic surfaces. 1. Formation and structural characterization of a self-consistent series of polyfunctional organic monolayers. *J. Am. Chem. Soc.* **1990,** *112,* 558-569.

[7] Malem, F.; Mandler. D.; Self-assembled monolayers in electoanalytical chemistry: application of ω-mercapto carboxylic acid monolayers for the electrochemical detection of dopamine in the presence of high concentration of ascorbic acid. *Analytical Chemistry* **1993,** *65,* 37-41.

[8] Lahiri, J.; Isaacs, L.; Tien, J.; Whitesides, G. M. A strategy for the generation of surfaces presenting ligands for studies of binding based on an active ester as a common reactive intermediate: A surface plasmon resonance study. *Anal. Chem.* **1999,** *71,* 777-790.

[9] Ista, L. K.; Callow, M. E.; Finlay, J. A.; Coleman, S. E.; Nolasco, A. C.; Simons, R. H.; Callow, J. A.; Lopez, G. P. Effect of substratum surface chemistry and surface energy on attachment of marine bacteria and algal spores. *Applied and Environmental Microbiology* **2004,** *70,* 4151-4157.

[10] Cheng, S. S.; Scherson, D. A.; Sukenik, C. N. In situ attenuated total reflectance fourier transform infrared spectroscopy of carboxylate-bearing, siloxane anchored, self-assembled monolayers: a study of carboxylate reactivity and acid-base properties. *Langmuir* **1995,** *11,* 1190-1195.

[11] Wasserman, S. R.; Tao, Y.-T.; Whitesides, G. M. Structure and reactivity of alkylsiloxane monolayers formed by reaction of alkyltrichlorosilanes on silicon substrates. *Langmuir* **1989,** *5,* 1074.

[12] Faucheux, N.; Tzoneva, R.; Magel, M.-D.; Groth, R. The dependence of fibrillar adhesions in human fibroblasts on substratum chemistry, *Biomaterials* **2006,** *27,* 234-245.

[13] Fryxell, G. E.; Rieke, P. C.; Wood, L. L.; Engelhard, M. H.; Williford, R. E.; Graff, G. L.; Campbell, A. A.; Wiacek, R. J.; Lee, L.; Halverson, A. Nucleophilic displacements in mixed self-assembled monolayers, *Langmuir* **1996,** *12,* 5064-5075.

[14] Masson, J.-F.; Battaglia, T. M.; Davidson, M. J.; Kim, Y.-C.; Prakash, A. M. C.; Beaudoin, S.; Booksh, K. S. Biocompatible polymers for antibody support on gold surfaces. *Talanta* **2005**, *67*, 918-925.

[15] Dai, J; Bao, Z.; Sun, L.; Hong, S. U.; Baker, G. L.; Bruening, M. L. High-capacity binding of proteins by poly(acrylic acid) brushes and their derivatives. *Langmuir* **2006**, *22*, 4274-4281.

[16] Wang, C.; Zhang, Y. Protein micropattering via self-assembly of nanoparticles. *Adv. Mater.* **2005**, *17*, 150-153.

[17] Senaratne, W.; Sengupta, P.; Harnett, C.; Craighead, H.; Baird, B.; Ober, C. K. Molecular templates for bio-specific recognition by low-energy electron beam lithography. *Nanobiotechnology* **2005**, *1*, 23-34.

[18] Gómez, R.; Bashir, R.; Sarikaya, A.; Ladisch, M. R.; Sturgis, J.; Robinson, J. P.; Geng, T.; Bhunia, A. K.; Apple, H. L.; Wereley, S. Microfluidic biochip for impedance spectroscopy of biological species, *Biomedical Microdevices* **2001,** *3,* 20l-209.

[19] Gómez, R.; Bashir, R.; Bhunia, A.K. Microscale electronic detection of bacterial metabolism, *Sensors and Actuators B* **2002,** *86,* 198-208.

[20] Boukherroub, R.; Wojtyk, J. T. C.; Wayner, D. D. M.; Lockwoodb, D. J. Thermal hydrosilylation of undecylenic acid with porous silicon, *J. Electrochem. Soc.* **2002,** *149,* H59-H63.

[21] Voicu, R.; Boukerroub, R.; Bartzoka, V.; Ward, T.; Wojtyk, J. T. C.; Wayner, D. D. M. Formation, characterization, and chemistry of undecanoic acid-terminated silicon surfaces: patterning and immobilization of DNA. *Langmuir* **2004,** *20,* 11713-11720.

[22] Asanuma, H.; Lopinski, G. P.; Yu, H.-Z. Kinetic control of the photochemical reactivity of hydrogen-terminated silicon with biofunctional molecules. *Langmuir* **2005,** *21,* 5013-5018.

[23] Asanuma, H.; Noguchi, H.; Uosaki, K.; Yu, H.-Z. Structure and reactivity of alkoxylcarbonyl (ester)-terminated monolayers on silicon: sum frequency generation spectroscopy. *J. Phys. Chem. B* **2006,** *110,* 4892-4899.

[24] Hyun, J.; Ma, H.; Banerjee, P.; Cole, J.; Gonsalves, K.; Chilkoti, A. Micropatterns of a cell-adhesive peptide on an amphiphilic comb polymer film. *Langmuir* **2002,** *18,* 2975-2979.

[25] Ostuni, E.; Chapman, R. G.; Holmli, R. E.; Takayama, S.; Whitesides, G. M. A survey of structure-property relationships of surfaces that resist the adsorption of proteins. *Langmuir* **2001,** *17,* 5605-5620.

[26] Sharma, S.; Johnson, R. W.; Desai, T. A. XPS and AFM analysis of antifouling PEG interfaces for microfabricated silicon biosensors. *Biosensors and Bioelectronics* **2004,** *20,* 227-239.

[27] Herrwerth, S.; Eck, W.; Reinhardt, S.; Grunze, M. Factors that determine the protein resistance of oligoether self-assembled monolayers—Internal hydrophilicity, terminal hydrophilicity, and lateral packing density. *J. Am. Chem. Soc.* **2003**, *125*, 9359-9366.

[28] Bhatnagar, P.; Mark, S. S.; Kim, I.; Chen, H.; Schmidt, B.; Lipson, M.; Batt, C. A.; Dendrimer-scaffold-based electron-beam patterning of biomolecules, *Adv. Mater.* **2006,** *18,* 315-319.

[29] Katz, J. S.; Doh, J.; Irvine, D. J. Composition-tunable properties of amphiphilic comb copolymers containing protected methacrylic acid groups for multicomponent protein patterning. *Langmuir* **2006,** *22,* 353-359.

[30] López, G. P.; Biebuyck, H. A.; Härter, R.; Kumar, A.; Whitesides, G. M. Fabrication and imaging of two-dimensional patterns of proteins adsorbed on self-assembled monolayers by scanning electron microscopy. *J. Am. Chem. Soc.* **1993,** *115,* 10774-10781.

[31] Brode III, P. F.; Erwin, C. R.; Rauch, D. S.; Lucas, D. S.; Rubingh, D. N. Enzyme behavior at surfaces: Site-specific variants of subtilisin-BPN′ with enhanced surface stability. *J. Biol. Chem.* **1994,** *269,* 23538-23543.

[32] Bouaidat, S.; Berendsen, C.; Thomsen, P.; Petersen, S. G.; Wolff, A.; Jonsmann, J. Micropatterning of cell and protein non-adhesive plasma polymerized coatings for biochip applications. *Lab Chip* **2004,** *4,* 632-637.

[33] Lahiri, J.; Ostuni, E.; Whitesides, G. M. Patterning ligands on reactive SAMs by microcontact printing. *Langmuir* **1999,** *15,* 2055-2060.

[34] Ruiz-Taylor, L. A.; Martin, T. L.; Zaugg, F. G.; Witte, K.; Indermuhle, P.; Nock, S.; Wagner, P. Monolayers of derivatized poly(L-lysine)-grafted poly(ethylene glycol) on metal oxides as a class of biomolecules interfaces. *Proc. Natl. Acad. Sci. U.S.A.* **2001,** *98,* 852-857.

[35] Sorribas, H.; Padeste, C.; Tiefenauer, L. Photolithographic generation of protein micropatterns for neuron culture applications. *Biomaterials* **2002,** *23,* 893-900.

[36] Lee, L. M.; Heimark, R. L.; Guzman, R.; Baygents, J. C.; Zohar, Y. Low melting point agarose as a protection layer in photolithographic patterning of aligned binary proteins. *Lab Chip* **2006**, *6*, 1080-1085.

[37] Jun, Y.; Cha, T.; Guo, A.; Zhu, X.-Y. Patterning protein molecules on poly(ethylene glycol) coated Si(1 1 1). *Biomaterials* **2004,** *25,* 3503-3509.

[38] Delamarche, E.; Bernard, A.; Schmid, H.; Michel, B.; Biebuyck, H. Patterned delivery of immunoglobulins to surfaces using microfluidic networks. *Science* **1997,** *276,* 779-781.

[39] Patel, N.; Sanders, G. H. W.; Shakesheff, K. M.; Cannizzaro, S. M.; Daviews, M. C.; Langer, R.; Roberts, C.; Tendler, S. J. B.; Williams, P. M. Atomic force microscope analysis of highly defined protein patterns formed by microfluidic networks. *Langmuir* **1999,** *15,* 7252-7257.

[40] Zhang, G.J.; Tanii, T.; Zako, T.; Hosaka, T.; Miyake, T.; Kanari, Y.; Funatsu, T.; Ohdomari, I. Nanoscale patterning of protein using electron beam lithography of organosilane self-assembled monolayers. *Small* **2005,** *1,* 833-837.

[41] Kumar, N.; Hahm, J. Nanoscale protein patterning using self-assembled diblock copolymers, Langmuir **2005,** *21,* 6652-6655.

[42] pK_a of MES is 6.269 at 25 °C. Roy, R. N.; Moore, C. P.; Carlsten, J. A.; Good, W. S.; Harris, P.; Rook, J. M.; Roy, L. N.; Kuhler, K. M. Second dissociation constant of two substituted aminomethanesulfonic acids in water from 5 to 55°C. *Journal of Solution Chemistry,* **1997,** *26,* 1209-1216.

[43] Ramakrishnan, A.; Dhamodharan, R.; Rühe, J. Controlled growth of PMMA brushes on silicon surfaces at room temperature. *Macromol. Rapid Commun.* **2002**, 23, 612-616.

[44] Coessens, V.; Pintauer, T.; Matyjaszewski, K. Functional polymers by atom transfer radical polymerization. *Prog. Polym. Sci.* **2001,** *26,* 337-377.

[45] Wu, T.; Genzer, J.; Gong, P.; Szleifer, I.; Vlček, P.; Šubr, V. Behavior of surface-anchored poly(acrylic acid) brushes with grafting density gradients on solid substrates. In *Polymer Brushes;* Advincula, R. C., Brittain, W. J., Caster, K. C., Rühe, J., Eds.; Wiley-VCH: Weinheim, 2004; pp 287-315.

[46] Matyjaszewski, K.; Miller, P. J.; Shukla, N.; Immaraporn, B.; Gelman, A.; Luokala, B. B.; Siclovan, T. M.; Kickelbick, G.; Vallant, T.; Hoffmann, H.; Pakula, T. Polymers at interfaces: using atom transfer radical polymerization in the controlled growth of homopolymers and block copolymers from silicon surfaces in the absence of untethered sacrificial initiator. *Macromolecules* **1999,** *32,* 8716-8724.

[47] Kurosawa, S.; Aizawa, H.; Talib, Z. A.; Atthoff, B.; Hilborn, J. Synthesis of tethered-polymer brush by atom transfer radical polymerization from a plasma-polymerized-film-coated quartz crystal microbalance and its application for immunosensors. *Biosensors and Bioelectronics* **2004,** *20,* 1165-1176.

[48] Treat, N. D.; Ayres, N.; Boyes, S. G.; Brittain, W. J. A facile route to poly(acrylic acid) brushes using atom transfer radical polymerization. *Macromolecules* **2006,** *39,* 26-29.

[49] Ashford, E. J.; Naldi, V.; O'Dell, R.; Billingham, N. C.; Armes, S. P. Novel routes to controlled structure water-soluble polymers: atom-transfer radical polymerization of sodium methacrylate in aqueous media. *Polymer Preprints (Am. Chem. Soc., Div. Polym. Chem.)* **1999,** *40,* 405-406.

[50] Ashford, E. J.; Naldi, V.; O'Dell, R.; Billingham, N. C.; Armes, S. P. First example of the atom transfer radical polymerisation of an acidic monomer: direct synthesis of methacrylic acid copolymers in aqueous media. *Chem. Commun.* **1999,** *14,* 1285-1286.

[51] Osborne,V.L.; Jones, D.M.; Huck, W T. S. Controlled growth of triblock polyelectrolyte brushes. *Chem. Commun.* **2002,** 1838-1839.

[52] Binding energy of the Na^+ 1s electron is expected to be about 1072.2 eV. [Hammond, J. S.; Holubka, J. W.; Devries, J. E.; Dickie, R. A. The application of X-ray photoelectron spectroscopy to a study of interfacial composition in corrosion-induced paint deadhesion. *Corros. Sci.* **1981,** *21,* 239].

[53] The binding energies of photoelectrons from CuBr and $CuBr_2$ are reported in the NIST X-ray Photoelectron Spectroscopy Database, Version 3.4, compiled and evaluated by Wagner, C. D.; Naumkin, A. V.; Kraut-Vass, A.; Allison, J. W.; Powell, C. J.; Rumble, J. R. and available online at http://srdata.nist.gov/xps.

[54] Hysemann, M.; Morrison, M.; Benoit, D.; Frommer, J.; Mate, C. M.; Hinsberg, W. D.; Hedrick, J. L.; Hawker, C. J. Manipulation of surface properties by patterning of covalently bound polymer brushes. *J. Am. Chem. Soc.* **2000,** *122,* 1844-1845.

[55] Beamson, G.; Briggs, D. High Resolution XPS of Organic Polymers - The Scienta ESCA300 Database, John Wiley & Sons: Chichester, 1992.

[56] High ionic strength solution is expected to result in desorption of physically adsorbed protein (cf. Wittemann, A.; Haupt, B.; Ballauf, M. Adsorption of protein on

spherical polyelectrolyte brushes in aqueous solution, *Phys. Chem. Chem. Phys.* **2003,** *5,* 1671-1677).

[57] Wissink, M. J. B.; Beernink, R.; Pieper, J. S.; Poot, A. A.; Engbers, G. H. M.; Beugeling, T.; van Aken, W. G.; Feijen, J. Immobilization of heparin to EDC/NHS-crosslinked collagen. Characterization and in vitro evaluation, *Biomaterials* **2001,** *22,* 151-163.

[58] Patrickios, C. S.; Yamasaki, E. N. Polypeptide amino acid composition and isoelectric point, *Analytical Biochemistry* **1995,** *231,* 82-91.

[59] Rao, S. V.; Anderson, K. W.; Bachas, L. G. Oriented immobilization of proteins. *Mikrochim. Acta.* **1998,** 128, 127-143.

[60] Rao, S. V.; Anderson, K. W.; Bachas, L. G. Controlled layer-by-layer immobilization of horseradish peroxidase. *Biotechnology and Bioengineering* **1999**, *65*, 389-396.

[61] Hiller, Y.; Gershoni, J. M.; Bayer, E. A.; Wilchek, M. Biotin binding to avidin. *Biochem. J.* **1987,** *248,* 167-171.

[62] Nehilla, B. J.; Popat, K. C.; Vu, T. Q.; Chowdhury, S.; Standaert, R. F.; Pepperberg, D. R.; Desai, T. A. Neurotransmitter analog tethered to a silicon platform for neuro-BioMEMS applications. *Biotechnology and Bioengineering* **2004,** *87,* 669-674.

[63] De Lange, R. J.; Huang, T.-S. Egg white avidin. *J. Biol. Chem.* **1971,** *246,* 698-709.

[64] Bruch, R. C.; White, H. B., III, Compositional and structural heterogeneity of avidin glycopeptides, *Biochemistry* **1982**, *21*, 5334-5341.

[65] Bomben, K. D.; Dev, S. B. Investigation of poly(L-amino acids) by X-ray photoelectron spectroscopy. *Anal. Chem.* **1988**, *60*, 1393-1397.

[66] Amino acid residues with aromatic rings are expected to show shakeup satellite peaks due to $\pi \rightarrow \pi^*$ excitation of the valence electrons. The shakeup satellite peak is

usually seen near 291 eV for phenyl rings. Bomben and Dev (ref. 62) have reported that, in the case of phenylalanine, tryptophan and tyrosine, the intensity of the shakeup satellite was bout 2 % of the total carbon intensity. These residues contribute to only about 17.5 % of the carbon atoms in avidin, so that the intensity of the shakeup satellites would be less than 0.5 % of the total carbon intensity. As such, no satellite peaks were observed near 291 eV.

[67] In addition to lysine, arginine and proline, each of which contains one carbon of the C̲N type (per residue), curve-fitting indicated that the α-carbon atoms along the protein backbone also contributed to the C̲N peak. All the carbon atoms in the phenyl group of phenylalanine, the indole group of tryptophan, and the phenol group of tyrosine were considered to be of the hydrocarbon type, in accordance with the analysis of Bomben and Dev (ref. 65). The carbon atoms in the imidazole group of histidine were similarly reckoned as C–C carbon atoms. The carboxylic C̲=O carbon atoms are expected from the aspartic acid and glutamic acid residues in avidin. However, we did not attempt to determine the percentage of PAA carboxylic acid groups that have reacted with the avidin amine groups. The number of amide linkages so formed will be small in comparison to the amide carbon atoms of the protein backbone, and the curve-fitting analysis is not sensitive enough to detect such small differences.

[68] Ebersole, R. C.; Miller, J. A.; Moran, J. R.; Ward, M. D. Spontaneously formed functionally active avidin monolayers on metal surfaces: a strategy for immobilizing biological reagents and design of piezoelectric biosensors. *J. Am. Chem. Soc.* **1990**, *112*, 3239-3241.

[69] Tan, Z.; Xia, Y.; Zhao, M.; Liu, X. Electron stopping power and inelastic mean free path in amino acids and protein over the energy range of 20–20,000 eV. *Radiat. Environ. Biophys.* **2006**, *45*, 135-143.

[70] To estimate the percentage contribution of avidin monolayer to C 1s peak area, a two-layer model was assumed wherein the top avidin monolayer, with a thickness of 4.8 nm, completely covers the bottom layer of pure PAA. The intensity of photoelectrons originating from a surface layer with a thickness, *d*, of 4.8 nm (and hence from the avidin layer) is given by $1–\exp(–d/\lambda)$, where λ is the electron escape depth. The inelastic mean free path (IMFP) of electron at a kinetic energy of about 1200 eV (close to kinetic energy of C 1s photoelectrons) was used as an estimate of the electron escape depth. The IMFP of electrons in protein was obtained from reference 69. It should be noted that the IMFP of electron in poly(acrylic acid) is quite similar (~ 3.2 nm).

[71] Czeslik, C.; Jackler, G.; Steitz, R.; von Grünberg H.-H. Protein binding to like-charged polyelectrolyte brushes by counterion evaporation. *J. Phys. Chem. B* **2004**, *108*, 13395-13402.

[72] Rosenfeldt, S.; Wittemann, A.; Ballauff, M.; Breininger, E.; Bolze, J.; Dingenouts, N. Interaction of proteins with spherical polyelectrolyte brushes in solution as studied by small-angle x-ray scattering. *Phys. Rev. E* **2004,** *70,* 61403.

[73] Lee, M. H.; Brass, D. A.; Morris, R.; Composto, R. J.; Ducheyne, P. The effect of nonspecific interactions on cellular adhesion using model surfaces. *Biomaterials* **2005,** *26,* 1721-1730.

CHAPTER 3

DISSOCIATION BEHAVIOR OF WEAK POLYELECTROLYTE BRUSHES ON A PLANAR SURFACE

Reproduced in part from: Dong, R.; Lindau, M.; Ober, C. K. *Langmuir* **2009,** 25, 4774-4779.

Abstract

Poly(acrylic acid) (PAA) brushes and poly(methacrylic acid)(PMAA) brushes on gold substrates were synthesized by surface-initiated atom transfer radical polymerization of sodium acrylate and sodium methacrylate in water media at room temperature. Fourier transform infrared spectroscopy (FTIR) titration and contact angle titration methods were used in combination to investigate the dissociation behavior of these two brushes. While FTIR titration gives effective bulk pK_a values of the polyacid brushes (pK_a^{bulk} of PAA brushes is 6.5-6.6, pK_a^{bulk} of PMAA brushes is 6.9-7.0), contact angle titration provides effective surface pK_a of the brushes (pK_a^{surf} of PAA brushes is 4.4 ± 0.01, pK_a^{surf} of PMAA brushes is ~ 4.6 ± 0.1). The difference between pK_a^{bulk} and pK_a^{surf} suggests that acid groups further from the substrate surface are easier to ionize and have smaller pK_a values. Angle-resolved X-ray photoelectron spectroscopy (ARXPS) was used to achieve the depth profile of charge distribution within PAA brushes. Although such behavior of weak polyelectrolyte brushes has been predicted by theoretical simulation, here we provide the first experimental evidence of this behavior.

Key words: FTIR titration, contact angle titration, poly(acrylic acid) brush, poly(methacrylic acid) brush, charge fraction

Introduction

Smart responsive surfaces can change their surface properties upon exposure to different environments, including a variety of solvents, aqueous media with different pH values, ionic strength, or temperature. Such surfaces have attracted recent interest because of their potential applications in drug delivery, biosensors, tissue engineering, colloidal stabilization and the like.[1] In particular, polyelectrolyte brushes have gained much attention due to their unique and complex physical properties.[1] Such systems generally remain poorly understood, despite significant efforts to better understand them, due partially to limitations of available characterization techniques. Among many physical properties, dissociation behavior of polyelectrolyte brushes is of particular interest because it is directly related to most of the applications of charged polymer brushes. Gaining a better understanding and control over the dissociation behavior of these brushes is very important. However, titration of acid or base groups on surfaces is not as straightforward as in solution. It is almost impossible to directly monitor the proton concentration within polymer brushes by common solution methods, for example, using a pH meter or pH indicator. Previous work has studied the dissociation behavior of functional groups on surfaces, primarily with self-assembled monolayers and polymer films bearing carboxylic acid groups. The most commonly used titration techniques are FTIR,[2,3] contact angle measurements,[4,5] chemical force microscopy,[6] and electrochemical methods.[7] For polymer brushes, the degree of brush swelling[8] and the polymer brush surface pressure[32] were reported to change with the pH of the surrounding solution, which provides more methods to study dissociation behavior of polymer brushes. Among these titration methods, contact angle and chemical force microscopy are only sensitive to the uppermost layer of polymer brushes and determine the effective pK_a of functional groups in the uppermost layer of the brush, which we define as effective pK_a^{surf}. On the other hand,

FTIR, and swelling behavior studies examine the entire brush layer, providing effective pK_a of the bulk polymer brushes, defined as effective pK_a^{bulk} in this paper. Theoretical simulations have shown that the fraction of charged groups within weak polyelectrolyte brushes increased with the distance from the substrate surface when the brushes are partially charged, [9,10,11,27] which leads to the prediction that pK_a^{bulk} is larger than pK_a^{surf}. Here, we combined both FTIR and contact angle titration to investigate pK_a values of polyelectrolyte brushes and our results show that indeed effective pK_a^{bulk} values do exceed effective pK_a^{surf} values by ~ 2 units for both PAA brushes and PMAA brushes. As far as we know, this is the first experimental evidence for the variation of charge fraction within weak polyelectrolyte brushes.

In this study, surface-initiated atom transfer radical polymerization (ATRP) was used to synthesize both PAA brushes and PMAA brushes on gold surfaces using a previously reported procedure.[12] The brush-modified gold substrates were incubated in buffer solution at different pH values and then characterized by grazing angle FTIR and contact angle measurements. FTIR titration results show that the effective pK_a^{bulk} of PAA brushes is 6.5-6.6 and the effective pK_a^{bulk} of PMAA brushes is 6.9-7.0. Contact angle titration reveal that the effective pK_a^{surf} of PAA brushes is 4.4 ± 0.01 and the effective pK_a^{surf} of PMAA brushes is 4.6 ± 0.1. These results clearly show that carboxylic acid groups further away from the substrate surface have a smaller pK_a and are more easily ionized. ARXPS of PAA brushes provided a detailed depth profile of charge distribution within PAA brushes. The factors determining this behavior of weak polyelectrolyte brushes will be discussed in detail later in the paper. We hope that this paper can shed light on the complex behavior of weak polyelectrolyte brushes and provide useful information for research utilizing such polymer brushes in the future.

Experimental section

Materials: 11-mercapto-1-undecanol, 2-bromo-2-methylpropionyl bromide, anhydrous pyridine, sodium acrylate, sodium methacrylate, 2,2′-bipyridine, copper (Ⅰ) bromide (CuBr), copper (Ⅱ) bromide ($CuBr_2$), 4-morpholineethanesulfonic acid (MES), sodium hydroxide, and ethylene diamine tetracetic acid (EDTA) and all solvents used were purchased from Sigma-Aldrich. All chemicals were used without further purification. Distilled deionized water and high-purity nitrogen gas (99.99 %, Airgas) were used throughout. A 1M sodium hydroxide solution was used to adjust pH of 0.1 M MES buffer solution into desired values and the accurate pH values were measured by pH meter at room temperature. The gold (~1000 Å) coated silicon wafers (4" diameter) with a titanium adhesion layer were purchased from Platypus Technologies. The wafers were cut into 1 cm x 2cm pieces before usage.

Synthesis of surface initiator and immobilization of initiator: Surface initiator was synthesized as described.[13] Gold substrates were rinsed with acetone, blown dry with nitrogen gas and cleaned using a Harrick Plasma Cleaner for 1- 2 minutes. The cleaned gold substrates were rinsed with ethanol, blown dry with nitrogen gas and kept in 1 mM initiator solution in anhydrous ethanol overnight under nitrogen. Before surface initiated polymerization, the gold substrates were taken out of the initiator solution, rinsed with ethanol and blown dry.

Surface initiated polymerization of sodium acrylate and sodium methacrylate: The gold substrates with initiator on were placed in a dry Schlenk flask. The flask was evacuated and back-filled with nitrogen three times. Sodium acrylate (1.88 g, 20 mmol), CuBr (28.7 mg, 0.2 mmol), $CuBr_2$ (9.0 mg, 0.04 mmol), and 2,2′-bipyridine (78.4 mg, 0.48 mmol) were added to another 25 mL Schlenk flask equipped with a magnetic stir bar. This flask was evacuated and backfilled with nitrogen three times concurrently with last flask. DI water (4 mL)with pH ~ 9[14] (pH was adjusted by 1 M

sodium hydroxide solution) was bubbled with nitrogen gas for at least 30 minutes, then transferred into the Schlenk flask containing sodium acrylate using a cannula. The mixture was stirred at room temperature under nitrogen for about 10 min until a viscous brown solution was obtained. The solution was then transferred by cannula into the Schlenk flask containing the gold substrates. Polymerization was carried out at room temperature for about 15 minutes, after which the substrates were taken out of the solution, rinsed with DI water thoroughly, sonicated in 0.1M EDTA solution gently for 1-2 minutes using a Fisher Ultrasonic Cleaner (Model FS6) to remove copper ions which might trapped inside the brushes. The films were then rinsed with water and ethanol and blown dry under nitrogen gas. In the case of polymerization of sodium methacrylate, every step is the same except that 2.12g of sodium methacrylate (20mmol) was used instead of 1.88g of sodium acrylate. The polymer brush-modified gold substrates were characterized by Grazing-angle Reflectance FTIR and contact angle measurement as described below.

Grazing-angle Reflectance FTIR titration of polyacid brushes on gold surfaces: Gold substrates covered by polymer brushes were incubated in MES buffer solutions with different pH values for about 10 minutes and then sonicated for 1 minute, after which the substrates were rinsed with anhydrous ethanol quickly and immediately blown dry with nitrogen gas. The substrates were then characterized using a VERTEX 80v vacuum FT-IR spectrometer from Bruker Optics equipped with a liquid nitrogen-cooled Mercury Cadmium Telluride (MCT) detector. Before collecting data, the system was left in vacuum for 10 minutes to minimize signal noise from air. IR spectra were taken with 2 cm^{-1} using 256 scans at 75° incident angle. Spectra from bare gold substrates were used for background. OPUS viewer was used to analyze FTIR spectra and Sperkwin32 was used to integrate peak areas in the spectra.

Contact angle titration of polyacid brushes on gold substrates: Gold substrates modified with polymer brushes were treated in the same manner as in the FTIR section before contact angle measurement. The advancing contact angle of buffer solution (same as the solution used to treat substrates) was measured on the polymer brush-covered substrate surface. All contact angles were measured using a NRL contact angle goniometer model 100-00 (Rame´-Hart Inc.), and values were averaged over several measurements in different locations. The differences between each measurement at a certain pH value were smaller than 3˚. All the FTIR and contact angle measurements were done at room temperature.

ARXPS of PAA brushes: Substrates covered with PAA brushes were pretreated with buffer solution (pH ~ 5.75, pH was adjusted by 1M KOH solution) in the same manner as describe above. X-ray photoelectron spectroscopy (XPS) measurements were performed using a SSX-100 instrument (Surface Science Instruments, Inc.) with a monochromatized Al Kα X-ray source (1486.6 eV) operating in a vacuum of 1×10^{-9} Torr. The spectra were acquired at various electron emission angles (electron emission along the surface normal). Charge neutralization was carried out by injection of low energy electrons. The spectra were analyzed using CasaXPS v. 2.1.9 software. Data fitting were done using ARXPS version 7.

Results and discussion

Polyacid brush synthesis: Both PAA and PMAA brushes were synthesized using surface-initiated ATRP in water media as described previously. It has been demonstrated that brush growth of sodium methacrylate by surface-initiated ATRP in water media depends on the monomer concentration, temperature and pH of the polymerization media.[14] When the polymerization is performed at pH ~ 9, the polymer brushes grow faster than at pH ~ 8, and the polymerization is more easily controlled than at pH 10. We found a large increase in brush thickness when the pH was adjusted

to 9. After only 15 minutes of polymerization, the thickness of the PAA brush was ~ 55 nm and the thickness of the PMAA brush was ~ 60nm. Thickness of polymer brushes was measured using a Woollam variable angle spectroscopic ellipsometer. A three layer model consisting of a 0.5 mm silicon layer, a 100 nm gold layer and a Cauchy layer, to represent the brush layer, was used to determine both the thickness and refractive index of the brush.

FTIR titration of polyacid brushes: Protonated carboxylic acid groups and deprotonated carboxylate groups absorb infrared light at different wavelengths, which allows the use of FTIR analysis to assess the degree of dissociation of carboxylic acid groups. FTIR titration has been used previously to study the pK_a of carboxylic acid terminated self-assembled monolayers (SAMs)[3] and spin-coated polymer films containing carboxylic acid groups.[2] FTIR has also been used to investigate the interaction of PMAA brushes with metal ions,[15] where Rühe et al. utilized FTIR to quantify the degree of dissociation of PMAA brushes in solution with a variety of metal ions at different concentrations. Their experiments have shown that at neutral pH, the dissociation of carboxylic acid groups in PMAA brushes increases with salt concentration and decreases with grafting density. Here we determined the degree of dissociation of both PAA and PMAA brushes at different pH values using FTIR.

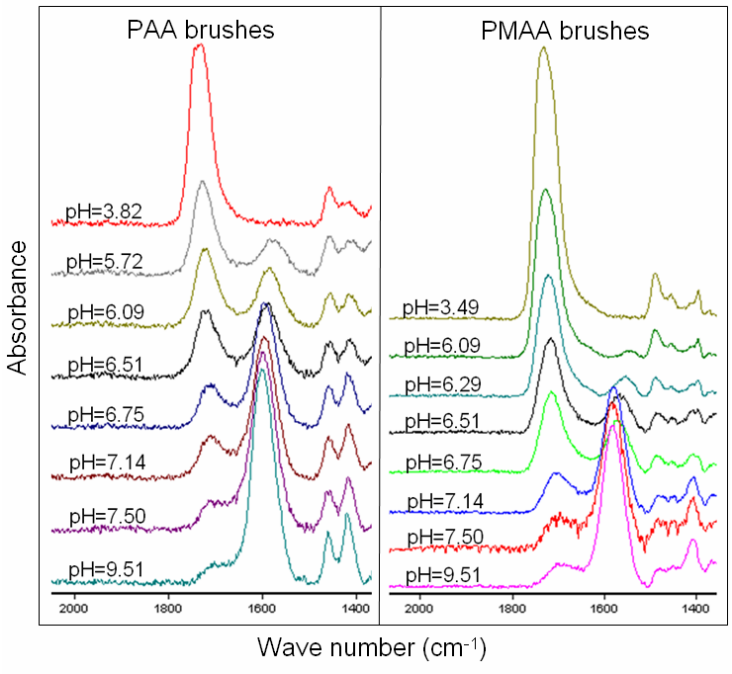

Figure 3.1. Grazing-angle reflectance FTIR spectra of PAA brushes and PMAA brushes on gold surfaces treated with buffer solutions at different pH values (only the carbonyl absorption region is shown).

Figure 3.1 shows a portion of the infrared spectrum for a series of PAA brushes and PMAA brushes treated with different buffer solutions. At pH < 4, carboxylic acid groups in the brushes are protonated and show the characteristic band peak at around 1732 cm^{-1}(C=O stretching of COOH), which decreases with pH. The size of an absorbance peak at ~1550 cm^{-1} (asymmetric stretching band of COO^-) increases with increasing pH.

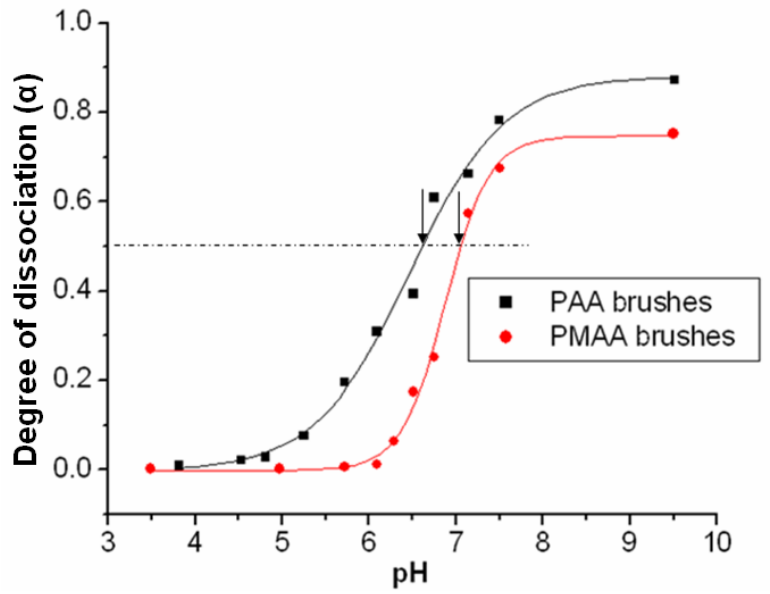

Figure 3.2. FTIR titration curves for PAA brushes (black filled squares) and PMAA brushes (red filled circles) on gold substrates. The arrows indicate the effective pK_a^{bulk} of PAA brushes and PMAA brushes corresponding to α = 0.5.

After integration of peak area, the degree of dissociation, α, was derived from Equation 1 as shown below. [29]

$$\alpha = [COO-] / \langle [COO-] + [COOH] * \varepsilon(COO-) / \varepsilon(COOH) \rangle \quad (1)$$

[COOH] and [COO-] are the integrated area of COOH and deprotonated COO- group in the FTIR spectra; $\varepsilon(COO-)$ and $\varepsilon(COOH)$ are extinction coefficients of the carboxylate and carboxylic acid peaks, respectively. According to Rühe et al.,[15] $\varepsilon(COO-)/\varepsilon(COOH)$ is ~ 1.8, which was used in our calculation. Titration curves of polyacid brushes were constructed by plotting the dissociation α versus pH, as shown in Figure 3.2.

Titration curves were obtained by fitting data points using the Sigmoid function. The pK_a^{bulk} value calculated from the curve varies depending on how it is defined. If pK_a is defined as the pH at which the degree of dissociation α = 0.5, the effective

pK_a^{bulk} of PAA brushes is ~ 6.6, and the effective pK_a^{bulk} of PMAA brushes is ~ 7.0. If pK_a is defined as pH at the mid-point of a titration curve, the effective pK_a^{bulk} of PAA brushes is 6.5 ± 0.1, and the effective pK_a^{bulk} of PMAA brushes is 6.9 ± 0.03. The pK_a^{bulk} values of polyacid brushes found here are larger than the pK_a of polyacids in solution reported in the literature. [16,17] The larger pK_a values of polyacid brushes are due to the unique properties of polymer brushes: high grafting density and polymer chain segment density, which lead to very little free volume. Because of the limited available volume, charged brushes must extend from the surface due to electrostatic repulsion with simultaneous loss of entropy of the associated counterions. To gain greater entropy and also to reduce the energy cost from repulsion, it is favorable for many acid groups within the brushes to remain uncharged at the cost of free energy of the acid-base reaction, thus minimizing the energy of the whole system.[9] As shown in Figure 3.1, it is very obvious that the absorption peak of undissociated carboxylic acid groups is still evident at pH values as high as 9.5. According to the simulation results of Uhlík et al.,[28] a non-negligible fraction of nondissociated carboxylic acid groups still exist close to the polystyrene core in micelles formed by polystyrene-block-poly(methacrylic acid) in aqueous solution at pH higher than pK_a of PMAA brushes, which was assumed to be 4.69 in their paper. Our observation again suggests that the acid groups buried in weak polyacid brushes near the substrate surface are very difficult to dissociate. It has to be pointed out that pK_a^{bulk} of weak polyacid brushes depends on many parameters. In addition to the acidity of the acid groups and ionic strength of the surrounding solution,[18] grafting density and thickness of the brushes also effects the pK_a^{bulk} of polyacid brushes.[10] In this paper, the incubation buffer solution is 0.1 M MES buffer solution and the pH of the solution is adjusted by 1 M sodium hydroxide solution. The thickness of PAA brushes used is ~ 55 nm and the thickness of PMAA brushes used is ~ 60 nm for all the surfaces used in the

experiment. When thickness and grafting density of the brushes change, different apparent pK_a^{bulk} values would be expected. One could study the relation between pK_a^{bulk} and such parameters by measuring pK_a^{bulk} of brushes at different thickness or grafting density. However, that is beyond the scope of this paper.

Contact angle titration of polyacid brushes: Whitesides et al.[19] have used contact angle values to study acid-base behavior of carboxylic acid groups attached to a polyethylene surface. They have demonstrated that surfaces with different degrees of ionization have different surface energy, and therefore have different contact angles. After their seminal work, contact angle titration has been used broadly to obtain the pK of self-assembled monolayers terminated by acid groups or basic groups.[20, 5, 21] Minko et al.[22] have also shown that contact angle values on weak polyelectrolyte brush surfaces changed with the pH of a bath solution used to treat the brushes.

Although theoretical correlation between surface ionization degree and contact angle might needs further perfection, contact angle titration method was proved to be very useful to study dissociation behavior of surfaces. Motivated by these studies, we decided to use contact angle titration to probe surface pK_a of polyacid brushes. Creager et al.[5] compared: i) a nonreactive spreading protocol, where samples were first pretreated with a solution identical to the buffered water droplets used for contact angle measurements, and ii) a reactive spreading protocol, where samples were not pretreated. Their results demonstrated that contact angle titration data acquired using nonreactive spreading protocol exhibited a smooth transition in contact angle between plateau regions at low and high pH.

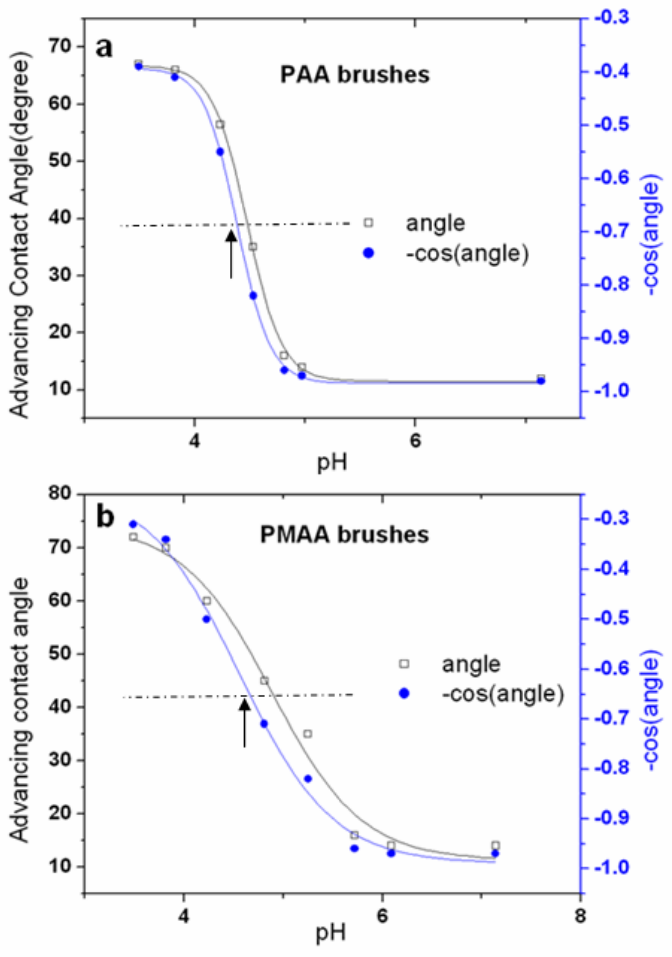

Figure 3.3. Contact angle titration curves measured using nonreactive spreading protocol for PAA brushes (graph a) and PMAA brushes (graph b) on gold substrates. The black rectangles correspond to the contact angle (θ) data points and the blue filled circles correspond to -cos(θ) data points. The arrows indicate the effective pK_a^{surf} of polyacid brushes in cos(θ) curves.

Here, we applied nonreactive spreading protocols for contact angle titration of polyacid brushes at different pH values ranging from 3 to 8. To avoid polymer chain cleavage due to hydrolysis of ester bonds, pH lower than 3 was not used. The contact angle titration curves for PAA brushes and PMAA brushes were shown below in

Figure 3.3. Titration curves were obtained by fitting data points using the Sigmoid function. According to Creager et al.,[5] cos(θ) has a linear relation with dissociation degree α. They plotted cos(θ) versus pH to construct titration curves. However, Homes-Farley et al. also plotted contact angle θ versus pH to obtain contact angle titration curves.[23] As shown in Figure 3.3, we compared the two types of titration curves achieved by plotting both cos(θ) and θ versus pH for each polymer brush. For both brushes, pK_a values derived from cos(θ) curves are slightly smaller than those from the contact angle θ curves. Homes-Farley et al.[23] also compared correlations between cos(θ) and the hydrophilicity of functional groups (π) with correlations between θ and π. They concluded that cos(θ) had better correlation with π than did θ, which might suggest that cos(θ) can better describe hydrophilicity of functional groups, and we therefore uses the pK_a values derived from cos(θ) curves in this paper. As mentioned before, the pK_a values determined by contact angle titration should give the pK_a of acid groups in the very uppermost layer of the brushes (pK_a^{surf}). From Figure 3.3, the effective pK_a^{surf} of PAA brushes is 4.4 ± 0.01; effective pK_a^{surf} of PMAA brushes is 4.6 ± 0.1. These values are considerably lower than most reported pK_a values of SAMs terminated by carboxylic acid groups,[4, 5, 20] but very close to pK_a of the corresponding monomers (pK_a of acrylic acid is 4.26;[24] pK_a of methacrylic acid is 4.69[25]). Significant effort has been made by other researchers to explain the larger pK_a of SAMs terminated by carboxylic acid groups. One hypothesis is that the hydrophobic and non-polar hydrocarbon chain segment between acid groups and the substrate surface created "hydrophobic pockets" around the carboxylic acid groups where the solvation of carboxylate anions is disfavored.[5,20] Creager et al.[5] and Liu et al.[20] have studied the relation between pK_a of acid-terminated SAMs and the length of the hydrocarbon chain between the substrate and functional groups. Both studies found that pK_a increases with the number of carbon units in the hydrocarbon chain,

which highlighted the important effect on pK_a of "hydrophobic pockets" in close proximity to the weak acid groups. Nevertheless, such effect can almost be ignored in the polyacid brush system because of the polar and hydrophilic nature of polyacid chains. It has been found that poly(methacrylic acid) brushes were already in a swollen state at pH as low as 2. [26] In a swollen state, carboxylic acid groups near the surface of the polymer brush are surrounded by the aqueous environment, which provides these acid groups access to ions in the solution. This environment is very similar to small organic acid molecules in solution, which explains why the pK_a^{surf} of polyacid brushes is similar to the pK_a of the corresponding monomer. The captive bubble contact angle method[30] was also used to measure the contact angle of air bubbles on inverted polymer brush modified surfaces immersed in selected buffer solutions. Titration curves based on the captive bubble method gave very similar pK_a^{surf} values compared to the nonreactive spreading method. A detailed depth profile of dissociation degree at specific pH was studied using ASXPS as described below.

Variation of degree of dissociation within weak polyacid brushes: Israëls et al. used self-consistent mean-field theory to simulate behavior of grafted weak polyacids.[11] Following their important work, Szlefier et al. have done extensive theoretical simulations of weak polyelectrolyte brushes on planar surfaces.[9,10,27] Uhlík et al. have also used lattice Monte Carlo methods to study behavior of poly(methacrylic acid) brushes on spherical surfaces using polystyrene-block-poly(methacrylic acid) micelles in water as a model.[28] Although different methods were used, all of these simulations predicted that the charge fraction, or dissociation degree, of acid groups within weak polyacid brushes increased with the distance from substrate surface. Szlefier et al. attributed such behavior to the result of minimization of the free energy of the system. Uhlík et al.[28] proposed several factors resulting in such properties. One factor is the inhomogeneous volume fraction within polymer

brushes. Segment density is much larger towards the substrate surface,[9] which works in favor of uncharged species as explained before. Another factor is larger relative permittivity and better accessibility of solution ions towards the brush periphery. Dissociation of outer acid groups leads to a double-layer and creates a boundary potential that reduces further ion transport across the boundary, therefore affecting acid dissociation inside the polymer brush. Our results show that the effective pK_a^{surf} is about two units smaller than the effective pK_a^{bulk}, which implies that carboxylic acid groups further away from the substrate are much easier to ionize than the acid groups near the substrate interface. Such results match well with previous theoretical simulations. This is the first experimental evidence for variation of dissociation degree within weak polyacid brushes. Based on previous theoretical simulation and the experimental results in this paper, a simple cartoon is shown in Figure 3.4 to illustrate how dissociation degree and swelling behavior of weak polyacid brushes change with pH.

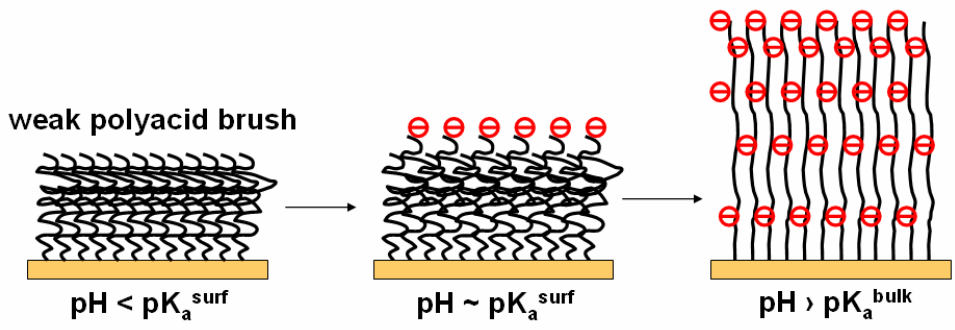

Figure 3.4: A cartoon (not to scale) showing how dissociation degree and swelling behavior of weak polyacid brushes change in solution at different pH

At pH values lower than pK_a^{surf}, all acid groups are protonated and the polymer brushes are relatively hydrophobic and collapsed, although the brushes are still in a swollen state. When the pH approaches pK_a^{surf}, acid groups in the uppermost layer

begin to ionize and the polymer brush surface becomes hydrophilic. Although the majority of the brushes remains collapsed, the ionized brush segments on the brush surface could stretch out into solution. When the pH increases to values around pK_a^{bulk}, more acid groups within the polyacid brushes become dissociated and the charge fraction of acid groups increases with distance away from substrate. When pH is larger than pK_a^{bulk}, most of the acid groups become charged, and the charged polymer chains stretch out as much as possible to reduce electrostatic repulsion. A small fraction of acid groups near the substrate still remained uncharged even at very high pH.

ARXPS characterization of partially charged PAA brush: ARXPS is a very useful nondestructive tool for depth profile analysis of near surface regions.[32] In the present work, we used ARXPS to characterize charge fraction of carboxylic acid groups along Z axis within PAA brushes pretreated with buffer solution. Figure 3.5 shows the C 1s spectrum of PAA brushes at emission angle (Φ) 0˚. All the spectra at different emission angles were fitted using a four-peak fitting model based on previous literature. Peak 3 and peak 4 are corresponding to COO^- and COOH accordingly. All the area percentage of four peaks at different emission angles were summarized in Table 3.1. Charge fraction of carboxylic acid groups was calculated using equation: $f = [\underline{C}OO^-]/([\underline{C}OO^-]+[\underline{C}OOH])$.

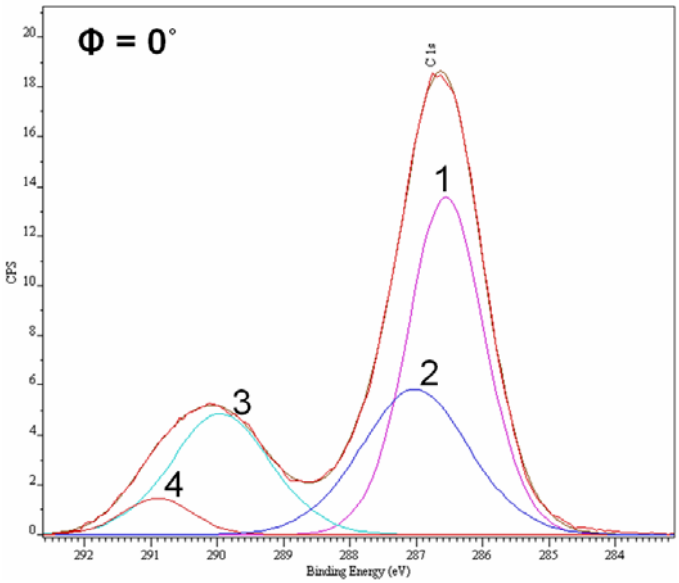

Figure 3.5: The C 1s spectrum of PAA brushes at emission angle 0˚ with a four-peak fit. Four peaks are corresponding to C-C/C-H, C-C=O, COO^-, COOH sequentially. The sample was pretreated with buffer solution at pH ~ 5.75.

Table 3.1: Area percentage of four peaks from the C 1s spectra of PAA brush at different emission angles

	C-C/C-H	C-C=O	COO^-	COOH
0˚	46.18	27.94	21.48	4.40
37˚	53.86	21.65	21.13	3.36
55˚	62.26	14.68	20.68	2.38
66˚	65.21	12.39	20.68	1.82

Figure 3.6a shows the relation between charge fraction (f) and emission angle. The theoretical fitting using model in Figure 3.6b matches with the experimental data very

well. As shown in Figure 3.6b, charge fraction in the top 2 nm layer almost remains the same. Then charge fraction decreases with depth almost linearly.

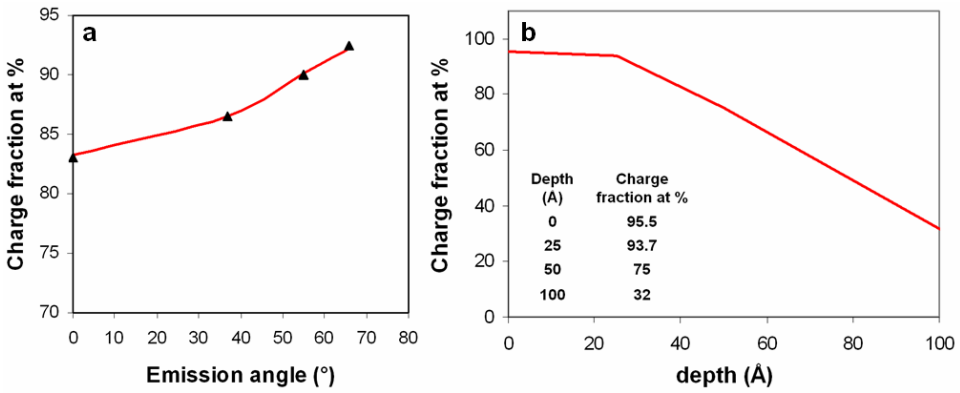

Figure 3.6. (a) Experimental dependence of charge fraction with emission angle, Φ. The curve is theoretical fit assuming the model shown in b. (b) Reconstructed depth profile of charge fraction within PAA brushes pretreated with buffer solution at pH ~ 5.75.

Conclusions

Surface-initiated atom transfer radical polymerization in water media was used to synthesize poly(sodium acrylate) brushes and poly(sodium methacrylate) brushes on gold surfaces. The fast polymerization results in polyacid brushes in 15 minutes with a thickness between 50 nm to 60 nm. These brushes were easily converted into PAA brushes and PMAA brushes by rinsing with thoroughly distilled water.

FTIR titration was used to determine effective bulk pK_a of the two polyacid brushes, defined as effective pK_a^{bulk}. Under the experimental conditions described in the paper, for PAA brushes, the effective pK_a^{bulk} is between 6.5 – 6.6; for PMAA brushes, the effective pK_a^{bulk} is between 6.9 – 7.0. Nonreactive contact angle titration was used to determine effective pK_a of the uppermost layer of polyacid brushes,

defined as effective pK_a^{surf}. For PAA brushes, the effective pK_a^{surf} is 4.4 ± 0.01 while for PMAA brushes, the effective pK_a^{surf} is 4.6 ± 0.1. The effective pK_a^{bulk} values of weak polyacid brushes are larger than the corresponding effective pK_a of polyacid chains in solution. However, the effective pK_a^{surf} values of weak polyacid brushes are similar to the pK_a of corresponding monomers, which are smaller than most reported pK_a values of SAMs bearing carboxylic acid groups on the chain end. Possible reasons for these differences are discussed in detail in this paper.

The large difference between the effective pK_a^{surf} and the effective pK_a^{bulk} provides the first experimental evidence for variation of the degree of dissociation within weak polyacid brushes on planar surfaces, although such behavior has been predicted previously in several theoretical simulations. The acid groups in the uppermost layer of weak polyacid brushes are easier to ionize than the acid groups buried near the substrate surface. Such properties could be very useful in varying charge density over the nanometer scale. Such aspects of polymer brushes may also play very important roles in studies involving interaction between nanomaterials on the interface and other systems sensitive to charges, such as biomolecules, cells, tissues, etc..

Acknowledgements

This research was supported by the NSF-funded Cornell Nanobiotechnology Center (NBTC). We have made use of the facilities at NBTC, Cornell NanoScale Science and Technology Facility (CNF), and Cornell Center for Materials Research (CCMR), all of which are supported by NSF. The NBTC support for RD and invaluable input from Joan K. Bosworth are gratefully acknowledged.

REFERENCES

[1] Handbook of Polyelectrolyes and Their Applications; Tripathy, S.; Kumar, J.; Nalwa, H.; Eds. American Scientific Publishers, 2002.

[2] Choi, J.; Rubner, M. F. *Macromolecules* **2005**, 38, 116-124.

[3] Gershevitz, Olga.; Sukenik, C.N. *J. Am. Chem. Soc.* **2004,** 126, 482-483.

[4] Holmes-Farley, S.R.; Reamey, R.H.; McCarthy, T.J.; Deutch, J.; Whitesides, G.M. *Langmuir* **1985**, 1, 725-740.

[5] Creager, S.E.; Clarke, J. *Langmuir* **1994**, 10, 3675-3683.

[6] Smith, D.A.; Wallwork, M.L.; Zhang, J.; Kirham, J.; Robinson, C.; Marsh, A.; Wong, M. *J. Phys. Chem. B* **2000**, 104, 8862-8870.

[7] Zhao, J.; Luo, L.; Yang, X.; Wang, E.; Dong, S. *Electroanalysis* **1999**, 11, 1108.

[8] Currie, E,P.K.; Sieval, A.B.; Avena, M.; Zuilhof, H.; SudhÖlter, E.J.R.; Cohen Stuart, M.A. *Langmuir* **1999**, 15, 7116.

[9] Nap, R.; Gong, P.; Szleifer, I. *J. Polym. Sci., Part B: Polym. Physics.* **2006**, 44, 2638-2662.

[10] Gong, P.; Genzer, J.; Szleifer, I. *Phys. Rev. Lett.* **2007,** 98, 018302.

[11] Israels, R.; Leermakers, F.A.M.; Fleer, G.J. *Macromolecules* **1994**,27, 3087-3093

[12] Dong, R; Krishnan, S.; Baird, B. A.; Lindau, M.; Ober, C. K. *Biomacromolecules* **2007,** 8, 3082-3092.

[13]Shah, R. R.; Merreceyes, D.; Husemann, M.; Rees, I.; Abbott, N.L.; Hawker, C. J.; Hedrick, J. L. *Macromolecules* **2000**, 33, 597-605.

[14] Tugulu, S.; Barbey, R.;Harms, M.; Fricke, M.; Volkmer, D.; Rossi, A.; Klok, H.- A. *Macromolecules* **2007,** *40,* 168-177.

[15] Konradi, R.; Rühe, J. *Macromolecules* **2005**, 38, 6954-6961.

[16] Colombani, O.; Ruppel, M.; Schubert,F.; Zettl, H.; Pergushov, D.V.;Axel H. E. Müller, A.H.E. *Macromolecules* **2007,** *40,* 4338-4350.

[17] Cho, J.; Hong, J.; Char, K.; Caruso F. *J. Am. Chem. Soc.* **2006**, 128, 9935- 9942.

[18] Smalley, J. F.; Chalfant, K.; Feldberg, S.W.; Nahir, T.M.; Bowden, E.F. *J. Phys. Chem. B* **1999,** *103,* 1676-1685.

[19] Holmes-Farley, S.R.; Reamey, R.H.; McCarthy, T.J.; Deutch, J.; Whitesides, G.M. *Langmuir* **1985**, 1, 725-740.

[20] Liu, Y.; Navasero, N.M.; Yu, H. *Langmuir* **2004**, 20, 4039-4050.

[21] Badre, C.; Mayaffre, A.; Letellier, P.; Turmine, M. *Langmuir* **2006**, 22, 8424-8430.

[22] Houbenov,N.; Minko,S.; Stamm**,** M. *Macromolecules* **2003,** *36,* 5897-5901.

[23] Holmes-Farley, S.R.; Bain, C.D.; Whitesides, G.M. *Langmuir* **1988**, 4, 921-937.

[24] Weast,R.C. *Handbook of Chemistry and Physics*, 69th edn (CRC Press, Inc., Boca Raton, Florida, 1988-1989)

[25] Lide, D.R. *CRC Handbook of Chemistry and Physics,* 76th ed. (CRC, Boca Raton, FL,1995).

[26] Biesalski,M.; Johannsmann, D.; Rühe, J. *J. Chem. Phys.* **2002,** 117, 4988-4994.

[27] Gong, P.; Wu, T.; Genzer, J.; Szleifer, I. *Macromolecules* **2007,** *40,* 8765-8773

[28] Uhlík, F.; Limpouchová, Z.; Jelínek, K.; Procházka, K. *J. Chem. Phys.* **2004**, 121, 2367-2375.

[29] Konradi, R.; Rühe, J. *Macromolecules* **2005**, 38, 6140-6151.

[30] Holly, F. J.; Refojo, M. F. *J. Biomed. Mater. Res.* **1975,** 9, 315-326.

[31] Li, F.; Balastre, M.; Schorr, P.; Argillier, J.-F.; Yang, J.; Mays, J. W.; Tirrell, M. *Langmuir* **2006,** *22,* 4084-4091.

[32]Alexandera, M.R.; Beamsonb, G.; Blomfieldc, C.J.; Leggettd, G.; Duce, T.M. *J. Electron Spectrosc. Relat. Phenom.* **2001,** 121, 19–32.

CHAPTER 4

INVESTIGATING RBL CELL BEHAVIOR ON PATTERNED POLYMER BRUSH SURFACES

Abstract

Patterned polymer brushes bearing functional groups are valuable for creating arrays of biomolecules to study cell-surface interactions and potentially for cell based biosensors. For these studies and for practical applications, it is important to understand how surface topography can affect the behavior of cells on such surfaces. In this study, we investigated the behavior of rat basophilic leukemia (RBL) mast cells on a series of patterned poly(acrylic acid) (PAA) brushes on silicon surfaces. Surface-initiated atom transfer radical polymerization (SI-ATRP) was used to synthesize PAA brushes. Brush thickness was controlled by monomer concentration in the polymerization media. PAA brushes were patterned into different size regions with various spacings between them using a procedure based on photolithography. With brush thickness of approximately 30 nm, cells responded to the patterned surfaces differently depending on the pattern morphology. When pattern size and spacing were larger than cell size, cells preferred to adhere to the silicon regions. However, when pattern size and spacing were smaller than the dimension of a cell, cells adhered to the patterned surface and cell membrane accumulated over the brush regions. Such membrane accumulation occurred at physiological temperature (37˚C) but not at room temperature, which suggests that this behavior is regulated by cellular processes. We also found that this membrane accumulation could be minimized when brush thickness was reduced to 10 nm or smaller. Finally, patterned short PAA brushes (with thickness below 10 nm) with pattern size smaller than RBL cell size were functionalized with

2,4-dinitrophenyl (DNP) ligand and used to study signaling of RBL cell sensitized by anti-DNP IgE.

Key Words

RBL mast cells, cell adhesion, poly(acrylic acid) brush, patterned surface, surface topography

Introduction

A good understanding of the cellular responses to surface chemistry and topography is critical in the fields of biomedical implantation, tissue engineering and cell-based sensors.[1] The advance of micro/nano technology enables well-defined arrays of biomolecules, which have been developed as useful tools for studying fundamental mechanisms of cell signaling.[2,3] Most reported work utilizes patterned self-assembled monolayers (SAMs) or protein arrays based on SAMs as platforms to study cell-surface interactions. Polymer brushes have attracted considerable attention recently for bio-functionalizing surfaces due to their unique properties. Compared to SAMs, polymer brushes provide much denser functional groups and can be used to immobilize multiple layers of proteins. Additionally, surface-initiated polymerization is a more universal method to introduce desired functional groups to surfaces simply by polymerizing monomers bearing these functional groups. Polymer brushes have been used to immobilize multiple layers of proteins[4] and generate protein arrays.[5] Due to the dynamic "brush-like" structure of polymer brushes in aqueous solution, hydrophilic polymer brushes might mimic *in vivo* extracellular matrix better than SAMs.

Before using chemically patterned surfaces to study specific cell-surface interactions, it is important to understand non-specific cell-surface interactions

induced by surface topography and, if desired, minimize these non-specific interactions. It is well known that surface topography alone can cause cells to adhere to varying degrees.[6,7] Due to the relatively large thicknesses of polymer brushes, surface topography of patterned polymer brushes might have some interesting effects on cell behavior. Using photolithography, PAA brushes with different thicknesses were patterned into a series of morphologies on silicon wafers. We found that the response of RBL cells to such patterned surfaces largely depends on brush thickness and pattern morphology. When the brush thickness was ~ 30 nm, cell behavior on patterned surfaces was tuned by pattern morphology. When spacing between PAA brush patterns was larger than the cell size, PAA brushes were cell repellent and the majority of cells adhered to silica regions. However, when pattern size and spacing were reduced to regions smaller than cell size, cells gradually adhered to the patterned surface in a time dependent manner. Moreover, the cell membrane consistently accumulated over the PAA brush regions. This ability to "tune" the adhesive nature of the cell membrane was lost when the brush thickness was reduced to 10 nm or smaller. Cells adhered to patterned short PAA brush surfaces in a manner very similar to their adherence to bare silica surfaces, which suggested that the non-specific cell-surface interaction induced by surface topography could be minimized when brush thickness was small enough. Thus, these patterned short PAA brushes could be extremely useful in generating arrays of biomolecules to study specific cell-surface interactions.

Clustering of receptors (anti-DNP IgE/FcεRI) on the cell surface by multivalent DNP ligands initiates intracellular signaling pathways associated with mast cell processes in allergic and inflammatory responses.[2] To synthesize surfaces which could specifically engage the anti-DNP IgE on cell surfaces, DNP was conjugated to patterned short PAA brushes through a polyethylene glycol (PEG) linker with hydroxyl group at each end. This PEG linker was included to further reduce non-

specific interaction between cells and patterned surfaces. Such DNP-brush microarrays on silica surfaces are valuable for studying fundamental mechanisms of IgE receptor-mediated RBL cell signaling. Mechanically, DNP-brushes are much more robust than previously used lipid bilayers containing DNP ligands[8], which, for example, enables preparation of cell membrane sheets on patterned surface. This opens a new avenue for combining patterned surfaces and electron microscopy, allowing a high resolution of protein spatial distribution in cell signaling processes.

Although patterned polymer brushes have been used to pattern cells previously,[9,10,11] pattern sizes were all bigger or close to the size of cells that were studied. In contrast, our study uses patterned polymer brushes with pattern size much smaller than the dimension of a cell to study both specific and non-specific cell-surface interactions. Our results showed that cell behavior is regulated by pattern morphology and dimension, especially when the brushes are thick (30 nm compared to 10 nm). Our results indicate that brush thickness and pattern morphology should be evaluated before patterned polymer brush surfaces are used to study specific cell-surface interactions. We find that that polymer brushes provide a versatile substrate for engineering biological-material interfaces for a variety of applications, such as fundamental cell biology research, bio-implanting, and tissue engineering.

Experimental Section

Materials: Allyl 2-bromo-2-methylpropionate, chlorodimethylhydrosilane, Pt on activated carbon (10 wt %), triethylamine, CuBr, $CuBr_2$, 2,2′-bipyridine, sodium acrylate and diisoproplycarbodiimide (DIPC) were purchased from Sigma-Aldrich. All solvents used were purchased from Sigma-Aldrich. All the chemicals were used without further purification. Distilled deionized water and high-purity nitrogen gas (99.99 %, Airgas) were used throughout. Silicon wafers covered with native silicon

oxide layer were purchased from Montco Silicon Technologies, Inc. Surface initiator for silica substrates was synthesized and immobilized to substrates as described.[5] 4-(dimethylamino)pyridinium-4-toluenesulfonate (DPTS) was synthesized according to a literature procedure. [12]

Patterning of PAA Brushes on Silicon Surfaces: PAA brushes were patterned on silicon surfaces using a procedure based on photolithography as shown below in Scheme 4.1. Detailed description and discussion about this patterning method was described elsewhere.[13] Briefly, a layer of lift-off resist 5A (LOR 5A) was spin-coated to silicon wafer before general photolithography was performed. LOR 5A has good solubility in the developer for photolithography which enables pattern to be transferred from the photoresist layer to the LOR 5A layer. However, LOR 5A does not dissolve in organic solvents, which protects the silica surface underneath from any chemical reaction. Patterned PAA brushes were characterized using atom force microscopy (AFM). Brush thickness was determined from both AFM images and ellipsometry.

Scheme 4.1: Patterning of PAA brushes on a silicon surface

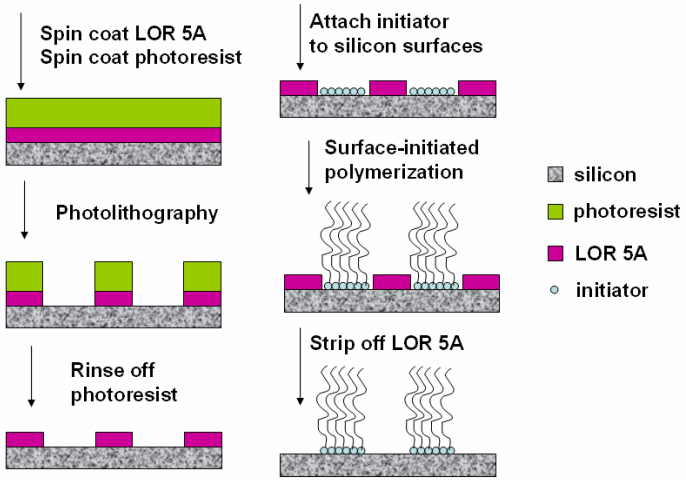

Synthesis of PAA-DNP Brushes: PAA brushes on silicon substrates were synthesized as described[5] with a short polymerization time (~ 20 minutes). Different

thicknesses of PAA brush were achieved using different monomer concentrations in the polymerization media. For thicknesses from large to small, 4mL, 5mL and 6mL DI water was used as solvent for 1.88g sodium acrylate. DNP was attached to PAA brushes through a PEG linker with hydroxyl group at each end, as shown in Scheme 4.2. DNP-PEG was synthesized according to a previously reported procedure.[3] A silicon chip covered with patterned PAA brushes and 75 mg DPTS was placed into a 25 mL Schlenk flask. The flask was evacuated and back-filled with nitrogen three times. After that, 4 mL anhydrous dichloromethane was transferred into the flask under nitrogen protection using a cannula. The flask was shaken gently until DPTS dissolved completely. Then 0.05 mL DNP-PEG and 0.05 mL DIPC were added into the solution. The solution was kept in dark at room temperature overnight. The modified silicon chip was taken out of the solution and rinsed with water, isopropanol and blown dry. The substrates covered with patterned PAA-DNP brushes were stored in dark area for less than a week before cell experiments. X-ray Photoelectron Spectroscopy (XPS) was used to characterize the PAA-DNP brushes. The appearance of a nitrogen peak in the XPS spectrum confirmed attachment of DNP groups.

Scheme 4.2: Attaching DNP to PAA brushes using a PEG linker

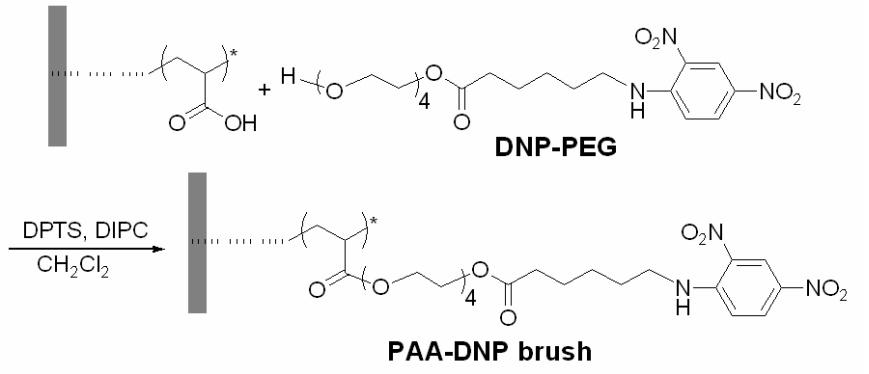

RBL Cells Incubated on Patterned Brush Surfaces: RBL-2H3 cells were maintained in tissue culture and harvested as previously described.[14] The cells were sensitized with fluorescently labeled anti-DNP IgE (3 μg mL^{-1}) for 1 hour and washed to remove unbound IgE. IgE binds very tightly to its high affinity receptor (FcεRI). One milliliter of cells suspended in cell media (0.5 X 10^6 cells/mL) was added on top of the patterned substrates in a 24 well culture plate. The plate was kept in an incubator at 37˚C or room temperature for ~ 20 minutes. Then the substrates were gently rinsed with Tyrode's buffer (150 mmol/L NaCl, 2.5 mmol/L KCl, 12 mmol/L $NaHCO_3$, 2 mmol/L $MgCl_2$, 2 mmol/L $CaCl_2$, 1 mg/mL bovine serum albumin, 1 mg/mL dextrose, pH 7.4) to remove the unattached cells. To label the cells on the surfaces with membrane dyes, a 200 μL solution containing the membrane dye (Texas Red DPPE or DiI C16) was added on top of each chip. After ~ 5 minutes, the chips were rinsed with Tyrode's buffer solution to remove free dye molecules. Finally, these substrates were placed in a plastic glass-bottomed petri dish filled with buffer solution and viewed under confocal microscopy.

Confocal Microscopy: Images of labeled RBL cells on patterned polymer brush surfaces were obtained with a Leica TCS SP2 confocal microscope. A 40x 0.8 NA long working distance water immersion lens was used for image acquisition. All images were acquired at room temperature. To visualize polymer brushes, reflection images with a highly attenuated laser were acquired. To quantify the number of cells adhered to patterned surfaces, 10 randomly selected views on patterned regions were collected.

Results and Discussion:

Effect of Pattern Morphology on Cell Adhesion: It is well known that surface morphology alone can regulate cell adhesion on surfaces. Turner et al.[15] showed that

astroglial cells prefer to attach to silica surfaces with micropillars. Surface topography can also control shape and behavior of cells, which has been defined as contact guidance.[16] Thus, it is important to understand how the surface morphology of biomaterials might affect the response of biological systems before such biomaterials can be utilized. Versatile polymer brushes offer new opportunities in creating bio-functionalized surfaces for various biomedical applications. Patterned PAA brushes have been shown to be useful for generating arrays of biomolecules,[5] which can be valuable in tissue engineering, biosensing and fundamental cell biology studies. It is worthwhile studying cell responses to patterned polymer brushes with different morphologies. In the present work, PAA brushes were patterned into different size regions with various spacings. PAA brush thickness was controlled by monomer concentration in the polymerization step. When pattern size and spacing were larger than the cell size, PAA brushes were cell repellent, i.e., the overwhelming majority of cells adhered to silica regions on surfaces patterned with 100 μm stripes of PAA brushes, as shown in Figure1a. But when pattern size and spacing were smaller than the cell size, particularly 2 μm x 2 μm squares with 2 μm spacing, cells were forced to adhere to the patterned surfaces (silica together with brushes). In this case, the cell membrane even accumulated over the brush regions as shown in Fig. 1b and 1c. In Fig. 1c, cell membrane was labeled with Texas Red DPPE. Clustering of Texas Red DPPE indicated that clustering of IgE shown in Figure 4.1b was due to accumulation of cell membrane.

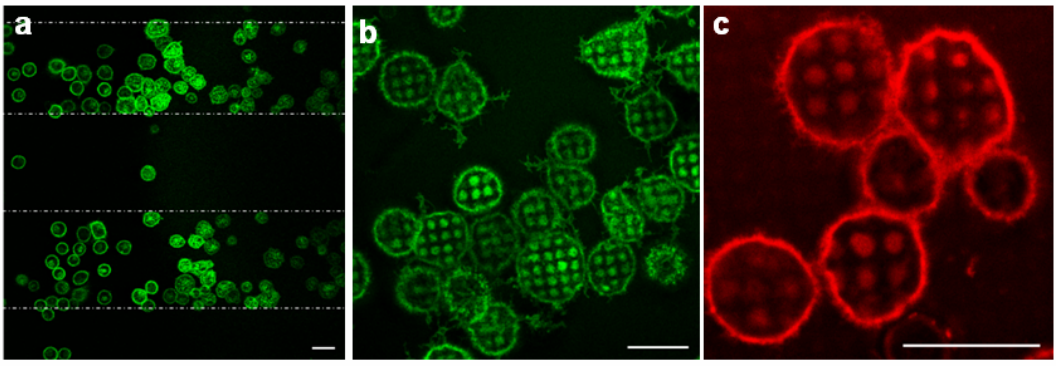

Figure 4.1: Confocal fluorescence images of RBL cells incubated on patterned PAA brush (~ 30 nm) surfaces at 37˚C for over twenty minutes. RBL cells sensitized with A488 anti-DNP IgE were incubated on 100 μm stripes of PAA brushes with 100 μm spacing in between (a) and 2 μm x 2 μm squares with 2 μm spacing (b, c). In panel c, cells were also labeled with Texas Red DPPE after incubation. The scale bar is 20 μm.

Cell adhesion was investigated on different surfaces with various patterned morphologies smaller than the cell size. The results are summarized in Figure 4.2 as shown below. As mentioned earlier, PAA brushes were cell repellent and over 95% cells adhered to silica regions when pattern size and spacing were larger than the cell size. However, cells adhered to the patterned surface and cell membrane accumulated over brush regions when pattern size and morphology were smaller than the cell size, as shown in Figure 4.1b. In addition, cell adhesion on these patterned surfaces with small pattern features varied a great deal depending on pattern morphology as shown in Figure 4.2. In general, the cell density on stripe-shaped patterns was much lower than on square-shaped patterns. It suggested that continuous occurrence of cell repellent PAA brushes, even with a width much smaller than the dimension of cells, is not favorable for stable cell adhesion. However, it is not yet well understood what caused the differences of cell adhesion on surfaces with different pattern morphologies.

Others have previously also reported the effect of surface morphology on cell adhesion. Turner et al.[15] showed that cell adhesion density on silica surfaces with micro-pillars was higher than on a smooth surface or a surface with micro-wells. Further experiments were required to determine whether such interesting phenomena are merely due to physicochemical interactions between cells and patterned surfaces, such as a capillary force,[17] or it is actually regulated by cellular events.

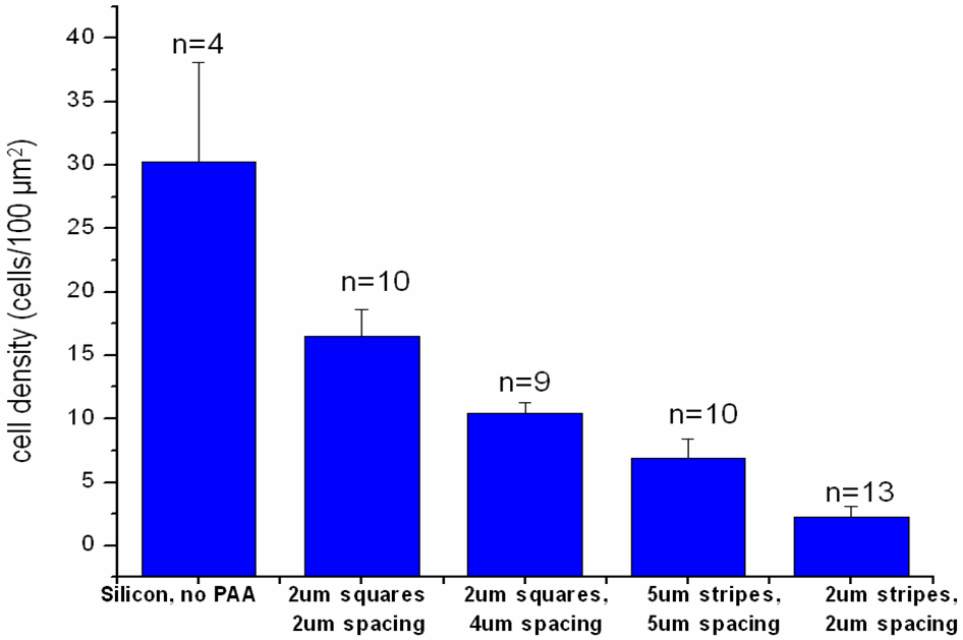

Figure 4.2: Density of cell adhesion on pure silicon surface and patterned PAA brush surfaces with different pattern morphology. Cells on an area of ~0.14 mm^2 were counted for each calculation.

Effect of Incubation Temperature on Cell Adhesion: Although physicochemical interactions between cells and the patterned surfaces are not quite different at room temperature (~ 25˚C) versus 37˚C, cellular behaviors at these two temperatures could be quite different.[18, 19] Many cellular events require physiological conditions,

including temperature. To determine whether the membrane accumulation observed in Figure 4.1c is due to physiochemical interactions or it is controlled by cellular events, RBL cells were incubated on these patterned surfaces at room temperature Interestingly, very few cells adhered and the cell membrane did not accumulate over brush regions, as shown in Figure 4.3a. Membrane even avoided the brush regions occasionally. However, when the same cells were put back in the incubator at 37˚C, membrane accumulation occurred, which suggested that such membrane accumulation required physiological temperature and was probably regulated by cellular processes, such as extension of filapodia. On the other hand, cells adhered at 37˚C did not dissociate from the surface when they were placed at room temperature. A series of follow-up experiments showed that such cell adhesion was mediated by integrin-fibronection interaction and driven by actin polymerization (data not shown). When the pattern size is larger than the size of cells, the cell adhesion is dominated by the combination of physicochemical interactions between cells and the patterned surfaces. Most cells adhered to the silica regions rather than the negatively charged PAA brushes. However, when the pattern size is smaller than the size of cells, cellular processes participated in the adhesion process and caused the cell adhesion and membrane accumulation. The mechanism for this intriguing phenomenon is described in a separate paper.[20]

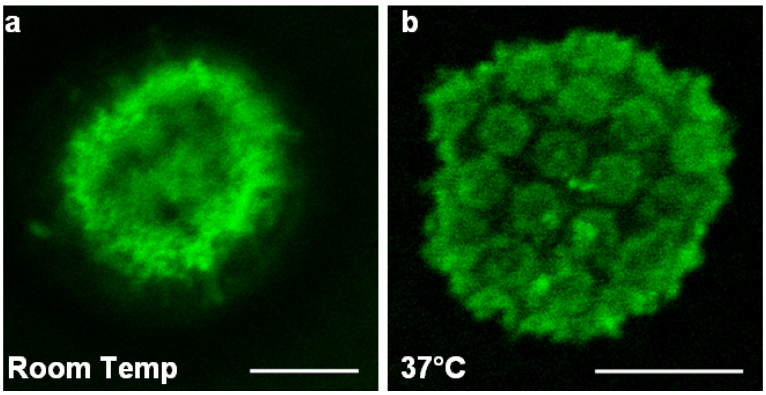

Figure 4.3: Confocal fluorescence images of RBL cells incubated on 2 μm x 2 μm squares with 2 μm spacing patterned PAA brush (~ 30 nm) surface at room temperature (a), followed by 37˚C (b). Cells were sensitized with A488 anti-DNP IgE before incubation. The scale bar is 10 μm.

Effect of Brush Thickness: It has been shown that the depth of patterned features plays a very important role in regulating cell behavior. Shallower features were shown to have less influence on cells.[21] Here, we explored the effects of brush thickness on cell adhesion. Thinner PAA brushes were synthesized by diluting monomer concentration in the polymerization medium. A series of brush thicknesses were achieved by using different monomer concentrations. As shown below in Figure 4.4b, when brush thickness was ~ 15 nm, membrane accumulation was still very pronounced. However, when brush thickness was further reduced to ~ 8 nm, the membrane accumulation was negligible, as shown in Figure 4.4a. Cells adhered to these patterned thin (< 10 nm) PAA brush surfaces in a very similar way as they did to bare silica surfaces. The presence of very short PAA brushes did not have a big impact on the adhesion of RBL cells.

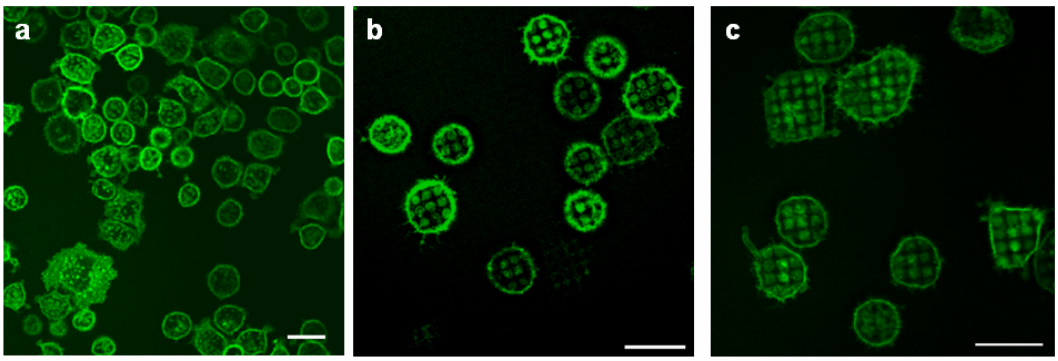

Figure 4.4: Confocal fluorescence images of RBL cells incubated on 2 μm x 2 μm squares with 2 μm spacing patterned PAA brush surface at 37˚C for over 20 minutes. Dry brush thickness in a, b, and c is ~ 8 nm, 15 nm, and 30 nm accordingly. Cells were sensitized with A488 anti-DNP IgE before incubation. The scale bar is 20 μm.

The cell behavior tuned by surface morphology is very interesting. It could provide very valuable information to better understand the fundamental mechanism of cell adhesion. However, such behavior could interfere with specific cell-surface interactions. In many cases, surfaces for studying specific cell-surface interactions should have negligible non-specific interaction with cells. In these cases, minimizing the effect of surface morphology on cell attachment is preferred. Since patterned short PAA brushes have minimal effect on cell attachment, these surfaces could be very useful in generating arrays of biomolecules to study specific cell-surface interactions.

RBL Cells on Patterned PAA-DNP Brush Surfaces: It is known that multivalent DNP ligands cluster IgE bound to its high affinity receptor (FcεRI) on the mast cell surface, which initiates intracellular signaling pathways and ultimately causes secretion of histamine resulting in allergic and inflammatory responses.[22] Recently, lipid bilayers[8, 23] and self-assembled monolayers[3] containing DNP ligands were patterned and used to control the location and size of IgE-FcεRI clusters. Well-defined patterns enabled good visualization of redistributed intracellular components in the

signaling process. However, all the imaging in these papers has been done using fluorescence microscopy. Detailed protein distribution on the nanometer scale cannot be distinguished due to the relatively poor resolution of fluorescence microscopy. Scanning electron microscopy (SEM) has nanometer scale resolution and it has been used to map protein distribution when proteins were labeled with gold nanoparticles.[24] Patterned brushes on silica surfaces are mechanically stable and compatible with gold nanoparticles in SEM imaging. To generate arrays of DNP ligands for mast cell signaling study, DNP ligands were linked to patterned short PAA brushes through PEG linker molecules. These patterned PAA-DNP brushes can be valuable substrates to study mast cell signaling on patterned surfaces using SEM. As shown in Scheme 4.2, DNP-caproic acid molecules were conjugated to PAA brushes using a PEG linker. The PEG linker reduced non-specific interaction between substrates and other proteins.[25] In addition, hydrophilic PEG linkers provide flexibility or mobility to the DNP-brush in cell media and provide DNP groups better accessibilities for IgE antibodies, which is necessary for clustering IgE- FcεRI on the cell surface. As shown in Figure 4.5a and 4.5b, patterned PAA-DNP brushes clustered anti-DNP IgE very well. Because of the short brush thickness, cell membrane visualized by a fluorescent lipid membrane probe was distributed uniformly over the patterned surfaces and did not accumulate over brush regions, as shown in Figure 4.5c.

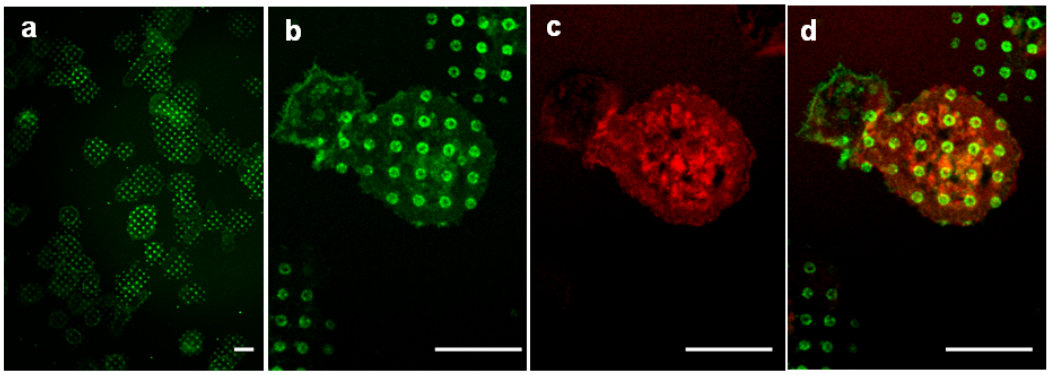

Figure 4.5: Confocal fluorescence images of RBL cells incubated on 2 μm x 2 μm squares with 4 μm spacing patterned PAA-DNP brush (~ 8 nm) surface at 37˚C for over 20 minutes. Green channel showed IgE clustering (a,b), red channel showed Di-16 labeled cell membrane (c), and overlay of b and c (d). The scale bar is 10 μm.

Such patterned bio-functionalized polymer brushes can be very useful for studying cell-surface interactions. Because of their "brush" shape and flexibility in aqueous solution, polymer brushes might mimic *in vivo* extra-cellular matrix better than SAMs providing a more physiologically realistic extra-cellular environment. Current efforts are being made to prepare cell membrane sheets on patterned brush surfaces for SEM imaging.

Conclusions

Surface-initiated ATRP was used to synthesize PAA brushes on silicon surfaces. PAA brushes with different thicknesses were patterned into regions of various size and spacing using photolithography. RBL cell behavior on these patterned polymer brush surfaces under different conditions was investigated. We found that the response of RBL cells to patterned polymer brush surfaces largely depended on brush thickness and pattern morphology. The substitutes of thick polymer brushes with very short PAA brushes did not greatly affect the adhesion behavior of cells on pure silicon

surfaces. However, when the dry brush thickness was increased to 15 nm or more, cells began to respond very differently to the patterned surface depending on the pattern size and spacing between patterns. When patterned at large dimensions greater than the dimension of cells, PAA brushes were cell repellent. When patterned into smaller regions with close spacing that were below the dimension of cells, cells adhered to patterned surfaces and the cell membrane even accumulated over the PAA brush regions. Cells did not adhere to surfaces patterned with small features at room temperature as much as they did at 37˚C. At room temperature, membranes of the adhered cells did not concentrate over brush regions, which implied that the membrane accumulation behavior required physiological temperature and was probably regulated by cellular processes, such as cytostructure rearrangements. DNP ligand molecules were attached to short PAA brushes (~ 8 nm) through a PEG linker. Patterned short PAA-DNP brushes clustered anti-DNP IgE on RBL cell surfaces very specifically without non-specific membrane accumulation over brush regions. We expect that bio-functionalized polymer brush surfaces will be valuable for biodiagnosis, tissue engineering and fundamental cell biology studies.

Acknowledgements

This research was supported by the NSF-funded Cornell Nanobiotechnology Center (NBTC) and Cornell Nanoscale Interdisciplinary Research Team (NIRT). We made use of the facilities at NBTC, Cornell NanoScale Science and Technology Facility (CNF), and Cornell Center for Materials Research (CCMR), all of which are supported by NSF. The NBTC support for RD and NIRT support for EC are gratefully acknowledged.

REFERENCES

[1] Senaratne, W.; Andruzzi, L.; Ober, C. K. *Biomacromolecules* **2005,** 6, 2427-2448.

[2] Torres, A. J.; Wu, M.; Holowka, D.; Baird, B. *Annu. Rev. Biophys. Biomol. Struct.* **2008,** 37, 265-288.

[3] Senaratne, W.; Sengupta, P.; Jakubek, V.; Holowka, D.; Ober, C. K.; Baird, B. *J. Am. Chem. Soc.* **2006,** 128, 5594-5595.

[4] Jain, P.; Sun, L.; Dai, J.; Baker, G. L.; Bruening, M. L. *Biomacromolecules* **2007**, 8(10), 3102- 3107.

[5] Dong, R; Krishnan, S.; Baird, B. A.; Lindau, M.; Ober, C. K. *Biomacromolecules* **2007,** 8, 3082-3092.

[6] Curtis, A.; Wilkinson, C. *Biomaterials,* **1997,** 18, 1573-1583.

[7] Reichert, J.; Brückner,S.; Bartelt, H.; Jandt, K. D. *Adv. Engr. Mater.* **2007,** 9, 1104-1113.

[8] Wu, M.; Holowka, D.; Craighead, H. G.; Baird, B. *Proc. Natl. Acad. Sci. USA* **2004,** 101, 13798-13803.

[9] Alarcón, C. D. H.; Farhan, T.; Osborne, V. L.; Huck, W. T. S.; Alexander, C. *J. Mater. Chem.* **2005,** 15, 2089–2094.

[10] Iwata, R.; Suk-In, P.; Hoven, V. P.; Takahara, A.; Akiyoshi, K.; Iwasaki, Y. *Biomacromolecules* **2004,** 5, 2308-2314.

[11] Andruzzi, L.; Senaratne, W.; Hexemer, A.; Sheets, E. D.; Ilic, B.; Kramer, E. J.; Baird, B.; Ober, C. K. *Langmuir* **2005,** 21, 2495-2504.

[12] Moore, J. S.; Stupp, S. I. *Macromolecules* **1990,** 23, 65.

[13] Dong, R.; Molloy, R. P.; Lindau, M.; Ober, C. K. *Direct synthesis of quaternized polymer brushes and their application for guiding neuronal growth, submitted to Nature Materials.*

[14] Sheets, E. D.; Holowka, D.; Baird, B. *J. Cell Biol.* **1999**, 145, 877.

[15] Turner, A. M. P.; Dowell, N.; Turner, S. W. P.; Kam, L.; Isaacson, M.; Turner, J. N.; Craighead, H. G.; Shain, W. *J. Biomed. Mat. Res. Part A,* **2000,** 51, 430-441.

[16] Dunn, G. A.; Heath, J. P. *Experimental Cell Res.* **1976**, 101, 1-14.

[17] Lenhert, S.; Sesma, A.; Hirtz, M.; Chi, L.; Fuchs, H.; Wiesmann, H. P.; Osbourn, A. E.; Moerschbacher, B. M. *Langmuir* **2007,** *23,* 10216-10223.

[18] Lepock, J. R. *International J. of Hyperthermia*, **2005,** 21, 681 - 687.

[19] Ducommun, P.; Ruffieux , P.-A.; Kadouri, A.; von Stockar, U.; Marison, I. W. *Biotechnology & Bioengineering* **2002,** 77, 838 - 842.

[20] Chiang, E.; Dong, R.; Holowka, D.; Ober, C. K.; Baird, B. *in preparation.*

[21] Wójciak-Stothard, B.; Curtis, A.; Monaghan, W.; Macdonald, K.; Wilkinson, C. *Experimental Cell Res.* **1996,** 223, 426–435.

[22] Holowka, D.; Baird, B. *Annu. Rev. Biophys. Biomol. Struct.* **1996**, *25*, 79-112.

[23] Orth, R. N.; Wu, M.; Holowka, D. A.; Craighead, H. G.; Baird, B. A. *Langmuir* **2003**, 19, 1599-1605.

[24] Thiberge, S.; Nechushtan, A.; Sprinzak, D.; Gileadi, O.; Behar, V.; Zik, O.; Chowers, Y.; Michaeli, S.; Schlessinger, J.; Moses, E. *Proc. Natl. Acad. Sci. USA* **2004,** 101, 3346-3351.

[25] Prime, K. L.; Whitesides, G. M. *J. Am. Chem. Soc.* **1993**, 115, 10714-10721.

CHAPTER 5

DIRECT SYNTHESIS OF QUATERNIZED POLYMER BRUSHES AND THEIR APPLICATIONS FOR GUIDING NEURONAL GROWTH

Abstract

Direct synthesis of quaternized poly(dimethylaminoethyl methacrylate) brushes was achieved by surface-initiated atom transfer radical polymerization (SI-ATRP) of [2-(methacryloyloxy)ethyl]trimethylammonium chloride (META) in protic media at room temperature. The kinetics of brush growth in three different solvents was compared. In pure water media, the polymer brush stopped growing after a very short time and the final brush thickness was ~15 nm. Polymer brush growth in isopropanol (IPA)/water mixture led to a final brush thickness of ~60 nm. Brush growth was faster in methanol/water mixture at the start of the polymerization but terminated at slightly smaller thickness. While quaternized polymer brush modified surfaces have previously been shown to be antibacterial, we show here that poly(META) (PMETA) brush modified surfaces are excellent substrates for growth of hippocampal neurons, which could prove useful for the surfaces of neural implants. PMETA brushes were photolithographically patterned on silicon substrates in combination with patterned regions backfilled with polyethylene glycol (PEG). The resulting hybrid patterned surfaces consisting of both "cytophilic" and "cytophobic" materials were successfully applied to guide neuron outgrowth. These surfaces can be further modified in chemical and photolithographic steps and should thus provide an excellent platform for studies of neuronal function, neuronal implants, cell-based biosensors and other applications.

Key words: Positively charged polymer brushes, ATRP, photolithography, hippocampal neuron culture

Introduction

Careful design of the interface between living tissue and the exposed surfaces of bioimplants is essential for the successful deployment of these devices.[1] Ideally, device surfaces should be compatible with both the growth of eukaryotic cells or tissue (biocompatible) and the suppression of prokaryotic infection (antibacterial), but this combination is difficult to achieve. We examined whether positively charged poly(quaternary ammonium) (PQA) compounds might meet these criteria.

A variety of positively charged PQA compounds have been shown to be antibacterial when applied to surfaces.[2,3] For example, a variety of quaternary poly(dimethylaminoethyl methacrylate) (PDMAEMA) compounds are known to have great antibacterial activity when deposited on surfaces as polymer brushes.[4,5,6] In this configuration, one polymer chain end is attached to the selected surface at a sufficiently high density that the polymer chains are forced to orient themselves away from the substrate. Inspired by previous literature about neuron culture on positively charged surfaces (e.g. poly-lysine),[7, 8,9,10] we examined several amine terminated polymer brushes for their ability to support neuronal growth. Here we show that quaternized antibacterial polymer brushes in pattern free and patterned surfaces are suitable substrates to support and guide growth of rat hippocampal neurons.

Polymer brushes with a selection of desired functional groups grown using surface-initiated polymerization can therefore provide a robust, tailored surface modification strategy. Among the many surface-initiated polymerization techniques, surface-initiated atom transfer radical polymerization (SI-ATRP) is most widely used. ATRP is compatible with protic solvents and monomers bearing many types of functional groups. Meanwhile, it also provides controlled polymerization, that is, control over molecular size. Quaternized PDMAEMA brushes have mainly been synthesized by quaternizing preformed PDMAEMA brushes with alkyl halogen.[5,6] This method

involves multiple synthetic steps and the use of toxic compounds. Direct synthesis of the quaternized brushes is therefore preferable. Osborne et al.[11] reported direct synthesis of PMETA brushes using SI-ATRP in a solution of water and methanol (MeOH/water). However, later Li et al.[12] showed that transesterification of the monomer with methanol produced significant amounts of methyl methacrylate when the polymerization was done in MeOH/water. Such transesterification can be avoided by using a solution of isopropanol and water (IPA/water) as polymerization solvent. We therefore grew PMETA brushes using SI-ATRP in IPA/water solution and compared the kinetics of brush growth in three different solvents: 3:2 v/v IPA/water mixture, 4:1 v/v MeOH/water mixture (water originally carried in the purchased monomer solution is not counted) and pure water.

The ability to guide neuron growth, especially synapse formation, is crucial in the field of neuroelectronic circuits, cell-based biosensors, neurological implants and pharmaceutical testing.[13] To generate surfaces for neuronal cell patterning, usually biomolecules promoting neuron growth, such as polylysine or laminin, are microstamped onto a surface.[14,15] Modification of the remaining surface to reduce non-specific interaction can be challenging due to the instability of physically adsorbed films. Such problems could, in principle, be resolved by using polymer brushes, which are covalently attached to substrates. Another potential advantage of this scheme is that surfaces with patterned polymer brushes can be backfilled with other surface tethered monolayers or polymer chains to form well-defined hybrid surfaces with multiple components.[16]

We applied photolithography to pattern PMETA brushes and backfilled the patterned surface with a monolayer containing polyethylene glycol (PEG). Hippocampal neurons were grown on the hybrid surfaces and their survival and neurite outgrowth were examined. We found that rat hippocampal neurons can grow

well and successfully extend neurites on PMETA brush-covered silicon substrates. By using well-defined hybrid surfaces containing both "cytophilic" PMETA brushes and "cytophobic" PEG[17] monolayers, we were able to guide neuron growth. Since the patterned hybrid surfaces are very stable and survive further chemical and photolithographic steps, they provide a versatile new tool for applications in cell-surface studies, cell-based biosensing, design of implants and other applications.

Experimental section

Materials: Allyl 2-bromo-2-methylpropionate, chlorodimethylhydrosilane, Pt on activated carbon (10 wt %), triethylamine, CuBr, $CuBr_2$, 2,2′-bipyridine, 11-mercapto-1-undecanol, 2-bromo-2-methylpropionyl bromide, anhydrous pyridine, 75% w/v aqueous solution of [2-(methacryloyloxy)ethyl]trimethylammonium chloride were purchased from Sigma-Aldrich. 2-[Methoxy(polyethylenoxy)propyl]trichlorosilane (PEGylated silane, $CH_3O(CH_2CH_2O)_{6-9}(CH_2)_3SiCl_3$, 90 %) was purchased from Gelest. All solvents used were purchased from Sigma-Aldrich. All the chemicals were used without further purification. Distilled deionized water and high-purity nitrogen gas (99.99 %, Airgas) were used throughout. All the Gold (~1000 Å) coated silicon wafers (4" diameter) with titanium adhesion layer were purchased from Platypus Technologies. The wafers were cut into 1 cm x 2cm pieces before their usage. Surface initiators for silica substrates and gold substrates were synthesized and immobilized to substrates as described.[18,19] Neurobasal Medium, GlutaMax supplement, pyruvate, antibiotics B27 supplement 0.2% Trypsin and calcein were obtained from InVitrogen. Hibernate Medium was obtained from Brainbits LLC. Poly-*D*-Lysine was obtained from Sigma. Fetal Bovine Serum was obtained from HyClone. Coverslips (Sargent) were obtained from Warner Instruments. The antagonists *D*-2-amino-5-phosphonopentanoic acid (D-AP5) and 2,3-Dioxo-6-nitro-1,2,3,4-tetrahydrobenzo

quinoxaline -7-sulfonamide disodium salt (NBQX) were from Tocris. Paraformaldehyde (37%) with 10% methanol (F-1268) was from Sigma. Anti-MAP2 antibody (#M9942) was obtained from Sigma. Secondary Cy3 labeled goat anti-mouse antibody (#115-165-146) and IgG-free BSA were obtained from Jackson Immunoresearch.

SI-ATRP of META: Silicon substrates covered with initiator were placed in a dry Schlenk flask. CuBr (28.7 mg, 0.2 mmol), $CuBr_2$ (4.5 mg, 0.02 mmol), and 2,2′-bipyridine (78.4 mg, 0.48 mmol) were added to another dry Schlenk flask tube equipped with a magnetic stir bar. Both flasks were evacuated and back-filled with nitrogen three times. META (2 mL aqueous solution), isopropanol (1.8 mL) and DI water (1.2 mL) were mixed together and bubbled by nitrogen gas for at least 30 minutes, then transferred into the Schlenk flask with copper catalysts using a cannula. The mixture was stirred at room temperature under nitrogen for about 10 min and transferred into the other Schlenk flask with silicon substrates using a cannula. Polymerization was carried out at room temperature for desired time, after which the substrates were taken out of the solution, rinsed with DI water, isopropanol thoroughly and blown dry by nitrogen gas. The same procedure was used when the polymerization solvent was methanol/water mixture (1.6 mL methanol and 0.4 mL water) or pure water (1.5 mL). To use grazing-angle reflectance Fourier transform infrared spectroscopy (FTIR) to characterize the synthesized polymer brushes, PMETA brushes were also grown on gold surfaces using the same procedure as describe above.

Characterization of polymer brushes by FTIR and Ellipsometry: Gold substrates coated with PMETA brushes were characterized using a VERTEX 80v vacuum FT-IR spectrometer from Bruker Optics equipped with a liquid nitrogen-cooled Mercury

Cadmium Telluride (MCT) detector. Before collecting data, the system was left in vacuum for 10 minutes to minimize signal noise from air. IR spectra were taken with 2 cm^{-1} resolution using 256 scans at 75˚ incident angle. Spectra from bare gold substrates were used to determine the background signal. OPUS viewer software from Bruker Optics was used to analyze FTIR spectra. Thickness of polymer brushes was measured using a Woollam variable angle spectroscopic ellipsometer. A two layer model consisting of a 0.5 mm silicon layer and a Cauchy layer, to represent the brush layer, was used to determine both the thickness and refractive index of the brush.

Patterning of polymer brushes by photolithography: PMETA brushes were patterned on silicon surfaces by photolithography as shown in Scheme 5.1. Lift off resist (LOR) 5A was spin coated on fresh silicon wafers, baked at 180˚C for 10 minutes and patterned by standard photolithography. The patterned wafers were cleaned with a Harrick oxygen plasma cleaner (PDC-32G) for 1-2 minutes. Photoresist was rinsed off with acetone. The silicon wafers covered by patterned LOR 5A were cleaned by plasma cleaner again for 1-2 minutes. Surface initiator for silicon oxide substrates was attached to the exposed silicon oxide regions on the patterned wafer. SI-ATRP of META was carried out on such surfaces, after which LOR 5A was stripped off by an AZ 300 MIF (tetramethylammonium hydroxide solution) developer, which yielded patterned PMETA brushes. The substrates with patterned brushes were back-filled with PEG-silane. Rat hippocampus neurons were cultured on such PMETA brush/PEG patterned surfaces as described below.

Scheme 5.1: Generation of polymer brushes/PEG patterned surfaces based on photolithography

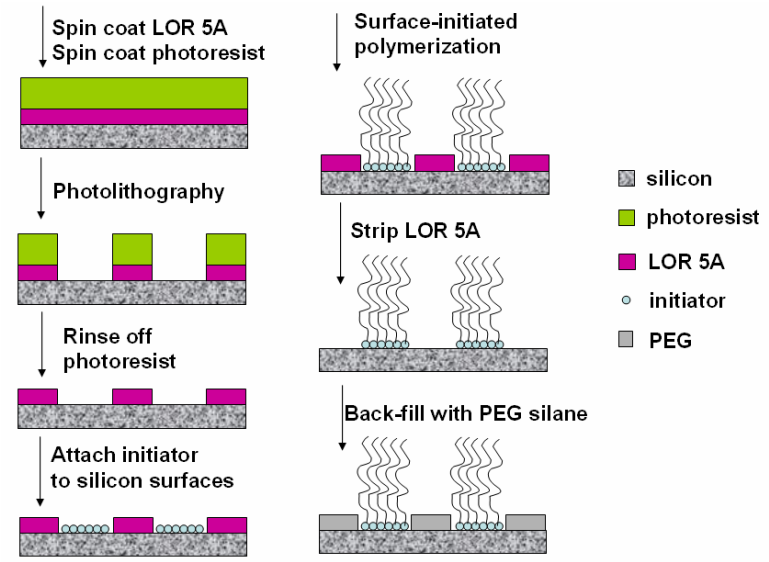

Rat hippocampus neuron culture: Rat Hippocampal neurons were obtained from newborn rats (P0-P5). Hippocampi were dissected in cold Hibernate E-Low Fluorescence medium (HibE, Brainbits LLC) and transferred to a 15 mL tube containing cold (4 °C) HibE. The solution was then exchanged for a freshly prepared 1:1 (v/v) mixture of room temperature 0.25% (w/v) Trypsin in Hank's balanced salts solution (Invitrogen) and warm (37 °C) HibE. Hippocampi were digested for 15 minutes at 37 °C. Trypsin was quenched with 3 changes of Neurobasal medium (Invitrogen) supplemented with 10% fetal bovine serum (FBS, Invitrogen). The hippocampi were then triturated 10 times with a 5 mL serological pipette and undissociated tissue allowed to settle. The supernatant, which contained dissociated neurons, was then transferred to a new 15 mL tube for counting and dilution. Prior to plating, the patterned PMETA brush/PEG surfaces were sterilized in Ethanol and transferred to Neurobasal medium supplemented with 10% FBS. Neurons were plated

in Neurobasal Medium supplemented with 1% GlutaMax (Invitrogen), 1 mM pyruvate (Invitrogen #11360), 1% penicillin/streptomycin (Invitrogen), 2% B27 supplement (Invitrogen) and 10% FBS After 12 hours the medium was changed to Neurobasal medium with the same supplements but no serum. Cells were maintained in a water-jacketed incubator maintained at 37 °C and 5% CO_2.

Microscopy of living hippocampal neurons labeled with calcein: To visualize living cells on the substrates, calcein-AM ester (1 mg/mL in DMSO) was diluted 1:2000 in HibE medium or Ringers solution for ten minutes. The solution was then exchanged for new HibE medium or Ringers solution interchangeably. Ringers solution contained in millimolar: NaCl, 119; KCl, 2.5; $CaCl_2$, 2; $MgCl_2$, 2; HEPES (pH 7.4), 25; glucose, 30). In both cases, the cell medium was supplemented with 50 μM AP-5 and 1 μM NBQX to block NMDA and AMPA/Kainate receptors respectively.

Immunocytochemistry of Hippocampal Neurons: Cells were fixed with 3.7% formaldehyde and 1-1.5% methanol in phosphate buffered saline (PBS) solution for 15 minutes. Free aldehydes were quenched with 50 mM NH_4Cl in PBS for 5 minutes. The cells were then permeabilized in the presence of 0.1% Tween-20 in PBS (PBST) for 5 minutes and blocked with 0.1% Tween-20 in PBS supplemented with 3% IgG free bovine serum albumin (Jackson Immunoresearch; PBSTB) for 30 minutes. Primary antibodies were added for 1-3 hours in PBSTB and rinsed 3 x 10 minutes in PBSTB. Secondary antibodies (Cy3 labeled anti-mouse, 1:500) were added for 1 hour in PBSTB and the cells rinsed 3x10 minutes in PBS. Patterned substrates with cultured cells atop were stored in PBS before imaging.

Confocal Microscopy: Images of labeled neurons were obtained with a Leica TCS SP2 confocal microscope equipped for spectral detection. A 40x 0.8 NA long working distance water immersion lens was used to acquire Z-series of labeled neurons. All

images were acquired at room temperature. To visualize polymer brushes and cell morphology, reflection images with a highly attenuated laser were acquired and enhanced using a shadow function in ImageJ.

Analysis of Neurites: Images were inspected using ImageJ[20] (v 1.41o) Z-Projections of confocal stacks were obtained by summing intensity values and the summed stacks used for subsequent analysis. Neurite lengths were measured interactively with the NeuronJ plugin.[21] Statistical analysis was conducted using Igor (v. 6.05, Wavemetrics, Lake Oswego, OR).

Results and discussion

Synthesis of PMETA brushes: Direct synthesis of PMETA brushes was first reported by Osborne et al.[11] They showed that PMETA brushes can be grown in a controlled manner on gold surfaces using SI-ATRP of META in methanol/water mixture at room temperature. However, it was shown by Li et al. [12] that transesterification of META occurred during polymerization, which produced significant amounts of methyl methacrylate in the final polymer. Unexpected transesterification of tertiary amine methacrylates during methanolic ATRP was reported before.[22] Li et al.[12] also showed that when methanol was replaced by IPA, such transesterification was avoided because the secondary alcohol was less prone to transesterification. In the present work, direct synthesis of PMETA brushes on silicon surfaces was carried out in IPA/water mixture to avoid transesterification as shown in Scheme 5.2. The kinetics of brush growth was also compared in three different solvents: IPA/water mixture, methanol/water mixture and pure water (Figure 5.1).

Scheme 5.2: Synthesis of cationic polymer brushes by SI-ATRP of [2-(methacryloyoxy)ethyl]trimethylammonium chloride (META)

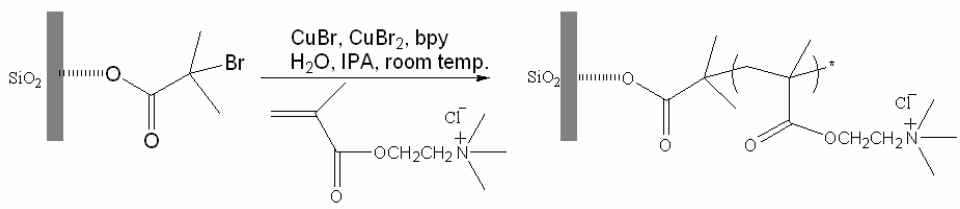

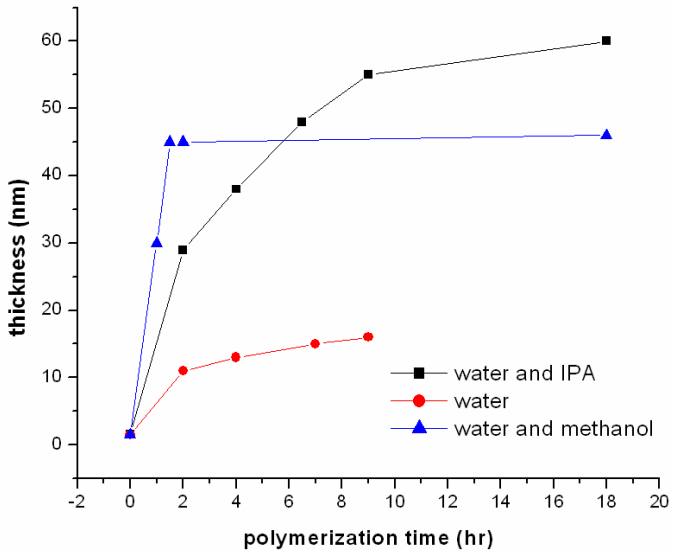

Figure 5.1: Thickness of PMETA brushes versus polymerization time in different solvents. Lines have been added to guide the eye.

The growth of PMETA brushes in water stopped after a short time of polymerization, and resulted in a small final thickness (~15 nm) of the brushes. In IPA/water mixture, PMETA brushes grew in a controllable manner for a long time (~10 hours) and the largest final brush thickness (~60 nm) was achieved. However, PMETA brushes grew faster in the early stage in methanol/water mixture than in IPA/water mixture. Such polymerization kinetics is quite different from the kinetics in solution reported by Li et al.[12] In solution, polymerization of META in IPA/water mixture was faster than in a

methanol/water mixture. Such differences imply that polymerization kinetics in solution and on a surface can be quite different. Also, the brush thickness observed in a methanol/water mixture is at variance with what Osborne et al.[11] reported. The difference could be due to different initiator efficiency or different initiator density on gold surfaces and silica surfaces.

An FTIR spectrum of PMETA brushes is shown in Figure 5.2. The absence of the absorption bands at ~ 2800 cm^{-1}, which are attributed to symmetric stretching vibrations of $-CH_3$ of the tertiary amine groups, indicated that the amine groups were quaternized in PMETA brushes synthesized directly from META. The absorption peak at 1734 cm^{-1} is a characteristic peak corresponding to the C=O stretching vibration.

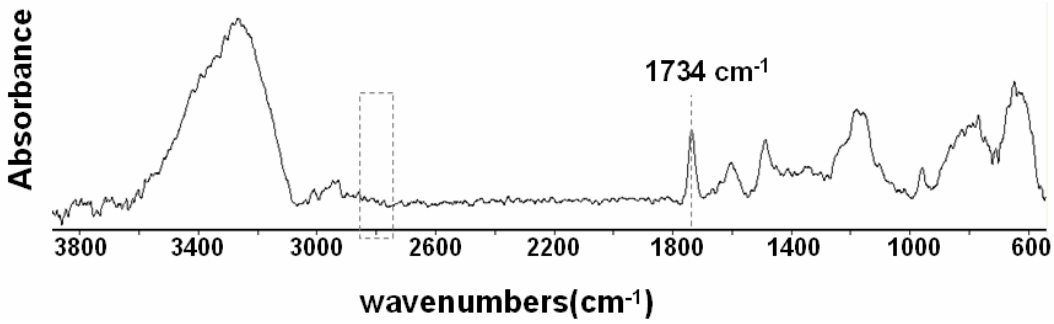

Figure 5.2: Grazing angle reflectance FTIR spectra of PMETA brushes synthesized directly from META. Absence of absorption peaks ~ 2800 cm^{-1} shows that amine groups in directly synthesized PMETA brushes are quaternized.

PMETA brush-modified surfaces for neuron culture: It is well known that neuronal cells grow well on surfaces covered with positively charged molecules.[23,24] Polylysine and laminin are the most commonly used compounds to promote neuron growth.[14,15] Surfaces covered by such molecules are, however, not stable over time and are thus usually freshly prepared before neuron culture. Polymer brushes provide

robust surface modification with desired functional groups for different applications. Rühe et al.[7] showed that cerebellar cells could grow on poly(2-methacryloyloxy)propyl trimethylammonium bromide) grafted surfaces. Quaternized PDMAEMA brushes were also shown to have antibacterial activity.[5] Thus quaternized PMETA brushes should be able to provide stable modified surfaces free of antibacterial contamination over time, suitable for neuron culture substrates. Rat hippocampal neurons were cultured on PMETA brush modified silicon substrates and labeled for the neuronal marker MAP2, the major microtubule associated protein of brain tissue (Fig. 5.3). MAP2 is localized to the cell bodies and dendrites, which are clearly evident in the immunofluorescence image (Fig. 5.3). With their simultaneous antibacterial and biocompatible activities, quaternized PMETA brush-modified surfaces are good candidates for biointerfaces to study neuronal function, for neuronal implants, cell-based biosensing and other applications.

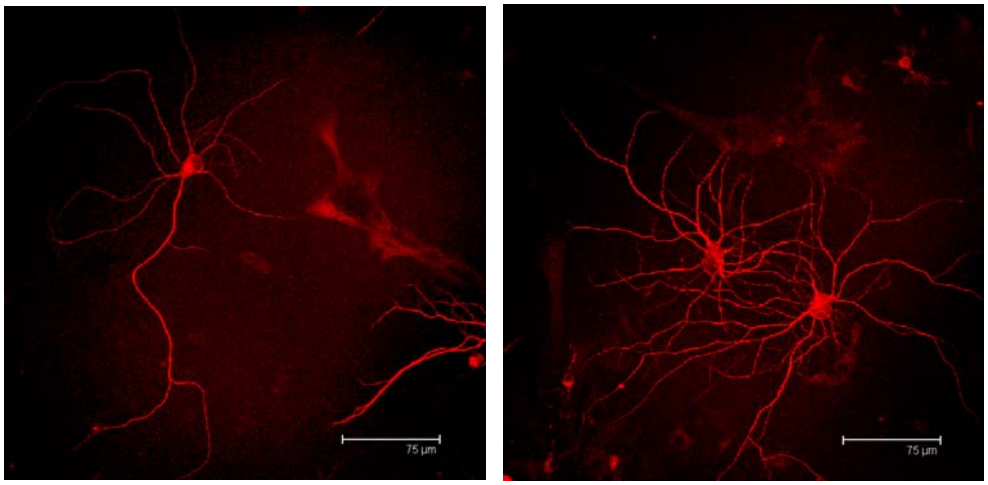

Figure 5.3: Confocal fluorescence image of rat hippocampal neurons cultured on PMETA brushes modified silicon substrates for ~20 days. Neurons were labeled by primary antibody raised against MAP2 and Cy3 labeled secondary antibody sequentially.

Creating patterned hybrid PMETA/PEG surfaces: The ability to control and direct neurite outgrowth is critical for neurological implants and neuroelectronic circuits. It can also be very useful for design of cell-based biosensors and fundamental studies of neuronal signaling. These studies require precise fabrication of hybrid patterned surfaces containing molecules that direct cell adhesion to precise locations and promote process outgrowth in desired directions. As mentioned before, chemical modification and lithographic processes can be performed on patterned polymer brush surfaces because of their high stability. The flexibility and robustness of the process can be very useful in generating multi-component hybrid patterned surfaces for various applications and are among the most promising features of the approach described here. To direct neuronal growth, we created a hybrid surface consisting of "cytophilic" PMETA brushes and "cytophobic" PEG monolayer.

As shown in Scheme 5.1, polymer brushes were patterned using a procedure based on photolithography, which is modified from a previously reported procedure[25]. Due to good solubility of ordinary photoresists in organic solvents, immobilizing surface initiator onto surfaces with patterned photoresists does not yield a well defined patterned initiator layer. As a result, most reported procedures for polymer brush patterning to date have been based on micro-contact printing.[14,24] Anderson et al.[25] showed that LOR 5A, a lift-off resist, is compatible with the chemical conditions required for molecular self-assembly. Here, we used a modification of the procedure reported by Anderson et al. to pattern PMETA brushes. Briefly, ordinary photolithography was done on a silicon wafer pre-coated with a layer of LOR 5A. The pattern generated on the photoresist layer was transferred into the LOR 5A layer. Because LOR 5A is stable in organic solvents, it prevents modification of the silica regions underneath. Surface-initiated polymerization took place in the exposed regions. After polymerization, LOR 5A was removed by a base developer. This process

provides a standard method to pattern polymer brushes on both silicon and gold surfaces. The unmodified silica regions were backfilled with a PEG layer. To avoid contamination or possible structural changes during the photolithography process, a PEG monolayer was deposited onto the patterned surface at the end of the whole process. An optical image of the patterned hybrid surface is shown in Figure 5.4. Large 10 μm x 10 μm squares were designed for neuron cell bodies to settle. Thin lines (2.5 μm wide) were designed for axon and dendrite processes. Such patterned hybrid surfaces were used to guide neurite outgrowth.

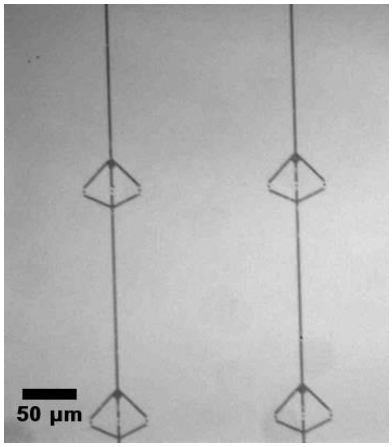

Figure 5.4: Optical image of a patterned PMETA brush/PEG surface. The black lines are PMETA brushes and the rest of the surface is covered with PEG monolayer.

Neurite outgrowth on patterned PMETA brush/PEG surfaces: Although much effort has been devoted to the creation of *in vitro* neuronal networks with geometrically defined features, most published procedures continue to rely on physically adsorbed polylysine or laminin, which is not stable over time. The polymer brushes are covalently attached to the substrate and are very stable in further chemical

or lithography processes. Hippocampal neurons localized to the brush patterns and, growth of neurites along the pattern line was clearly evident (Fig. 5.5A, B)

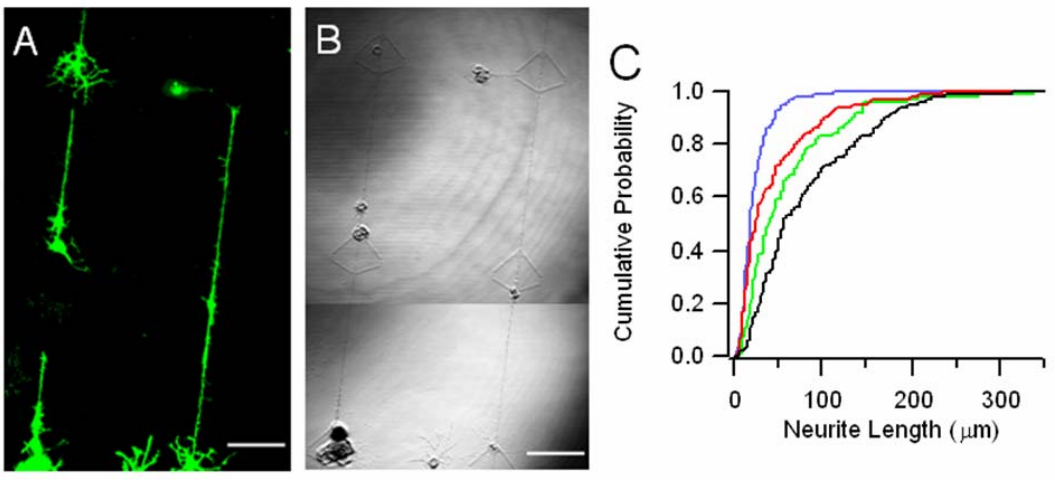

Figure 5.5: Fluorescence (A) and reflectance (B) image of living hippocampal neurons using confocal microscopy. The neurons were cultured on a PMETA brush/PEG hybrid patterned surface for ~ 10 days and labeled with calcein. (C) Cumulative histograms of neurite length on patterned lines (green), on PEG-surface between PMETA patterns (blue), on unpatterned PMETA surface (red), and unpatterned poly-lysine (black). The scale bar is 75 μm.

Although the PEG between patterned polymer brush surfaces was designed to minimize cell attachment and neurite outgrowth, we found that some cells did attach to this surface and extend neurites. To assess the utility of the brush surface, we compared neurite lengths on the patterned brush to that on the intervening PEG areas of patterned chips. Cumulative histograms (Figure 5.5C) of neurite length indicate that neurites on the PMETA pattern lines (Fig 5.5C, blue line) were markedly longer than those extending on the cytophobic PEG surface (Fig 5.5C, green line) (brush median length 39 μm, mean 60 μm; PEG median length = 20 μm, mean = 24 μm; H =

48, p<.0001, Kruskal-Wallis test). For comparison also the neurite length distribution of cells grown on conventional polylysine surface (Fig 5.5C black line) is shown (median length = 57 μm, mean = 81 μm). On unpatterned PMETA surfaces neurite length was intermediate (Fig 5.5C, red line). This suggests that the constrained geometry of the pattern promotes neurite outgrowth, perhaps by limiting the metabolic cost of outgrowth in the non-preferred (pegylated) directions.

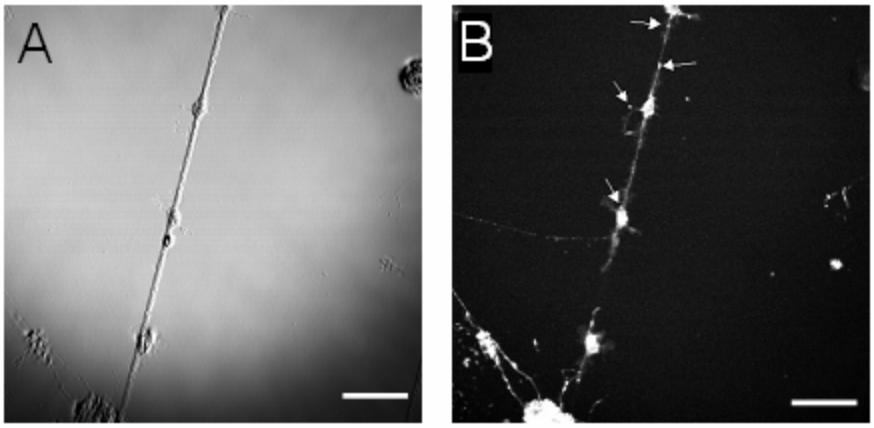

Figure 5.6: Reflectance (A) and fluorescence (B) images of hippocampal neurons acquired by confocal microscopy. The neurons were cultured on a PMETA brush/PEG hybrid patterned surface for ~ 10 days and labeled with anti-synaptobrevin antibody. The scale bar is 50 μm.

Immunofluorescence labeling of neurons for the synaptic vesicle protein synaptobrevin (Fig 5.6) showed that there is directed growth of axons along the PMETA brush pattern and puncta (arrows) indicating synaptic varicosities are clearly evident. Future applications may extend to spotting proteins to promote synapse formation at the predesigned location in the neuronal network. Neuronal networks with precise control of synapses should be extremely useful for hybrid neuronal-electronic circuits and investigating neuronal signaling.

Conclusions

PMETA brushes were directly synthesized by SI-ATRP of META in protic media. Kinetics of polymer brush growth was compared in three different solvents: IPA/water mixture, methanol/water mixture and pure water. Brush growth terminated after a short period of polymerization in pure water and the final brush thickness is only around ~ 15 nm. When an IPA/water mixture was used as solvent, PMETA brushes grew in a controllable manner for ~ 8 hours, resulting in the largest final brush thickness (~ 60nm) among three solvents. However, in the first couple of hours, polymer brushes grew faster in methanol/water mixture than in IPA/water mixture, which is different from the polymerization kinetics in solution.

PMETA brushes modified surfaces were shown to be excellent neuron culture substrates. Rat hippocampal neurons showed long-term viability and formed extensive neurites on PMETA brushes coated silicon substrates. With previously reported antibacterial activity and the ability to provide good neuronal cell viability demonstrated here, quaternized PMETA polymer brushes are excellent candidates for biointerface materials in bioimplanting, biosensing and the like.

Hybrid surfaces with both “cytophilic” PMETA brushes and “cytophobic” PEG monolayers were patterned by a procedure based on photolithography. Such hybrid surfaces showed good spatial control on rat hippocampal neuron outgrowth. The compatibility with more chemical modification techniques and lithography steps suggests that such hybrid surfaces may be a very useful platform to build up more complex biomedical micro-devices for cell-based biosensors, fundamental studies of neuron signaling, neuronal implants and further applications.

Acknowledgements

This research was supported by the NSF-funded Cornell Nanobiotechnology Center (NBTC). We made use of the facilities at NBTC, Cornell NanoScale Science and Technology Facility (CNF), and Cornell Center for Materials Research (CCMR), all of which are supported by NSF. We also acknowledge partial support of NSF grant DMR-0518785. The NBTC support for RD and RPM are gratefully acknowledged. The authors also would like to thank the helpful discussion and valuable information about polymerization conditions from Wilhelm T. S. Huck group at University of Cambridge, UK.

REFERENCES

[1] Kasemo, B. *Curr. Opin. Solid State Mater. Sci.* **1998**, 3, 451-459.

[2] Ikeda, T.; Hirayama, H.; Yamaguchi, H.; Tazuke, S.; Watanabe, M. *Antimicrob. Agents Chemother.* **1986**, *30*, 132-136.

[3] Krishnan, S.; Ward, R. J.; Hexemer, A.; Sohn, K. E.; Lee, K. L.; Angert, E. R.; Fischer, D. A.; Kramer, E. J.; Ober, C. K. *Langmuir* **2006,** 22, 11255-11266.

[4] Cheng, Z.; Zhu, X.; Shi, Z. L.; Neoh, K. G.; Kang, E. T. *Ind. Eng. Chem. Res.* **2005,** *44,* 7098-7104.

[5] Huang, J.; Murata,H.; Koepsel, R. R.; Russell, A. J.; Matyjaszewski, K. *Biomacromolecules* **2007**, 8, 1396-1399

[6] Roy, D.; Knapp, J. S.; Guthrie, J. T.; Perrier, S. *Biomacromolecules* **2008,** *9,* 91–99.

[7] Rühe, J.; Yano, R.; Lee, J.-S.; Koberle, P.; Knoll, W.; Offenhausser, A. *J. Biomater. Sci. Polym. Ed.* **1999**, 10, 859-874.

[8] Soekarno, A.; Lom, B.; Hockberger, P. E. *Neuroimage* **1993,** 1, 129-144.

[9] Bledi, Y.; Domb, A. J.; Linial, M. *Brain Research Protocols* **2000**, 5, 282-289.

[10] Wang, J-H.; Hung, C-H.; Young, T-H. *Biomaterials* **2006,** 27, 3441-3450.

[11] Osborne, V. L.; Jones D. M.; Huck. W. T. S. *Chem. Commun.*, **2002,** 1838–1839.

[12] Li, Y.; Armes, S. P.; Jin, X.; Zhu, S. *Macromolecules* **2003,** *36,* 8268-8275.

[13] Senaratne, W.; Andruzzi, L.; Ober, C. K. *Biomacromolecules* **2005,** 6, 2427-2448.

[14] Kam, L.; Shain, W.; Turner, J.N.; Bizios, R. *Biomaterials* **2001,** 22, 1049-1054.

[15] Changa, J. C.; Brewerb, G. J.; Wheeler, B. C. *Biomaterials* **2003**, 24, 2863–2870.

[16] Zhou, F.; Zheng, Z.; Yu, B.; Liu, W.; Huck, W. T. S. *J. Am. Chem. Soc.* **2006**, 128, 16253-16258.

[17] Harris, J. M. *Poly(ethylene glycol) chemistry: Biotechnical and Biomedical Applications;* Plenum Press: New York, 1992.

[18] Dong, R; Krishnan, S.; Baird, B. A.; Lindau, M.; Ober, C. K. *Biomacromolecules* **2007,** 8, 3082-3092.

[19] Shah, R. R.; Merreceyes, D.; Husemann, M.; Rees, I.; Abbott, N.L.; Hawker, C. J.; Hedrick, J. L. *Macromolecules* **2000**, 33, 597-605.

[20] Rasband, W.S. (U.S. National Institutes of Health, Bethesda, MD, USA; 1997-2009).

[21] Meijering, E.; Jacob, M.; Sarria, J.-C. F.; Steiner, P.; Hirling, H.; Unser, M. *Cytometry A* **2004,** 58, 167-176.

[22] Bories-Azeau, X.; Armes, S. P. *Macromolecules* **2002,** 35, 10241-10243.

[23] Yavin, E.; Yavin, Z. *J. Cell Biol.* **1974,** 62, 540-546.

[24] Ruegg, U. T.; Hefti, F. *Neurosci. Lett.* **1984,** 49, 319-324.

[25] Anderson, M. E.; Srinivasan, C.; Hohman, J. N.; Carter, E. M.; Horn, M. W.; Weiss, P. S.; *Adv. Mater.* **2006**, 18, 3258–3260.

CHAPTER 6

TAILORING ELECTRODE PROPERTIES TOWARDS BIOSENSOR APPLICATIONS USING pH-SENSITIVE POLYMER BRUSHES

Abstract

Gold electrode surfaces were modified with pH-sensitive polymer brushes using surface-initiated atom transfer radical polymerization. Cyclic voltammetry (CV) of potassium ferricyanide ($K_3Fe(CN)_6$) was used to study pH response of the brush modified electrodes. On poly((2-dimethylamino)ethyl methacrylate) (PDMAEMA) brush covered electrode surfaces, CV for $K_3Fe(CN)_6$ changed dramatically as a function of pH. When pH was decreased from ~9 to ~7.5, PDMAEMA brushes changed from prohibitive to permissive for the redox process of negatively charged $Fe(CN)_6^{3-/4-}$. However, on poly(acrylic acid) (PAA) brush modified electrode surfaces, the redox process of $Fe(CN)_6^{3-/4-}$ was markedly inhibited at all pH values studied, from acidic to neutral (pH 2-7). Reasons for the different pH responses of electrodes modified with the different brushes are discussed. The negatively charged ascorbic acid, is a common interference chemical during *in vivo* measurements of neurotransmitters in the brain. At physiological pH, PAA brush modified gold electrodes show much stronger suppression of ascorbic acid oxidation than Nafion™ coated gold electrodes. Such polyelectrolyte brushes could be very useful in enhancing selectivity and biocompatibility of biosensors.

Key words: polyelectrolyte brush, pH-sensitive, electrochemical, cyclic voltammetry, biosensor, charge screen, ascorbic acid

Introduction

Surface modification is usually a critical part in building up a biosensor, especially when the target species cannot be directly detected by the detector and functionalization with specific biomolecules is required to convert these target species into other molecules and into detectable signals.[1] These biomolecules are usually covalently immobilized to self-assembled monolayers (SAMs) or physically trapped inside polymer films. In electrochemical biosensors, SAMs or coating films have also been used to selectively screen electrodes against interfering agents and improve selectivity of electrodes. For instance, ascorbic acid is present in the brain at high concentration and is usually the major interfering chemical during *in vivo* measurements of neurotransmitters.[2] Many attempts have been made to reduce the sensitivity of electrodes towards ascorbic acid. SAMs with acid end groups[3] and Nafion™,[4,5]a negatively charged polymer, have been widely used to coat electrodes and enhance selectivity of electrodes towards electroactive neurotransmitters such as dopamine. However, physically adhered polymer films usually suffer from swelling or peeling off, which decreases the lifetime of the biosensors. There are usually pinholes in SAMs that result in incomplete coverage of the surfaces. These issues could potentially be avoided by utilizing polymer brushes for surface modification of electrochemical biosensors.

Polymer brushes are surface-grafted polymer chains with sufficiently high grafting density such that polymer chains are forced to stretch away from the surfaces.[6] Polymer brushes provide a powerful means to tailor surface properties.[7] Compared to SAMs, polymer brushes provide much higher density of desired functional groups. Long polymer chains also ensure better surface coverage. Polymer brushes are covalently attached to the interface which makes them much more chemically and mechanically robust than physically coated polymer films. These advantages of

polymer brushes make them very attractive for surface modifications. Recently, polymer brushes have been used to modify electrode surfaces.[8,9,10,11] However, most of the studies used electrochemical methods to study properties of polymer brushes, instead of utilizing polymer brushes to tailor electrode properties. Here, we extended the application of polymer brushes to the field of biosensors.

We used surface-initiated atom radical polymerization (ATRP) to synthesize both PDMAEMA and PAA brushes on gold electrode surfaces and characterized these electrodes by CV. On PDMAEMA brush covered electrodes, the CV signals for $K_3Fe(CN)_6$ changed dramatically depending on the pH of the solution. However, PAA brushes largely prohibited the redox process of negatively charged $Fe(CN)_6^{3-/4-}$ over a large pH range, suggesting that PAA brushes could mimic the role of Nafion^{TM} in decreasing interference introduced by negatively charged ascorbic acid. Our results show that the oxidation peak in CV of ascorbic acid was shifted from ~ 0.23V (vs. Ag/AgCl sat. KCl) on bare gold electrodes to ~ 0.8V on PAA brush modified electrodes at neutral pH, demonstrating that oxidation of ascorbic acid on gold electrodes is significantly hindered by negatively charged PAA brushes. Comparison of CVs for ascorbic acid on Nafion^{TM} coated electrodes and PAA brushes modified electrodes showed that PAA brushes are more effective than Nafion^{TM} in suppressing ascorbic acid CV signals, which makes PAA brushes very promising in tailoring electrode properties towards biosensor applications.

Experimental section

Materials: 11-mercapto-1-undecanol, 2-bromo-2-methylpropionyl bromide, anhydrous pyridine, sodium acrylate, 2-(dimethylamino)ethyl methacrylate, 2,2′-bipyridine, copper (Ⅰ) bromide (CuBr), copper (Ⅱ) bromide ($CuBr_2$), 4-morpholineethanesulfonic acid (MES), sodium hydroxide, ethylene diamine tetracetic

acid (EDTA), potassium sulfate (K_2SO_4), Nafion^{TM} solution (20 wt. % in lower aliphatic alcohols and water, contains 34% water) and all solvents used were purchased from Sigma-Aldrich. All chemicals were used without further purification. Distilled deionized water and high-purity nitrogen gas (99.99 %, Airgas) were used throughout. A 1M sodium hydroxide solution was used to adjust pH of 0.1 M MES buffer solution into desired values and the accurate pH values were measured by pH meter at room temperature. Gold coated (~100 nm) silicon wafers (4" diameter) with a titanium adhesion layer were purchased from Platypus Technologies. The wafers were cut into 1 cm x 2cm chips before usage.

Modification of gold electrodes: Surface initiator was synthesized and immobilized to pre-cleaned gold surfaces as described.[12] PAA brushes[13] and PDMAEMA brushes[14] were synthesized using published procedures. Poly(styrene sulfonate) brushes were synthesized according to the following procedure. The substrate chips covered with surface initiator were placed in a dry Schlenk flask. The flask was evacuated and back-filled with nitrogen three times. Sodium styrene sulfonate (2.06 g, 10 mmol), CuBr (57.4 mg, 0.4 mmol), $CuBr_2$ (9.0 mg, 0.04 mmol), and 2,2′-bipyridine (137.4 mg, 0.88 mmol) were added to another 25 mL Schlenk flask equipped with a magnetic stir bar. Air in this flask was evacuated and replaced with nitrogen three times. Four mL of water, which was purged with nitrogen for at least 30 min, was transferred to the Schlenk flask containing the monomer using a cannula. The mixture was stirred at room temperature under nitrogen for about 10 min until a brown solution was obtained. The solution was then transferred into the Schlenk flask containing the patterned substrates using a cannula. Polymerization was carried out at 30 °C for 2 hours, after which the substrates were taken out of the solution and rinsed with water and ethanol, then blown dry under nitrogen gas. All brush modified chips were sonicated in 0.1 M EDTA solution (pH was adjusted to ~ 7 by 1M NaOH

solution) for 30 seconds right after polymerization to remove trapped copper ions. Then the chips were rinsed with DI water, ethanol sequentially and blown dry with pure nitrogen gas. Nafion^{TM} solution was spin-coated on pre-cleaned gold substrates. The substrates were baked at 100 ˚C for 1 minute afterwards.

Surface characterization: Gold substrate chips covered with polymer brushes were incubated in MES buffer solutions of different pH values for about 10 minutes and subsequently sonicated for 1 min, after which the substrates were rinsed with anhydrous ethanol quickly and immediately blown dry with nitrogen gas. The substrates were then characterized using a VERTEX 80v vacuum FT-IR spectrometer from Bruker Optics equipped with a liquid nitrogen-cooled Mercury Cadmium Telluride (MCT) detector. Before collecting data, the system was left in vacuum for 10 minutes to minimize signal noise introduced by air. IR spectra were taken with 2 cm^{-1} resolution using 256 scans at 75˚ incident angle. Spectra from bare gold substrates were used as background. OPUS viewer software was used to analyze FTIR spectra. Thickness of polymer brushes and Nafion^{TM} film was measured using a Woollam variable angle spectroscopic ellipsometer. A three layer model consisting of a 0.5 mm silicon layer, a 100 nm gold layer and a Cauchy layer, to represent the brush layer, was used to determine both the thickness and refractive index of the brush.

Cyclic voltammetry: Before measuring cyclic voltammograms, gold chips were cut into ~ 5 mm x 1 cm pieces. Electrochemical measurements were carried out using a BAS Voltammograph CV-27 electrochemical analyzer at room temperature. The measurements were conducted in a standard three-electrode cell, containing ~ 0.25 cm^2 polymer brush modified gold as the working electrode, Ag/AgCl in saturated KCl solution as the reference electrode and a Pt wire as the counter electrode. Cyclic voltammograms were recorded using a National Instrument Data Acquisition Card at home-written software interface. For each recording, several cycles were recorded

until a stable cyclic voltammogram was obtained. Scan rate was 25 mV/s. Data was analyzed using Origin 6.

Results and discussion

CV of PDMAEMA brushes modified electrodes: SAMs and thin polymer films have been widely used to tailor the properties of electrodes in the field of electrochemical sensors, [15,16,17,18,19] where CV was used to characterize changes induced by the surface modification in the redox processes of redox-active compounds. In a cyclic voltammogram, the position of redox peaks indicates how easily the compound can be oxidized or reduced on the electrode. To tailor electrode properties, materials containing acid or basic groups were usually used to coat electrodes. For a redox-active compound, its redox process in a slow-scan CV could be tuned mainly by its diffusion process from bulk solution to the electrode surface. Its diffusion process is regulated by the sum of physicochemical interactions between the compound and the surface coating material. Among several physicochemical interactions, electrostatic forces usually dominate. Sometimes, hydrophobicity and chain conformation of the surface materials also play very important roles.[20,21]

Polyelectrolyte brushes provide another powerful means to tailor surface properties. Because of their advantages over SAMs and polymer films as discussed before, polyelectrolyte brushes have a great potential in tuning properties of electrodes for biosensor applications. PDMAEMA brushes are pH-sensitive polybase brushes. Schepelina et al.[10] used CV to study the diffusion rate of redox-active $Ru(NH_3)_6^{3+}$ through PDMAEMA brushes modified colloidal nanopores on platinum electrode surfaces. They have shown that the diffusion rate decreased with decreasing pH as a result of electrostatic interactions and steric hindrance. They also found that the limiting current in the cyclic voltammograms had an abrupt change at pH ~ 4-5.

The pH dependence of cyclic voltammograms was investigated for negatively charged $Fe(CN)_6^{3-/4-}$ on PDMAEMA brush modified electrodes. Thickness of dry PDMAEMA brushes is ~ 50 nm. As expected, the redox current in cyclic voltammograms of $Fe(CN)_6^{3-/4-}$ increased with decreasing pH (Figure 6.1). At low pH, the PDMAEMA brushes became more positively charged, which produces larger attractive forces between $Fe(CN)_6^{3-/4-}$ and the brushes, facilitating the diffusion of redox-active $Fe(CN)_6^{3-/4-}$ to the electrodes. As shown in Figure 6.2, the characteristic absorption band for $-N(CH_3)_2$ around 2800 cm^{-1} in their IR spectra disappeared at pH ~6, indicating that the $-N(CH_3)_2$ groups become charged at lower pH. Accordingly, the absorption band for the counter ion, $Fe(CN)_6^{3-/4-}$, appears with decreasing pH. In addition, PDMAEMA brushes become more hydrophilic and exhibit larger swelling ratios with decreasing pH,[22] which further facilitates the diffusion of $Fe(CN)_6^{3-/4-}$. At lower pH, both electrostatic interaction and chain conformation of PDMAEMA brushes, facilitate the diffusion of $Fe(CN)_6^{3-/4-}$ and result in larger and more reversible redox currents in the cyclic voltammograms. At pH>8, however, we observed a dramatic change in the cyclic voltammograms for $Fe(CN)_6^{3-/4-}$, which is very different from what Schepelina et al.[10] have reported. This discrepancy may be due to the fact that the redox-active compound we studied was negatively charged, while the redox-active compound Schepelina et al. have studied was positively charged. As mentioned before, two properties of polymer brushes contribute to the diffusion rate of the redox-active compound: charge status and chain conformation (swelling ratio, hydrophobicity). When pH decreases, PMAEMA brushes become more hydrophilic and a larger brush swelling ratio enables better permeability of molecules, for both negatively and positively charged compounds. However, a larger charge fraction in positively charged PDMAEMA brushes at lower pH values facilitates diffusion of negatively charged $Fe(CN)_6^{3-/4-}$, but hinders diffusion of positively charged

$Ru(NH_3)_6^{3+}$. Thus, the two properties work in the same direction in affecting diffusion of $Fe(CN)_6^{3-/4-}$, but in the opposite manner in affecting diffusion of $Ru(NH_3)_6^{3+}$. This might explain why the dramatic change in the CVs of the two oppositely charged compounds occurred at very different pH values. CVs of PDMAEMA brushes for charged redox-active compounds can be tuned by pH values of the surrounding solution. This may be extremely useful in generating smart pH-sensitive sensors or switches at the nanometer scale.

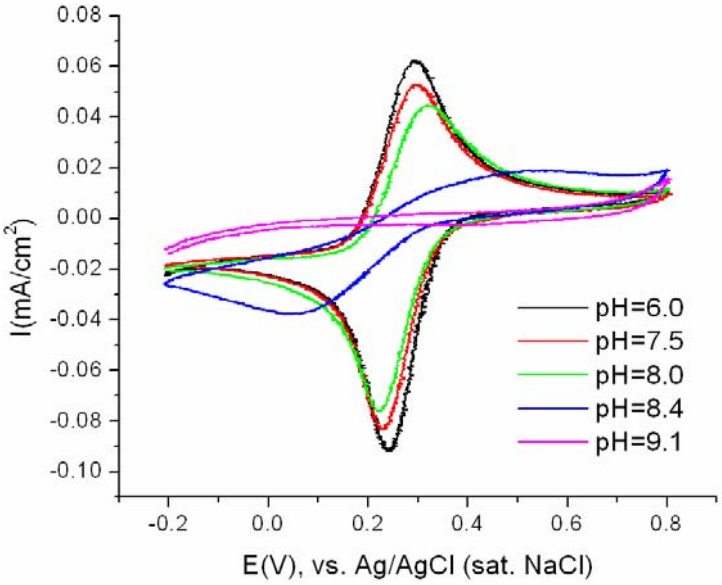

Figure 6.1: Cyclic voltammograms of PDMAEMA brush modified gold electrodes for 1 mM $K_3Fe(CN)_6$ solution in 0.1 M MES buffer solution at different pH values. The scan rate is 25 mV/s.

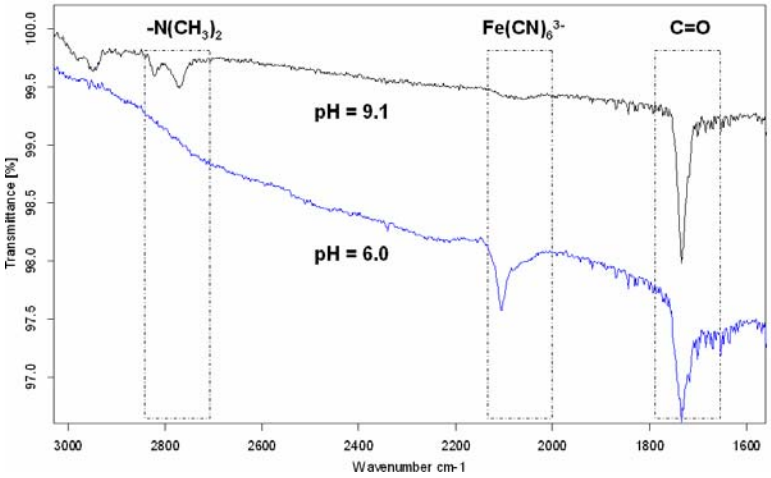

Figure 6.2: FTIR spectra of PDMAEMA brushes on gold surfaces pretreated by solution used in the electrochemical experiments.

CV of PAA brushes modified electrodes: PAA brushes are also pH-sensitive polymer brushes.[6] In contrast to PDMAEMA brushes, PAA brushes are negatively charged at pH values higher than the pKa.[12] For the reasons discussed in the previous section, the charge status and polymer chain conformation of PAA brushes work in the opposite manner in CV for negatively charged $Fe(CN)_6^{3-/4-}$. At neutral pH, PAA brushes were negatively charged, resulting in strong repulsion between the brushes and $Fe(CN)_6^{3-/4-}$. Virtually no redox reactions took place on PAA brush modified electrodes at potentials where peak redox currents were clearly obtained on bare gold electrodes (Fig 6.4). The redox process of $Fe(CN)_6^{3-/4-}$ was thus markedly reduced. At low pH, PAA brushes collapse and become hydrophobic,[12] which also reduces access of the redox-active compounds to the electrode surface. Only at intermediate pH (~4-6), when the brushes are still hydrophilic but not too highly charged, small redox peaks are discernible (Fig 6.3). PAA brushes effectively hindered redox process of negatively charged compounds at neutral pH. This may be very useful in creating

biosensors for neurotransmitters with small sensitivity towards the interfering ascorbic acid.

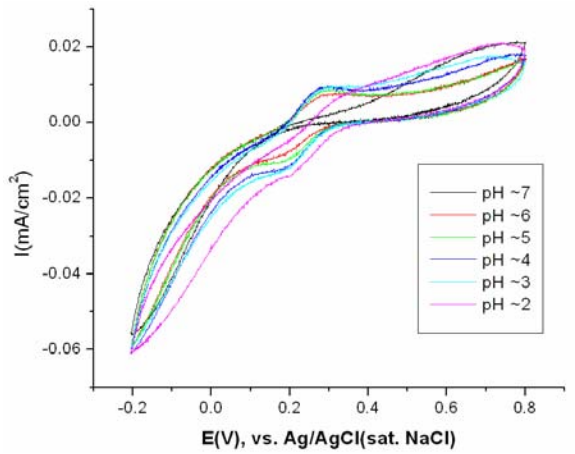

Figure 6.3: Cyclic voltammograms of PAA brush modified gold electrodes for 1 mM $K_3Fe(CN)_6$ solution in 0.1 M K_2SO_4 solution at different pH values (pH were adjusted by adding 1M H_2SO_4). The scan rate is 25 mV/s.

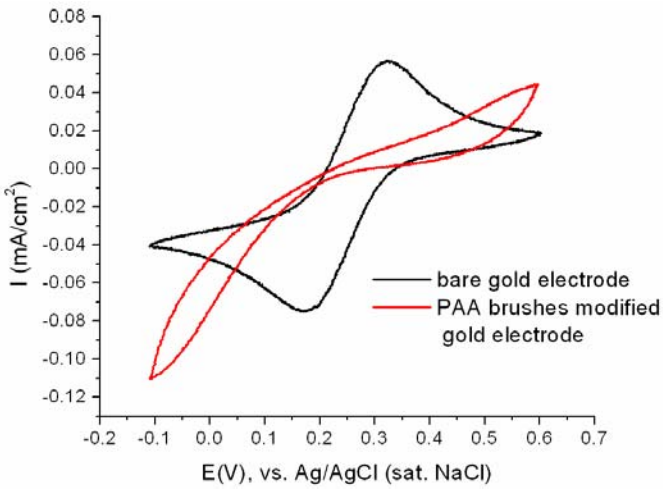

Figure 6.4: Cyclic voltammograms of PAA brush modified gold electrode (red line) and bare gold electrode (black line) for 1 mM $K_3Fe(CN)_6$ solution in 0.1 M K_2SO_4 solution at neutral pH. The scan rate is 25 mV/s.

Screening ascorbic acid using PAA brushes: Neurotransmitters in the brain are very important compounds and they are related to many neural diseases.[2] The ability to measure neurotransmitters accurately is crucial in diagnosing these diseases and also in developing suitable treatments. Many efforts have been made to develop electrochemical biosensors for neurotransmitters. A major challenge in developing a neurotransmitter biosensor is the interference caused by ascorbic acid. To reduce the interfering ascorbic acid signal, negatively charged Nafion™ film has been widely used to screen electrodes against negatively charged ascorbic acid .[23,24,25] Nafion™ film was usually applied to electrode surfaces by dip-coating or drop-coating, which resulted in thick and uncontrollable film thickness. In addition, physically adsorbed Nafion™ film is mechanically unstable and suffers from swelling, peeling off from electrode surface. PAA brushes are covalently attached to surfaces, which makes them mechanically and chemically stable. Moreover, the thickness of the brushes can be easily controlled at nanometer scale by varying polymerization conditions. At physiological pH, PAA brushes are negatively charged.[12] Thus, PAA brushes could potentially replace the role of Nafion™ in biosensors to screen ascorbic acid.

To compare the performance of PAA brush modified electrodes with that of Nafion™ modified electrodes, Nafion™ film (~ 100 nm thick) was cast on a gold electrode surface by spin-coating. Cyclic voltammograms of PAA brush modified electrodes and Nafion™ covered electrodes are shown in Figure 6.5. Both, Nafion™ and PAA brushes hindered oxidation of ascorbic acid on gold electrodes, with PAA brushes being more effective than Nafion™. Compared with bare gold electrodes, oxidation current peak for ascorbic acid was shifted towards more positive potential by ~ 570 mV on PAA brushes modified electrodes, while was only shifted by ~ 40 mV on Nafion™ covered electrodes.

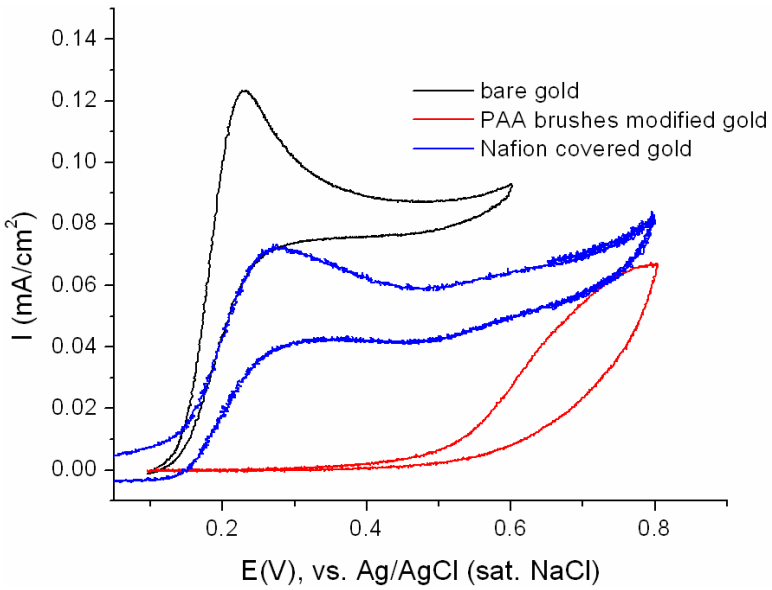

Figure 6.5: Cyclic voltammograms of PAA brush modified gold electrode (red line), Nafion^{TM} coated gold electrode (blue line) and bare gold electrode (black line) for 1 mM ascorbic acid solution in 0.1 M K_2SO_4 solution at neutral pH. The scan rate is 25 mV/s.

It seems surprising that weak polyacid (PAA) brushes screen ascorbic acid much better than a strong polyacid film (Nafion^{TM}). One reason could be that weak polyelectrolyte brushes have larger Gouy-Chapman length[26] and a substantial fraction of counterions leave the brush, resulting in an increased overall negative charge density of the brush system. Counterions associate more tightly with strong acid groups than with weak acid groups. In a solution with moderate or high ionic strength, strong acid groups form tight ion pairs with counterions and a strong polyacid behaves very much like a neutral polymer.[27] We also observed that PAA brushes screened ascorbic acid better than poly(styrene sulfonate) brushes (thickness ~40 nm), as shown in Figure 6.6, which further supports this interpretation. Another reason could be that spin-coated films have different chain conformation than polymer brushes, which

might also cause different electrochemical properties of the modified electrodes. Our results showed that PAA brushes worked better than Nafion^{TM} in screening electrodes against ascorbic acid. The screening is mainly due to the electrostatic repulsion between the charged brushes and ascorbic acid, because PAA brushes do not make pronounced changes to the CVs of other compounds, such as dopamine. Amperometry currents of dopamine and ascorbic acid measured at 0.7V showed that the selectivity of the gold electrodes towards dopamine versus ascorbic acid was increased around one hundred times by modifying the electrodes with PAA brushes. In addition, carboxylic acid groups on PAA brushes can be used to conjugate biomolecules under mild conditions.[13] PAA brushes are valuable in building up biosensors for *in vivo* neurotransmitter measurements.

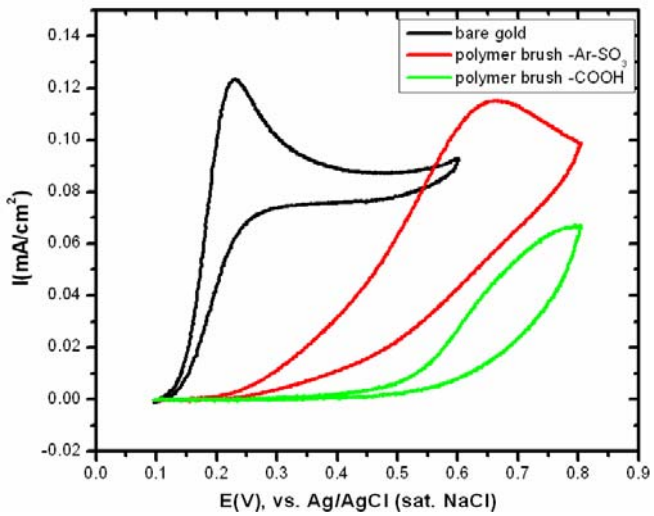

Figure 6.6: Cyclic voltammograms of PAA brush modified gold electrode (green line), poly(styrene sulfonate) brush modified gold electrode (red line) and bare gold electrode (black line) for 1 mM ascorbic acid solution in 0.1 M K_2SO_4 solution at neutral pH. The scan rate is 25 mV/s.

Conclusions

Gold electrodes were modified with pH-sensitive PDMAEMA brushes and PAA brushes using surface-initiated atom transfer radical polymerization. Cyclic voltammetry for $K_3Fe(CN)_6$ was used to study pH responses of the brush modified electrodes. On PDMAEMA brush modified electrodes, CV for $K_3Fe(CN)_6$ changed dramatically at pH ~ 8. Redox processes for $Fe(CN)_6^{3-/4-}$ became much more reversible and easier with decreasing pH. On PAA brush modified electrodes, redox process for $Fe(CN)_6^{3-/4-}$ was greatly hindered at studied pH values, from acidic to neutral. Reasons for the different responses of the two brushes were discussed in detail. PAA brushes were shown to work better than Nafion™ in screening electrodes against ascorbic acid, a common interference involved in neurotransmitter biosensing. At neutral pH, oxidation current peak in cyclic coltammogram for ascorbic acid was shifted from ~ 230 mV on bare gold electrodes to ~ 800 mV on PAA brush modified gold electrodes, indicating that PAA brushes made the oxidation of ascorbic acid much harder. Such a big shift caused by PAA brushes is much bigger than the voltage shift caused by Nafion™ film, which means that PAA brushes work better than Nafion™ in screening ascorbic acid.

We have shown here that electrochemical electrode properties can be tailored by pH-sensitive polymer brushes. Depending on the charge of the brushes and the redox-active compounds, CV of pH-sensitive brush modified electrodes could respond to pH in very different ways. We have also shown that PAA brushes work even better than Nafion™ in screening ascorbic acid, which can be extremely useful in enhancing selectivity for *in vivo* neurotransmitter biosensors.

Acknowledgements

This research was supported by the NSF-funded Cornell Nanobiotechnology Center (NBTC). We have made use of the facilities at NBTC, Cornell NanoScale Science and Technology Facility (CNF), and Cornell Center for Materials Research (CCMR), all of which are supported by NSF. The NBTC support for RD, CCMR support for YL, and generous help from Khajak Berberian are gratefully acknowledged.

REFERENCES

[1] Willner, I.; Katz. E. *Angew. Chem. Int. Ed.,* **2000,** 39, 1180-1218.

[2] Hu, Y.; Mitchell, K.M.; Albahadily, F.N.; Michaelis, E.K.; Wilson, G.S. *Brain Res*. **1994,** 659,117-25.

[3] Dalmia, A.; Liu, C.C.; Savinell. R. F. *J. Electroanal. Chem.* **1997,** 430, 205-214.

[4] Rice, M.E.; Oke, A.F.; Bradberry, C.W.; Adams, R.N. *Brain Res.* **1985,** 340, 151.

[5] Wightman, R.M.; May, L.J.; Michael, A.C. *Anal. Chem.* **1988,** 60, 769A.

[6] Advincula, R. C.; Brittain, W. J.; Caster, K. C.; Rühe, J. *Polymer Brushes: Synthesis, Characterization, Applications* **2004,** 1. Edition.

[7] Prucker, O.; Rühe, J. *Macromolecules,* **1998,** 31, 592-601.

[8] (a) Choi, E.; Azzaroni, O.; Cheng, N.; Zhou, F.; Kelby, T.; Huck, W. T. S. *Langmuir* **2007,** *23,* 10389-10394. (b) Zhou, F.; Hu, A.; Yu, B.; Osborne, V. L.; Huck, W. T. S.; Liu, W. *Anal. Chem.* **2007,** 79, 176-182. (c) Yu, B.; Zhou, F.; Hua, H.; Wang, C.; Liu, W. *Electrochimica Acta* **2007,** 53, 487–494.

[9] (a) Zhou, J.; Wang, G.; Hu, J.; Lu, X.; Li, J. *Chem. Commun.* **2006,** 4820–4822. (b) Zhou, J.; Lu, X.; Hu, J.; Li, J. *Chem. Eur. J.* **2007,** 13, 2847–2853.

[10] Schepelina, O.; Zharov, I. *Langmuir* **2008,** 24, 14188-14194.

[11] Fulghum, T. M.; Estillore, N. C.; Vo, C.; Armes, S. P.; Advincula, R. C.; *Macromolecules* **2008,** 41, 429-435.

[12] Dong, R.; Lindau, M.; Ober, C. K. *Langmuir,* **2009,** 25, 4774-4779.

[13] Dong, R; Krishnan, S.; Baird, B. A.; Lindau, M.; Ober, C. K. *Biomacromolecules* **2007,** 8, 3082-3092.

[14] Huang, J.; Murata,H.; Koepsel, R. R.; Russell, A. J.; Matyjaszewski, K. *Biomacromolecules* **2007**, 8, 1396-1399.

[15] Roy, P. R.; Okajima, T.; Ohsaka, T. *Bioelectrochemistry* **2003,** 59, 11 – 19.

[16] Zhang, L.; Jia, J.; Zou, X.; Dong, S. *Electroanalysis* **2004,** 16, 1413-1418.

[17] Cecchet, F.; Marcaccio, M.; Margotti, M.; Paolucci, F.; Rapino, S.; Rudolf, P. *J. Phys. Chem. B* **2006,** *110,* 2241-2248.

[18] Hwang, I.; Baek, K.; Jung, M.; Kim, Y.; Park, K. M.; Lee, D.; Selvapalam, N.; Kim, K. *J. Am. Chem. Soc.* **2007**, 129, 4170-4171.

[19] Shervedani, R. K.; Bagherzadeh, M.; Mozaffari, S. A. *Sens. Actuators B:* **2006,**115, 614–621.

[20] Hamdi, N.; Wang, J.; Monbouquette, H. G. *J. Electroanal. Chem.* **2005,** 581, 258.

[21] Tam, T. K.; Ornatska, M.; Pita, M.; Minko, S.; Katz, E. *J. Phys. Chem. C* **2008,** 112, 8438–8445.

[22] Sanjuan, S.; Perrin, P. ; Pantoustier, N.; Tran, Y. *Langmuir* **2007,** 23, 5769-5778.

[23] Burmeister, J. J.; Gerhardt, G. A. *Anal. Chem.* **2001,** 73, 1037-1042.

[24] Kulagina, N. V.; Shankar, L.; Michael, A. C. *Anal. Chem.* **1999,** 71, 5093-5100.

[25] Pan, S.; Arnold, M. A. *Talanta* **1996,** 43, 1157-1162.

[26] Seidel, C. *Macromolecules* **2003,** *36,* 2536-2543.

[27] Hehmeyer, O. J.; Arya, G.; Panagiotopoulos, A. Z.; Szleifer, I. *J. Chem. Phys.* **2007,** 126, 244902.

CHAPTER 7

CONCLUSIONS

This dissertation describes the synthesis, characterization and biological applications of several types of polyelectrolyte (PE) brushes on planar surfaces. Surface-initiated ATRP in protic solvents was used to synthesize PE brushes directly from their ionizable monomers. A fabrication procedure compatible with organic solvents was developed to pattern polymer brushes based on photolithography. A variety of surface characterization techniques, including AFM, FTIR, contact angle, XPS and ellipsometry, were used to determine surface morphology, chemical structure and physiochemical properties of the PE brushes. Patterned PE brushes were further functionalized with biomolecules to create arrays of biomolecules, which were used to study cell signaling processes and guide growing of neuronal cells. PE brushes were also used to tailor the electrochemical properties of electrodes and increase their selectivity during biosensing.

Poly(acrylic acid) (PAA) brushes were directly synthesized by SI-ATRP of sodium acrylate in aqueous media, without the need of further deprotection steps used by traditional methods. Patterned PAA brushes were achieved by growing the brushes on silicon surfaces covered with pre-patterned polyethylene glycol (PEG) monolayers. These patterned PAA/PEG surfaces were used to immobilize proteins by several different strategies. Well-defined protein arrays with very clean background were achieved. The immobilized proteins were also shown to keep their activity very well.

FTIR, contact angle and angle-resolved XPS were used to characterize the dissociation behavior of PAA brushes and poly(methacrylic acid) (PMAA) brushes on gold surfaces. Carboxylic acid groups and deprotonated carboxylate groups absorb IR at different wavelengths, which gives FTIR the ability to quantify the degree of

dissociation of PAA brushes and PMAA brushes. Water contact angle decreases with increasing charge fraction of ionizable groups on the surface. By measuring the FTIR spectra and contact angles of the brush modified surfaces at different pH values, titration curves of the weak polyacid brushes were achieved. While FTIR probes the dissociation behavior of the whole brush layer, contact angle is only sensitive to the uppermost layer of the brushes. The pKa values extracted from FTIR titration are higher than the pKa values from contact angle titration for both brushes, indicating a variation of pKa inside the brushes. Angle-resolved XPS results also suggested that the charge fraction towards the brush periphery was larger than the charge fraction deeper inside the weak PE brushes when the brushes were partially charged. These results provide the first experimental evidence for this unique dissociation behavior of weak PE brushes.

Patterned PAA brushes were functionalized with 2,4-dinitrophenyl (DNP) groups to study rat basophilic leukemia (RBL) cell signaling processes. Although the RBL cell behavior on patterned short brush surfaces looked similar as on patterned self-assembled monolayers or lipid bilayers, the cell behavior on surfaces with patterned thick PAA brushes were very different and tuned by the pattern morphology. When pattern size was larger than the size of cells, PAA brushes were cell resistant. However, when pattern size was smaller than the size of cells, especially when the pattern size was reduced to ~2 μm, RBL cells gradually adhered to the patterned surfaces and the cell membrane concentrated over the brush regions after ~ 20 minutes at 37˚C. Such cell adhesion and membrane clustering did not occur at room temperature, which suggests that such phenomenon is regulated by cellular events, not the physiochemical interactions between cells and the patterned brush surfaces. Further experiments showed that such cell adhesion behavior was mediated by fibronection-integrin interactions and also driven by actin polymerization. These

results provide rich information about the cell adhesion process. On surfaces with large pattern size, cells could easily settle on “cytophilic” regions. In this case, the repulsion between negatively charged PAA brushes and cell membranes makes PAA brushes cell repulsive. However, when the pattern size is smaller than the size of cells, cells can not adhere to the surfaces easily because of the cell repellent PAA brushes. After enough accumulation of fibronection on the PAA brushes, the affinity force between fibronection and integrin can overcome the repulsion and cells can adhere to the patterned surfaces.

Positively charged poly([2-(Methacryloyloxy)ethyl]trimethylammonium chloride) (PMETA) brushes were directly synthesized using SI-ATRP of META in 2-isopropanol/water mixture at room temperature. This synthesis method provides good control over the brush growth and avoids the quaternization step which involves hazardous chemicals. Although quaternary brushes were shown to be antibacterial by other research groups, we hereby showed that PMETA brush modified surfaces worked well as culture substrates for rat hippocampal neurons. Surfaces with patterned PMETA brushes surrounded by PEG monolayers could guide neurons to grow following the designed patterns. These properties of quaternary brushes make them good candidates of biomaterials used for bioimplanting.

Several types of pH-responsive polymer brushes, PAA brushes and poly(dimethylaminoethyl methacrylate) (PDMAEMA) brushes, were synthesized on gold electrode surfaces to tailor the electrochemical properties of the electrodes. Cyclic voltammetry of the modified electrodes in a solution containing $K_3Fe(CN)_6$ changed with pH of the solution very differently depending on the nature of the charge carried by the brushes. For PDMAEMA brush modified electrodes, the cyclic voltammograms changed dramatically with the pH values of the solution. However, the cyclic voltammograms of PAA brush modified electrodes looked very similar at

different pH values ranging from 2 to 7. PAA brushes were very prohibitive for redox processes of negatively charged $Fe(CN)_6^{3-/4-}$ at all examined pH values. These properties of PE brushes were used to change the selectivity of electrodes. PAA brushes were shown to screen electrodes well against negatively charged ascorbic acid, a major interference in brain for *in vivo* biosensors. It was also shown that weak PE brushes could screen charged species better than strong PE brushes and casted thin polyelectrolyte films.

Polymer brushes combined the good features of SAMs and casted polymer films. They provide powerful tools to tailor surface properties. In particular, PE brushes are very interesting systems both theoretically and experimentally. PE brushes might provide good realistic models to study many inaccessible biological interfaces with "brush-like" structures, which could be extremely useful for better understanding of biological systems. The stimuli-responsive properties of PE brushes make them very attractive for various applications in the fields of, for example, protein engineering, tissue engineering, sensors, lubrication, nanoparticle encapsulation, functional coating, water purification, and proton exchange membrane in fuel cells.